BIOCHEMICAL AND SINGLE-MOLECULE ANALYSIS OF SIGNALING MOLECULES

BY

EDWIN X. ARAUZ DIAZ

DISSERTATION

Submitted in partial fulfillment of the requirements
for the degree of Doctor of Philosophy in Cell and Developmental Biology
in the Graduate College of the
University of Illinois at Urbana-Champaign, 2015

Urbana, Illinois

Doctoral Committee:

Professor Jie Chen, Chair and Director of Research
Associate Professor Craig Mizzen
Associate Professor Supriya Prasanth
Professor James Morrissey

Abstract

Mammalian cells use a variety of molecules to receive, process, and transmit information from the extracellular environment. Proteins receive and transmit signals through direct protein-protein interaction at the membrane surface and within the cytoplasm. Similarly, membrane lipids facilitate signal transmission across the membrane by direct interaction with intracellular proteins. In this disertation, I have investigated protein-protein and lipid-protein interactions of important signaling molecules by employing biochemical methods and novel single-molecule approaches.

Mammalian target of rapamycin (mTOR) is a master regulator of mammalian cell growth and proliferation. Phosphatidic acid (PA) is a critical mediator of mitogenic activation of mammalian target of rapamycin complex 1 (mTORC1) signaling, a master regulator of mammalian cell growth and proliferation. However the mechanism by which PA activates mTORC1 signaling has remained unknown. In Chapter I of my thesis, I discovered a new mechanism by which the lipid second messenger phosphatidic acid (PA) regulates mTORC1 complex. PA competes with the mTORC1 inhibitor, FK506 binding protein 38 (FKBP38), for mTOR binding at a site encompassing the rapamycin-FKBP12 binding domain. This leads to PA antagonizing FKBP38 inhibition of mTORC1 kinase activity in vitro and rescuing mTORC1 signaling from FKBP38 in cells. Additionally, PA binding to mTORC1 leads to an increase in kinase activity by an allosteric effect, independently of FKBP38. In conclusion, a dual mechanism for PA activation of mTORC1 is proposed– PA displaces FKBP38 from mTOR and allosterically stimulates the catalytic activity of mTORC1.

mTOR functions as part of either of the two multisubunit complexes, mTORC1 and mTORC2, but molecular details about the assembly and oligomerization of mTORCs are currently lacking. In chapter III of my thesis, in collaboration with Dr. Ankur Jain from Dr. Taekjip Ha laboratory, I used the single-molecule pulldown (SiMPull) assay to investigate the stoichiometry and assembly of mTORCs. After validating this novel approach with mTORC1, confirming a dimeric assembly as previously reported, I show that all major components of mTORC2 exist in two copies per complex, indicating that mTORC2 assembles as a homodimer. Interestingly, each mTORC component, when free from the complexes, is present as a monomer and no single subunit serves as the

dimerizing component. Instead, the data suggest that dimerization of mTORCs is the result of multiple subunits forming a composite surface. SiMPull also allowed the distinction of complex disassembly from stoichiometry changes. Physiological conditions that abrogate mTOR signaling such as nutrient deprivation or energy stress did not alter the stoichiometry of mTORCs. On the other hand, rapamycin treatment leads to transient appearance of monomeric mTORC1 before complete disruption of the mTOR–raptor interaction, whereas mTORC2 stoichiometry is unaffected. These insights into assembly of mTORCs may guide future mechanistic studies and exploration of therapeutic potential.

Signaling phospholipids are critical mediator of biological processes such as cell growth, proliferation, and metabolism. Recognition of signaling phospholipids by proteins is important for the targeting and initiation of many signaling cascades, but the mechanisms that regulate such interactions are not completely understood. The majority of the biophysical methods used to measure these interactions are performed with pure proteins *in-vitro*. In Chapter IV, in collaboration with graduate student Vasudha Aggarwal from Dr. Taekjip Ha laboratory, I have developed a single-molecule fluorescence approach to analyze lipid-protein interaction using crude cell extracts. The assay is applicable to a variety of lipid-binding domains (LBDs) expressed in cell lysates, and these LBDs are specifically pulled down by their target phospholipids. The single-molecule analysis quantitatively describes the interaction of LBDs on the lipids in real-time. These allowed the distinction of assembly features and kinetics for the different LBDs uncovering novel interaction behaviors. As an extension to cellular proteins, I determined the assembly properties of protein kinase Akt. Overall, this study demonstrates the strength of our assay to investigate protein-lipid interaction mechanisms in a new light.

This dissertation is dedicated to my wonderful siblings Eric and Karina Arauz and to the memory of my parents Aromelia Diaz and Diogenes Arauz.

ACKNOWLEDGEMENTS

I thank my advisor Professor Jie Chen for her gracious support, guidance, and availability throughout my PhD. I am thankful for her vast knowledge, scientific vision, patience, and support of my pursuit of challenging projects.

I thank the members of my thesis committee; Dr. Supriya Prasanth for her insightful comments and guidance in the cell biology of my projects; Dr. Craig Mizzen for his scientific and career advices; and Dr. James Morrissey for his help and expertise in lipid biochemistry.

I thank members of the Chen laboratory for their continued support. I thank Dr. Nidhi Khanna, Dr. Min Zeng, and Dr. MeeSup Yoon not only for their scientific advice, but also for sharing in my moments of frustration and excitement during my research studies. I thank all current and former members of the Chen lab for their help and support during my studies: Dr. Yejing Ge, Christina Rosenberger, Rachel Waldemer, Nick Ikon, Nilmani Singh, Kook Son, and Rongping Zhang. I'd also like to thank Dr. Yuting Sun for helping me get my feet underneath me during my first 5 months in the laboratory.

I thank my family, especially my siblings Karina and Eric, for their love and support through out the course of my studies. Their words of inspiration and motivation have been a vital part of my success.

I thank my collaborators from the Ha laboratory, Dr. Ankur Jain and Vasudha Aggarval, for their sincere dedication and hard work. Finally, I want to thank Dr. Taekjip Ha for his guidance and helpful advice on the projects and manuscripts.

TABLE OF CONTENTS

CHAPTER I
Introduction

I.1. Mammalian target of rapamycin (mTOR)

Eukaryotic cells have acquired complex regulatory mechanisms that monitor nutrient and energy levels to regulate cell growth and division. An evolutionarily conserved protein from yeast to mammals called target of rapamycin (TOR), is a key regulator of these processes. Mammalian TOR (mTOR) integrates the sensing of nutrients, growth factors, oxygen, energy and cellular stress to regulate a myriad of processes such cell growth, proliferation and survival (Fig. I. 1). Accordingly, misregulation of mTOR activity is implicated in genetic diseases (Inoki, Corradetti et al. 2005), cancer (Guertin and Sabatini 2007), obesity, diabetes (Dann, Selvaraj et al. 2007; Vodenik, Rovira et al. 2009), and lifespan extension (Harrison, Strong et al. 2009; Selman, Tullet et al. 2009; Stanfel, Shamieh et al. 2009) (Fig. I. 2). Therefore, it is important to understand in molecular detail how mTOR signaling network works. Such understanding may aid in the development of disease treatment and drug design.

mTOR is a 290 kDa serine/threonine protein kinase that belongs to the PI3K related kinases family (PIKK) (Keith and Schreiber 1995). Other members of this family include the kinases ATM, ATR, DNA-PK, SMG-1, and TRRAP (Baretic and Williams 2014). All members of this family share a similar domain composition: a kinase domain that is functional in all members except for TRRAP (McMahon, Van Buskirk et al. 1998); a short FATC domain, present at the C-terminus of the kinase domain; a helical solenoid FAT domain just N-terminal to their kinase domain; and HEAT (huntinting, elongation factor 3, A subunit of PP2A, TOR) repeats. HEAT repeats are rod-like helical domains involved in protein-protein interactions and intracellular transport. Interestingly, only mTOR has an FRB (FKBP12 rapamycin binding) domain. As implied, FRB is the binding site for the drug rapamycin when complexed with the protein FKBP12. FRB serves as the binding site for the lipid second messenger phosphatidic acid (PA) (Fang, Vilella-Bach et al. 2001) and is part of the binding site for FKBP38, a negative regulator of mTOR signaling (Bai, Ma et al. 2007) (Fig. I. 3). Although all the members share

structural similarities and domain composition, they participate in distinct cellular processes. Among them,. mTOR is the only member that responds to nutrients and hormone signals.

I.2. Rapamycin

Rapamycin is a natural product produced by *Streptomyces hygroscopicus*. It was first discovered on Eastern Island as a potent fungicide (Vezina, Kudelski et al. 1975; Singh, Sun et al. 1979). Subsequently, it was found to have immunosuppressive activity and anti-tumor activity (Eng, Sehgal et al. 1984). The molecular target of rapamycin, TOR, was first identified in yeast (Heitman, Movva et al. 1991; Sabatini, Erdjument-Bromage et al. 1994). Due to its exceptional specificity and potency towards mTOR, rapamycin has been an invaluable tool in dissecting the biological functions of this protein. Rapamycin is even an FDA approved drug for organ transplantation immunosuppression and certain types of cancer. Rapamycin is known to limit substrate access to the kinase domain (McMahon, Choi et al. 2002; Yang, Rudge et al. 2013) as well as induce raptor dissociation from mTOR (Kim, Sarbassov et al. 2002; Oshiro, Yoshino et al. 2004; Yip, Murata et al. 2010). Rapamycin is also known to displace key activators of mTOR, thereby inhibiting downstream signaling (Fang, Vilella-Bach et al. 2001).

I.3. mTOR complexes, biological functions and regulation

mTOR nucleates two biochemically and functionally distinct complexes, mTORC1 and mTORC2 (Fig. I. 4). mTORC1 is composed of the proteins Raptor, mLST8/GBL, (Hara, Maruki et al. 2002; Kim, Sarbassov et al. 2002; Kim, Sarbassov et al. 2003), and the regulatory proteins PRAS40 and Deptor, which function as inhibitors of mTORC1 (Sancak, Thoreen et al. 2007; Peterson, Laplante et al. 2009). mTORC1 regulates cell growth and proliferation and its activation depends on nutrient (in particular, amino acids) availability and growth factors (Dunlop and Tee 2009). The best-known substrates of the mTORC1 kinase are the ribosomal subunit kinase S6K1 and the eIF4E binding protein 4EBP1 (Brown, Beal et al. 1995; Burnett, Barrow et al. 1998). When

phosphorylated by mTORC1, these proteins regulate translation initiation and ribosome biogenesis. mTORC1 function is specifically inhibited by rapamycin.

mTORC2 consists of Rictor, mLST8, mSIN1 (Sarbassov, Ali et al. 2004; Frias, Thoreen et al. 2006; Jacinto, Facchinetti et al. 2006; Yang, Inoki et al. 2006), the regulatory protein Protor, (Pearce, Huang et al. 2007), the inhibitory protein Deptor (Peterson, Laplante et al. 2009), and XPLN, an mTORC2-specific inhibitor (Khanna, Fang et al. 2013). mTORC2 is involved in actin cytoskeleton organization and cell survival by regulating members of the AGC kinase family such as AKT, SGK1 and PKC (Jacinto and Lorberg 2008; Alessi, Pearce et al. 2009). Contrary to mTORC1, mTORC2 is considered rapamycin insensitive. However, in some cell and tissue types prolonged treatment of cells with rapamycin induces the dissociation of mTORC2 and de-phosphorylation of its downstream targets (Sarbassov, Ali et al. 2006).

I.4. mTOR signaling network

Many regulators of mTOR signaling have been reported. There are many negative and positive feedbacks between several of the regulatory proteins, highlighting the complexity of the network. Here I highlight the key regulators of this network (Fig. I. 5).

TSC1/2: A key regulator of mTORC1 signaling is the TSC complex, which is a heterodimer composed of hamartin and tuberin, the products of tumor suppressor genes TSC1 and TSC2, respectively. When mutated, they are responsible for the tuberous sclerosis complex disease, which is characterized by development of hamartoma in a variety of organs (Gomez 1991). The TSC complex regulates mTORC1 signaling by working as a GTPase activating protein (GAP) for the small Rheb GTPase (Tee, Manning et al. 2003). Rheb binds and activates mTORC1 signaling by a mechanism not completely understood (Long, Lin et al. 2005; Avruch, Long et al. 2009).

FKBP38: A member of the FKBP (FK506 binding protein) family. Members of this family function as chaperones by facilitating protein folding (Somarelli, Lee et al. 2008). FKBP38 was found to be important in size regulation by the TSC complex (Rosner, Hofer et al. 2003). Consistent with this function, FKBP38 was found to negatively regulate mTORC1 signaling (Bai, Ma et al. 2007). FKBP38 binds to mTOR in

a region including the FRB domain where phosphatidic acid and the FKBP12-Rapamycin complex bind (Bai, Ma et al. 2007).

Phosphatidic acid (PA) and Phospholipase D (PLD): Our lab identified the lipid second messenger phosphatidic acid, and subsequently phospholipase D1 enzyme, which produces PA, as critical mediators of mTOR signaling (Fang, Vilella-Bach et al. 2001; Fang, Park et al. 2003; Sun, Fang et al. 2008). Additional reports indicate that both mammalian PLD isoforms (PLD1 and PLD2) are involved in mTOR signaling (Ha, Kim et al. 2006; Toschi, Lee et al. 2009). The enzymatic activity of PLD1 and PLD2 increases upon mitogenic and oncogenic signals (Foster 2009). The identification of the mTOR-PLD connection provides a mechanistic explanation for the mitogenic and oncogenic activities of PLD. PA binds to the FRB domain of mTOR and this interaction is specific for PA, as other lipids did not show any affinity for this domain (Fang, Vilella-Bach et al. 2001). A key residue for this interaction is Arg 2109 (Fang, Vilella-Bach et al. 2001), which has now been shown to interact directly with the phosphate group of PA (Veverka, Crabbe et al. 2008). Therefore, an increasing body of evidence supports a critical role of PA and PLD enzymes in the regulation of mTOR signaling. However, how PA activates mTOR remains incompletely understood. Direct activation of mTORC1 kinase by PA has been discovered by our lab (Yoon, Sun et al. 2011). My thesis work in Chapter II describes a novel mechanism of PA activation of mTORC1.

I.5. Single-molecule microscopy

Our knowledge of mTOR complexes is largely derived from conventional biochemical approaches. However, these approaches suffer from limitations that may hinder the complete understanding of protein complexes. To fully decipher the complicated processes of mTOR complex formation and signaling, my thesis work delved into single-molecule approaches.

Before the 1980's, it was not possible to observe single molecule dynamics in real time. Spectroscopy and experiments performed at low temperatures proved it was possible to detect single molecules (Moerner and Kador 1989). This allowed the direct observation of new molecular behaviors, heterogeneity, and dynamics over time. With

additional technological advancements, it is now possible to investigate the behavior of single molecules in real-time at room temperature.

The imaging of individual biomolecules has had a tremendous impact on biomedical research. We can study the fluctuations of different enzymatic states, biological processes in live cells, membrane behaviors, and structural analysis (Sako and Yanagida 2003). Importantly, studying individual molecules allows direct observation of the behavior of each molecule rather than an average behavior of many molecules.

To observe individual molecules in single-molecule microscopy, the molecules must first be present at a very low concentration. If attached to a surface, molecule density should be in the range of 0.2 molecules/μm^2. This surface density ensures that each molecule is sufficiently apart from each other allowing the optical detection of each individual molecule. Molecules are then visualized using total internal reflection fluorescent (TIRF) microscopy. TIRF microscopy is based on the creation of an evanescent wave generated by a beam of light entering between two optical media (glass and oil) in a critical angle. The evanescent wave penetrates the sample to a depth of approximately 100 nm. This allows the molecules that are very closed to the surface to be excited by the evanescent wave. The emitted signal is usually recorded by a high-sensitivity camera that allows the recording of hundreds of individual molecules with millisecond-time resolution.

I.6. Single-molecule pulldown (SiMPull)

Most proteins in the cell do not work alone. Instead, they are found in protein complexes. These complexes are regulated in many ways, but one of the most important mechanisms is by interacting with other cellular proteins. Traditional biochemical methods to study protein-protein interactions have been instrumental in our current understanding of signaling networks. The most common way to detect protein-protein interactions is by performing a pulldown assay. In this assay, a protein of interest (bait) will bring along its binding partners (prey). These binding partners are then identified using Western blotting or mass spectrometry.

However, this ensemble assay presents several limitations: 1) Most detected interacting partners must be tightly associated in order to survive the cell lysis and

stringent washing conditions used to remove non-specific binding proteins. 2) After the pulldown assay is completed, interacting proteins are detected via western blotting. This presents a concern since proteins must be separated by size during gel electrophoresis and then transferred to a membrane for subsequent blotting with primary and secondary antibodies. This leads to the detecting of fewer molecules than the true number in the complex, and thus loss of sensitivity. 3) Because many steps are involved, conventional pull-down assays take several hours, making them cumbersome as well as non-physiological. 4) It is not possible to determine the stoichiometry of a particular protein in a complex, and it cannot be revealed the physiological permutations of these protein-protein interactions. Therefore, deeper understanding of the complexity of protein-protein interacting networks will require molecular dissection beyond the current state of traditional biochemical assays.

Recently, a new approach was developed that addresses these limitations. This new assay, named single-molecule pulldown (SiMPull) and developed by our collaborator Prof. Taekjip Ha's laboratory, combines the principles of conventional pulldown assay and the power of single-molecule fluorescent microscopy (Jain, Liu et al. 2011). In SiMPull, protein complexes are pulled down from freshly lysed cells directly onto quartz slides prepared for single-molecule fluorescence microscopy (Fig. I. 6). SiMPull presents several advantages over conventional pulldown assays: 1) It enables direct visualization of individual cellular protein complexes. 2) It has the potential to differentiate between multiple subcomplexes and configurations. 3) When proteins are stoichiometrically labeled, for example, using fluorescent protein tags such as YFP, SiMPull can reveal the stoichiometry of the protein complexes via single-molecule fluorescence photobleaching step analysis. 3) The whole assay can be completed in a short time, 1-30 minutes. 4) SiMPull can serve as a preparatory tool, in which functional macromolecules can be pulled-down directly from cell extracts for subsequent single-molecule biochemistry in situ. In Chapter III, I will describe the application of SiMPull to determine the stoichiometry and assembly of mTORC1 and mTORC2 in freshly prepared cell lysates, as well as the effects of nutrients, growth factors, and the drug rapamycin on these complexes.

I.7. Lipid-protein interactions

Signaling lipids, such as phospholipids, regulate a myriad of cellular processes. For example, Phosphatidylinositol 3-phosphate (PI(3)P) is a key regulator of membrane trafficking, autophagy, and cell growth (Burman and Ktistakis 2010; Yoon, Du et al. 2011). Phosphatidylinositol 4,5-bisphosphate ($PI(4,5)P_2$) is involved in vesicle fusion, membrane trafficking, and actin cytoskeletal assembly (Di Paolo and De Camilli 2006). Phosphatidylinositol 3,4,5-triphosphate ($PI(3,4,5)P_3$) regulates cell growth, proliferation, survival and metabolism. Consistent with this, PIP_3 is involved in diseases such as diabetes and cancer (Cantley 2002). Phosphatidic acid (PA) regulates cell growth and proliferation via mTORC1 and membrane trafficking (Jenkins and Frohman 2005; Sun and Chen 2008).

Lipid-protein interactions play critical roles in the assembly of signaling complexes. However, the mechanisms that regulate such interactions are not well understood. Signaling lipids can bind to specific proteins and recruit them to membranes in different cellular compartments, or regulate the assembly with other cellular proteins. Additionally, lipids can induce activation or inhibition of enzymes by allosteric effects.

The majority of the biophysical methods used to measure lipid-protein interactions are performed with purified proteins. Examples of these methods include surface-plasmon resonance, isothermal titration calorimeter, and size-based methods using chromatography or centrifugation. To date, only a handful of studies have probed these interactions with single-molecule resolution (Scott, Musselman et al. 2012). A major limitation of these studies lies in using purified recombinant proteins, which may not recapitulate function *in vivo*. Additionally, these assays are not performed in equilibrium since the unbound protein or lipids are separated from the lipid-protein complex before final detection. Finally, transient lipid-protein interactions cannot be detected by these methods due to non-equilibrium conditions and low detection sensitivity. In Chapter IV of my thesis, I describe the development of a new assay to probe lipid-protein interactions with single-molecule resolution in real-time with whole cell lysates.

I. 8. Figures

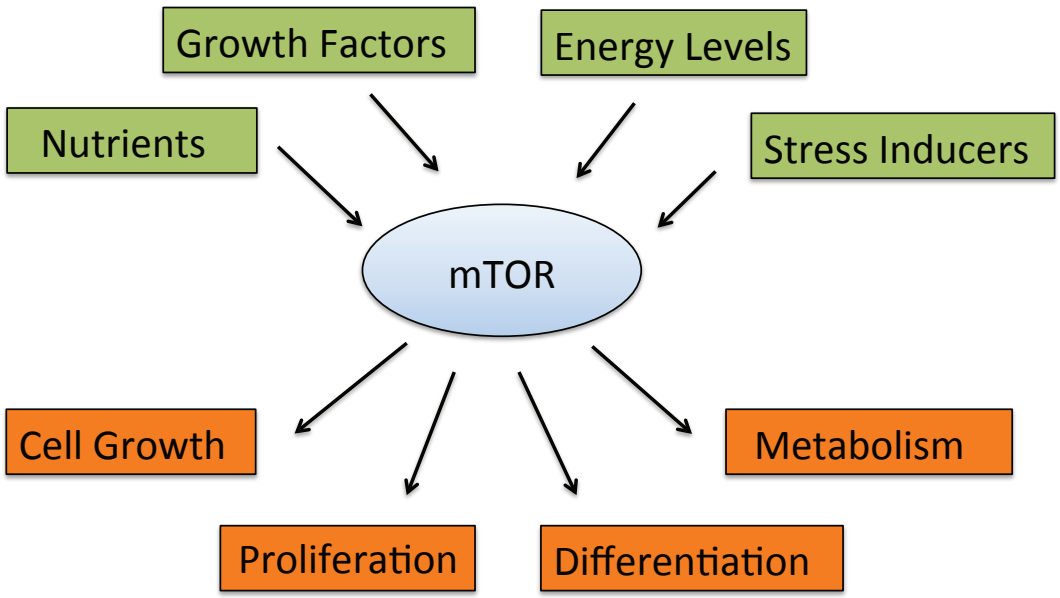

Figure I. 1. Upstream and dowmstream of mTOR. The Schematic shows different stimuli, such as nutrients, growth factors, energy levels, and stress inducers that transmit signals to mTOR. mTOR integrates these signals to regulate biological processes such as cell growth, proliferation, differentiation, and metabolism.

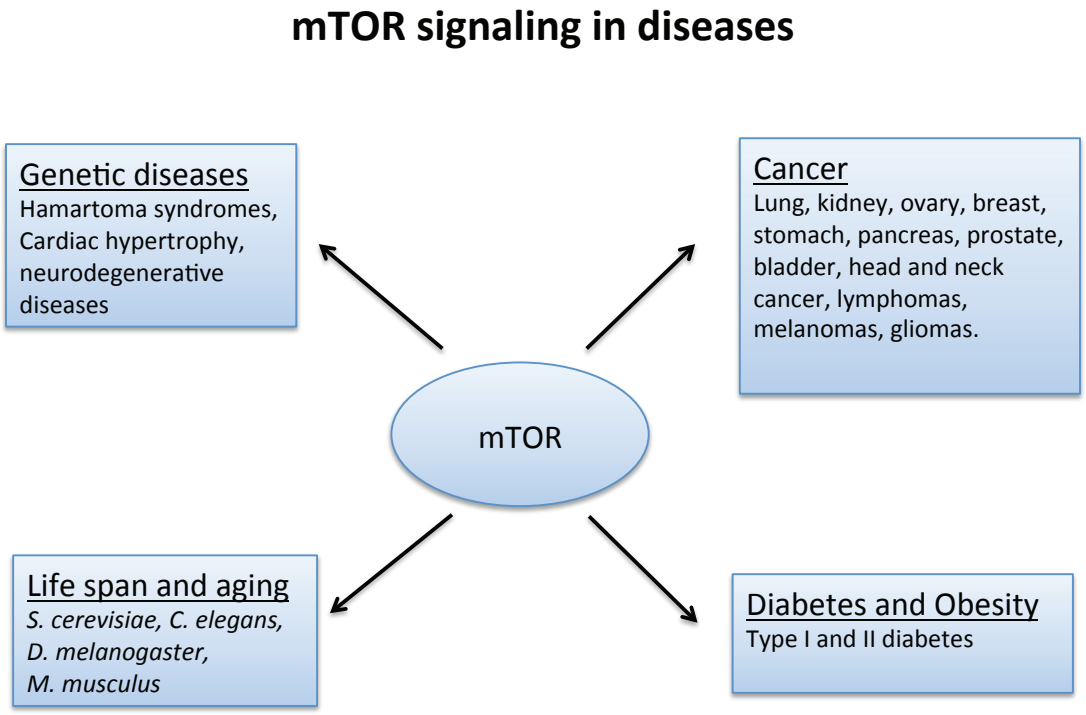

Figure I. 2. mTOR signaling in disease. The schematic shows human diseases where mTOR signaling is involved. Although mTOR itself is not genetically mutated in diseases, key upstream regulators of mTOR signaling are mutated in genetic diseases. mTOR is also involved in cancer, diabetes and obesity, and aging.

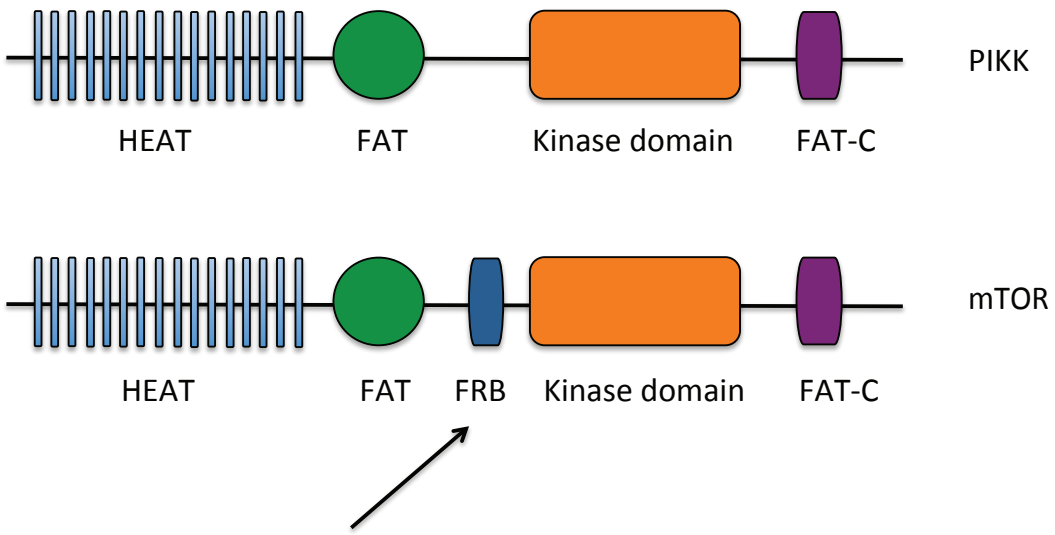

Figure I. 3. Domain composition of PIKK-family members. The schematic shows the domains present in all members of the PIKK family. mTOR has an additional domain named FRB (Fkbp12-rapamycin binding domain), which is not present in other PIKK-family members.

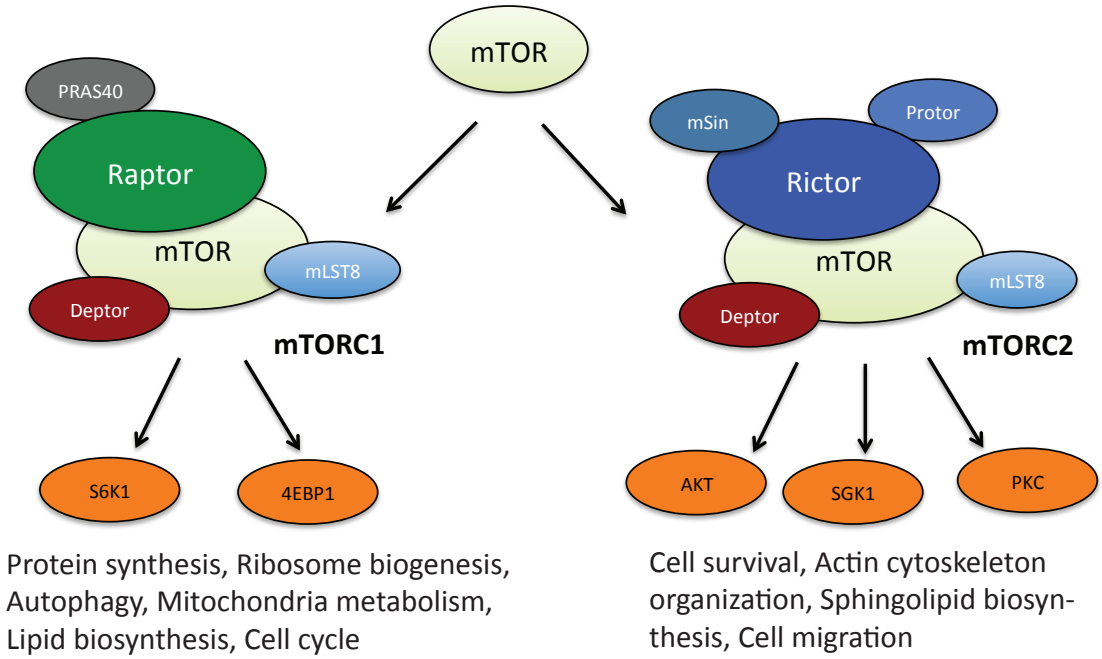

Figure I. 4. mTOR complexes. The diagram shows the subunit compositions of mTORC1 and mTORC2. Each complex has unique components (Raptor-PRAS40 in mTORC1 and Rictor-mSin in mTORC2) and shared components (mTOR, mLST8, Deptor). These subunit compositions allow substrate selectivity and participation of the two complexes in different biological processes.

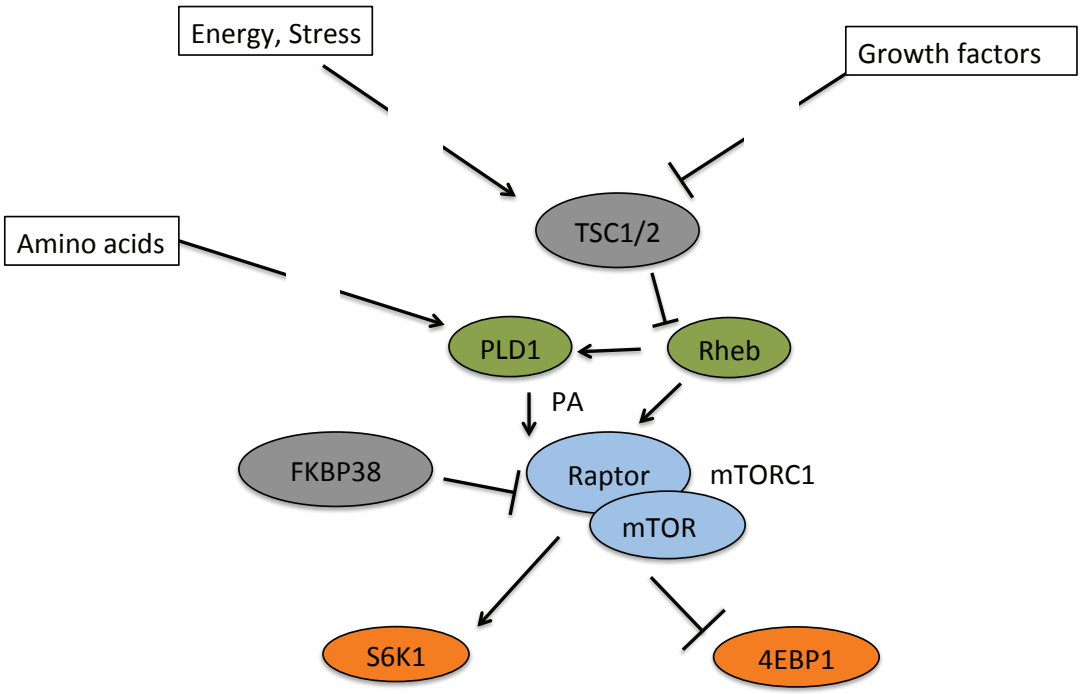

Figure I. 5. Key regulators of mTOR signaling. TSC1/2 is an upstream regulator of mTORC1. TSV1/2 has GAP (GTPase activating protein) activity toward the small G protein Rheb. PLD1 produces PA and synergizes with Rheb to activate mTORC1. FKBP38 is an inhibitor of mTORC1 that binds to a region including the FRB (FKBP12-rapamycin binding domain). Activated mTORC1 phosphorylates the substrates S6K1 and 4EBP1.

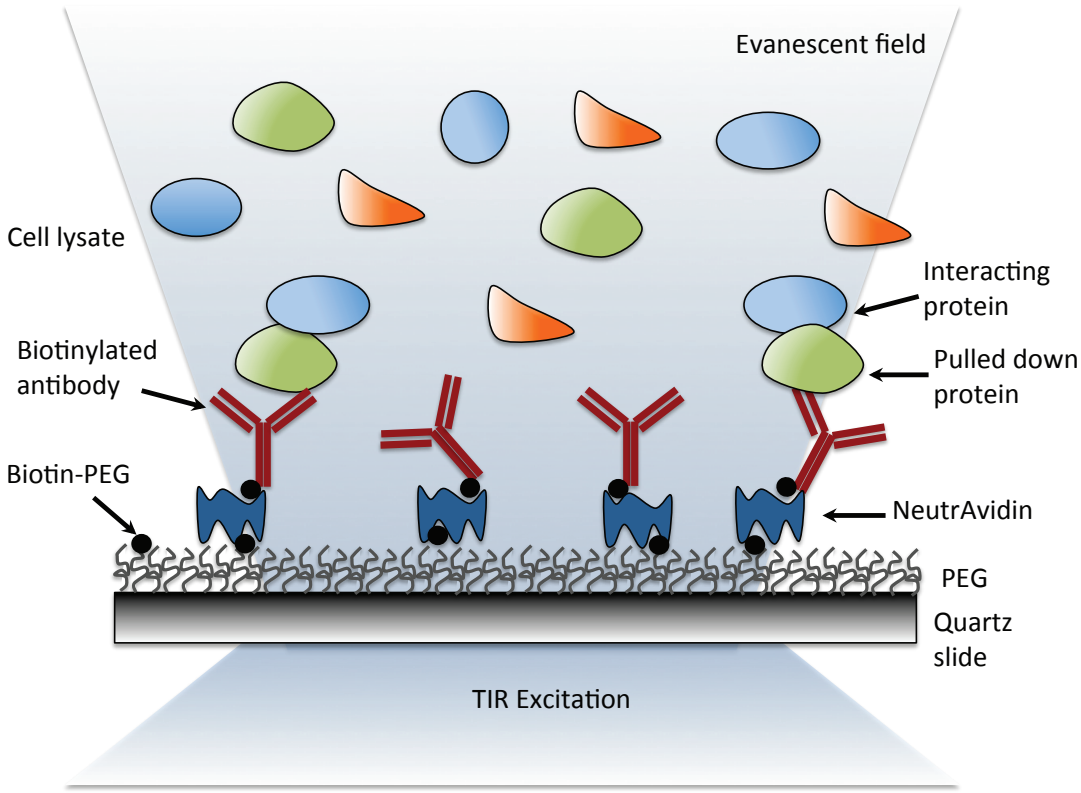

Figure I. 6. Single molecule pulldown (SIMPull). Quartz slides are functionalized with PEG and doped with PEG-biotin. Biotinylated antibodies against a protein of interest are immobilized using NeutrAvidin. When a cell extract is added to the chamber, the antibody captures the protein of interest together with its associating proteins. When the protein is fluorescently tagged, it can be directly visualized using a single-molecule fluorescent microscope.

I. 9. References

Alessi, D. R., L. R. Pearce, et al. (2009). "New insights into mTOR signaling: mTORC2 and beyond." Sci Signal 2(67): pe27.

Avruch, J., X. Long, et al. (2009). "Activation of mTORC1 in two steps: Rheb-GTP activation of catalytic function and increased binding of substrates to raptor." Biochem Soc Trans 37(Pt 1): 223-226.

Bai, X., D. Ma, et al. (2007). "Rheb activates mTOR by antagonizing its endogenous inhibitor, FKBP38." Science 318(5852): 977-980.

Baretic, D. and R. L. Williams (2014). "PIKKs - the solenoid nest where partners and kinases meet." Curr Opin Struct Biol 29C: 134-142.

Brown, E. J., P. A. Beal, et al. (1995). "Control of p70 s6 kinase by kinase activity of FRAP in vivo." Nature 377(6548): 441-446.

Burman, C. and N. T. Ktistakis (2010). "Regulation of autophagy by phosphatidylinositol 3-phosphate." FEBS Lett 584(7): 1302-1312.

Burnett, P. E., R. K. Barrow, et al. (1998). "RAFT1 phosphorylation of the translational regulators p70 S6 kinase and 4E-BP1." Proc Natl Acad Sci U S A 95(4): 1432-1437.

Cantley, L. C. (2002). "The phosphoinositide 3-kinase pathway." Science 296(5573): 1655-1657.

Dann, S. G., A. Selvaraj, et al. (2007). "mTOR Complex1-S6K1 signaling: at the crossroads of obesity, diabetes and cancer." Trends Mol Med 13(6): 252-259.

Di Paolo, G. and P. De Camilli (2006). "Phosphoinositides in cell regulation and membrane dynamics." Nature 443(7112): 651-657.

Dunlop, E. A. and A. R. Tee (2009). "Mammalian target of rapamycin complex 1: signalling inputs, substrates and feedback mechanisms." Cell Signal 21(6): 827-835.

Eng, C. P., S. N. Sehgal, et al. (1984). "Activity of rapamycin (AY-22,989) against transplanted tumors." J Antibiot (Tokyo) 37(10): 1231-1237.

Fang, Y., I. H. Park, et al. (2003). "PLD1 regulates mTOR signaling and mediates Cdc42 activation of S6K1." Curr Biol 13(23): 2037-2044.

Fang, Y., M. Vilella-Bach, et al. (2001). "Phosphatidic acid-mediated mitogenic activation of mTOR signaling." Science 294(5548): 1942-1945.

Foster, D. A. (2009). "Phosphatidic acid signaling to mTOR: signals for the survival of human cancer cells." Biochim Biophys Acta 1791(9): 949-955.

Frias, M. A., C. C. Thoreen, et al. (2006). "mSin1 is necessary for Akt/PKB phosphorylation, and its isoforms define three distinct mTORC2s." Curr Biol 16(18): 1865-1870.

Gomez, M. R. (1991). "Phenotypes of the tuberous sclerosis complex with a revision of diagnostic criteria." Ann N Y Acad Sci 615: 1-7.

Guertin, D. A. and D. M. Sabatini (2007). "Defining the role of mTOR in cancer." Cancer Cell 12(1): 9-22.

Ha, S. H., D. H. Kim, et al. (2006). "PLD2 forms a functional complex with mTOR/raptor to transduce mitogenic signals." Cell Signal 18(12): 2283-2291.

Hara, K., Y. Maruki, et al. (2002). "Raptor, a binding partner of target of rapamycin (TOR), mediates TOR action." Cell 110(2): 177-189.

Harrison, D. E., R. Strong, et al. (2009). "Rapamycin fed late in life extends lifespan in genetically heterogeneous mice." Nature 460(7253): 392-395.

Heitman, J., N. R. Movva, et al. (1991). "Targets for cell cycle arrest by the immunosuppressant rapamycin in yeast." Science 253(5022): 905-909.

Inoki, K., M. N. Corradetti, et al. (2005). "Dysregulation of the TSC-mTOR pathway in human disease." Nat Genet 37(1): 19-24.

Jacinto, E., V. Facchinetti, et al. (2006). "SIN1/MIP1 maintains rictor-mTOR complex integrity and regulates Akt phosphorylation and substrate specificity." Cell 127(1): 125-137.

Jacinto, E. and A. Lorberg (2008). "TOR regulation of AGC kinases in yeast and mammals." Biochem J 410(1): 19-37.

Jain, A., R. Liu, et al. (2011). "Probing cellular protein complexes using single-molecule pull-down." Nature 473(7348): 484-488.

Jenkins, G. M. and M. A. Frohman (2005). "Phospholipase D: a lipid centric review." Cell Mol Life Sci 62(19-20): 2305-2316.

Keith, C. T. and S. L. Schreiber (1995). "PIK-related kinases: DNA repair, recombination, and cell cycle checkpoints." Science 270(5233): 50-51.

Khanna, N., Y. Fang, et al. (2013). "XPLN is an endogenous inhibitor of mTORC2." Proc Natl Acad Sci U S A 110(40): 15979-15984.

Kim, D. H., D. D. Sarbassov, et al. (2002). "mTOR interacts with raptor to form a nutrient-sensitive complex that signals to the cell growth machinery." Cell 110(2): 163-175.

Kim, D. H., D. D. Sarbassov, et al. (2003). "GbetaL, a positive regulator of the rapamycin-sensitive pathway required for the nutrient-sensitive interaction between raptor and mTOR." Mol Cell 11(4): 895-904.

Long, X., Y. Lin, et al. (2005). "Rheb binds and regulates the mTOR kinase." Curr Biol 15(8): 702-713.

McMahon, L. P., K. M. Choi, et al. (2002). "The rapamycin-binding domain governs substrate selectivity by the mammalian target of rapamycin." Mol Cell Biol 22(21): 7428-7438.

McMahon, S. B., H. A. Van Buskirk, et al. (1998). "The novel ATM-related protein TRRAP is an essential cofactor for the c-Myc and E2F oncoproteins." Cell 94(3): 363-374.

Moerner, W. E. and L. Kador (1989). "Optical detection and spectroscopy of single molecules in a solid." Phys Rev Lett 62(21): 2535-2538.

Oshiro, N., K. Yoshino, et al. (2004). "Dissociation of raptor from mTOR is a mechanism of rapamycin-induced inhibition of mTOR function." Genes Cells 9(4): 359-366.

Pearce, L. R., X. Huang, et al. (2007). "Identification of Protor as a novel Rictor-binding component of mTOR complex-2." Biochem J 405(3): 513-522.

Peterson, T. R., M. Laplante, et al. (2009). "DEPTOR is an mTOR inhibitor frequently overexpressed in multiple myeloma cells and required for their survival." Cell 137(5): 873-886.

Rosner, M., K. Hofer, et al. (2003). "Cell size regulation by the human TSC tumor suppressor proteins depends on PI3K and FKBP38." Oncogene 22(31): 4786-4798.

Sabatini, D. M., H. Erdjument-Bromage, et al. (1994). "RAFT1: a mammalian protein that binds to FKBP12 in a rapamycin-dependent fashion and is homologous to yeast TORs." Cell 78(1): 35-43.

Sako, Y. and T. Yanagida (2003). "Single-molecule visualization in cell biology." Nat Rev Mol Cell Biol Suppl: SS1-5.

Sancak, Y., C. C. Thoreen, et al. (2007). "PRAS40 is an insulin-regulated inhibitor of the mTORC1 protein kinase." Mol Cell 25(6): 903-915.

Sarbassov, D. D., S. M. Ali, et al. (2004). "Rictor, a novel binding partner of mTOR, defines a rapamycin-insensitive and raptor-independent pathway that regulates the cytoskeleton." Curr Biol 14(14): 1296-1302.

Sarbassov, D. D., S. M. Ali, et al. (2006). "Prolonged rapamycin treatment inhibits mTORC2 assembly and Akt/PKB." Mol Cell 22(2): 159-168.

Scott, J. L., C. A. Musselman, et al. (2012). "Emerging methodologies to investigate lipid-protein interactions." Integr Biol (Camb) 4(3): 247-258.

Selman, C., J. M. Tullet, et al. (2009). "Ribosomal protein S6 kinase 1 signaling regulates mammalian life span." Science 326(5949): 140-144.

Singh, K., S. Sun, et al. (1979). "Rapamycin (AY-22,989), a new antifungal antibiotic. IV. Mechanism of action." J Antibiot (Tokyo) 32(6): 630-645.

Somarelli, J. A., S. Y. Lee, et al. (2008). "Structure-based classification of 45 FK506-binding proteins." Proteins 72(1): 197-208.

Stanfel, M. N., L. S. Shamieh, et al. (2009). "The TOR pathway comes of age." Biochim Biophys Acta 1790(10): 1067-1074.

Sun, Y. and J. Chen (2008). "mTOR signaling: PLD takes center stage." Cell Cycle 7(20): 3118-3123.

Sun, Y., Y. Fang, et al. (2008). "Phospholipase D1 is an effector of Rheb in the mTOR pathway." Proc Natl Acad Sci U S A 105(24): 8286-8291.

Tee, A. R., B. D. Manning, et al. (2003). "Tuberous sclerosis complex gene products, Tuberin and Hamartin, control mTOR signaling by acting as a GTPase-activating protein complex toward Rheb." Curr Biol 13(15): 1259-1268.

Toschi, A., E. Lee, et al. (2009). "Regulation of mTORC1 and mTORC2 complex assembly by phosphatidic acid: competition with rapamycin." Mol Cell Biol 29(6): 1411-1420.

Veverka, V., T. Crabbe, et al. (2008). "Structural characterization of the interaction of mTOR with phosphatidic acid and a novel class of inhibitor: compelling evidence for a central role of the FRB domain in small molecule-mediated regulation of mTOR." Oncogene 27(5): 585-595.

Vezina, C., A. Kudelski, et al. (1975). "Rapamycin (AY-22,989), a new antifungal antibiotic. I. Taxonomy of the producing streptomycete and isolation of the active principle." J Antibiot (Tokyo) 28(10): 721-726.

Vodenik, B., J. Rovira, et al. (2009). "Mammalian target of rapamycin and diabetes: what does the current evidence tell us?" Transplant Proc 41(6 Suppl): S31-38.

Yang, H., D. G. Rudge, et al. (2013). "mTOR kinase structure, mechanism and regulation." Nature 497(7448): 217-223.

Yang, Q., K. Inoki, et al. (2006). "Identification of Sin1 as an essential TORC2 component required for complex formation and kinase activity." Genes Dev 20(20): 2820-2832.

Yip, C. K., K. Murata, et al. (2010). "Structure of the human mTOR complex I and its implications for rapamycin inhibition." Mol Cell 38(5): 768-774.

Yoon, M. S., G. Du, et al. (2011). "Class III PI-3-kinase activates phospholipase D in an amino acid-sensing mTORC1 pathway." J Cell Biol 195(3): 435-447.

Yoon, M. S., Y. Sun, et al. (2011). "Phosphatidic acid activates mammalian target of rapamycin complex 1 (mTORC1) kinase by displacing FK506 binding protein 38 (FKBP38) and exerting an allosteric effect." J Biol Chem 286(34): 29568-29574.

CHAPTER II

Phosphatidic acid activates mammalian target of rapamycin complex 1 (mTORC1) kinase by displacing FK506 binding protein 38 (FKBP38) and exerting an allosteric effect[1]

II. 1. Introduction

The mammalian target of rapamycin (mTOR) assembles a signaling network that regulates a myriad of cellular and developmental processes and has emerged as a promising therapeutic target in various diseases including cancer (Martin and Hall 2005; Sarbassov, Ali et al. 2005; Guertin and Sabatini 2007). As a protein Ser/Thr kinase, mTOR exists in two biochemically and functionally distinct complexes – mTORC1 and mTORC2 – that mediate rapamycin-sensitive and rapamycin-insensitive signaling, respectively. The two complexes are defined by the presence of raptor in mTORC1 and rictor in mTORC2, although they also contain other components (Sarbassov, Ali et al. 2005). The best characterized substrates of mTORC1 kinase are ribosomal S6 kinase 1 (S6K1, phosphorylation at Thr389) and eukaryotic initiation factor 4E binding protein 1 (4E-BP1, phosphorylation at Thr37/46), both regulators of protein synthesis and both critically involved in mTOR regulation of cell growth and proliferation (Fingar and Blenis 2004; Ma and Blenis 2009). mTORC2 phosphorylates Akt at the hydrophobic motif (Ser473), which is required for Akt activation. In addition, mTORC2 phosphorylates Akt and cPKC at their turn motif, which stabilizes the kinases (Facchinetti, Ouyang et al. 2008; Ikenoue, Inoki et al. 2008).

Two major types of upstream signals impinge on the mTORC1 pathway in cell growth: mitogens and amino acids. The Rag small G proteins, and separately, the class III phosphatidylinositol 3-kinase hVps34, mediate amino acid signaling to mTORC1 (Avruch, Long et al. 2009). The tuberous sclerosis complex TSC1/TSC2 receives mitogenic signals, among other signals, upstream of mTORC1 (Li,

[1]This chapter appeared in its entirety in The Journal of Biological Chemistry 286 (2011), pages 29568-74 by MeeSup Yoon*, Yuting Sun*, **Edwin Arauz***, Yu Jiang and Jie Chen. (*Co-first authors)

Corradetti et al. 2004). The target of TSC's GTPase activating protein (GAP) activity is the small G protein Rheb, which activates mTORC1 signaling (Manning and Cantley 2003). Several mechanisms have been proposed for Rheb activation of mTORC1: (a) direct binding of Rheb to mTOR stimulates the kinase activity of mTORC1 (Long, Lin et al. 2005); (b) as an effector for Rheb, phospholipase D (PLD) mediates Rheb activation of mTORC1 (Sun, Fang et al. 2008); (c) Rheb displaces FKBP38, an inhibitor of mTORC1 kinase, and consequently activates mTORC1 (Bai, Ma et al. 2007).

Work from our laboratory, and subsequently many others, has established the lipid second messenger phosphatidic acid (PA) as a key mediator of mitogenic activation of mTORC1 (Fang, Vilella-Bach et al. 2001; Foster 2007; Sun and Chen 2008). Phospholipase D (PLD), an enzyme that converts phosphatidylcholine (PC) to PA (Frohman, Sung et al. 1999), is a critical component upstream of the mTORC1 pathway in the regulation of cell growth (Fang, Park et al. 2003; Foster 2007; Sun and Chen 2008). PA, with remarkable specificity, interacts with the FKBP12-rapamycin binding domain (FRB) of mTOR located N-terminal to the kinase domain, in competition with FKBP12-rapamycin binding (Fang, Vilella-Bach et al. 2001). Recently, a solution structure of the FRB-PA complex (Veverka, Crabbe et al. 2008) has validated the biochemically derived knowledge of FRB-PA interaction.

As a signaling lipid, PA has been found to have many effectors (Stace and Ktistakis 2006). Membrane translocation of the protein upon binding to PA is a major mechanism by which PA regulates its effectors, but PA is also believed to allosterically regulate the enzymatic activities of some of its effectors (Stace and Ktistakis 2006). The exact mechanism or a common mode for the allosteric effect of PA has not emerged, partly due to the lack of any well-defined PA-binding module in PA effectors. Although it is well established that PA activates mTORC1 signaling in cells, the mechanism behind this activation has remained a long-standing puzzle. There is no evidence for PA induction of mTOR membrane translocation, and our earlier experimental evidence also argued against the possibility of PA activating mTOR catalytic activity (Fang, Vilella-Bach et al. 2001; Chen and Fang 2002). However, recent advances in the understanding of the biochemistry and signaling of

mTOR have prompted us to reconsider the role of PA in the context of mTOR kinase activity. Here we report that PA directly activates mTORC1 kinase through a dual mechanism – displacement of the endogenous inhibitor FKBP38 from mTOR and allosteric activation of the kinase.

II. 2. Materials and methods

II. 2. 1. Reagents

The antibodies used in this study were obtained from the following commercial sources: Flag M2, Sigma; HA (16B12) and Myc (9E10.2), Covance; FKBP38, R&D Systems; GST and His, Santa Cruz; tubulin, Abcam; raptor and rictor, Bethyl laboratory, Inc.; all other antibodies, Cell Signaling. C8-PA, 1-palmitoyl-2-oleoyl-PA and -PC were from Avanti Lipids. Glutathione beads were from GE Healthcare. Protein G-agarose and His-Akt were from Millipore. All other reagents were from Sigma.

II. 2. 2. Plasmids

GST-S6K1 (a.a.332-421) was constructed by inserting the corresponding S6K1 cDNA into pGEX-2T (GE Healthcare). Raptor shRNA constructs were obtained from Addgene (Kim, Sarbassov et al. 2002). The following plasmids were previously described: Myc-S6K1 (Fang, Vilella-Bach et al. 2001); Flag-4EBP1 (Kim and Chen 2000); Flag-mTOR (Vilella-Bach, Nuzzi et al. 1999); HA-FKBP38, GST-FKBP38, and GST-mTOR-225 (Bai, Ma et al. 2007).

II. 2. 3. Cell culture

Human embryonic kidney (HEK) 293 cells were grown in DMEM containing 10% fetal bovine serum (FBS) at 37 °C with 5% CO_2. Transient transfections were performed with PolyFect (Qiagen) or Lipofectamine (Invitrogen) following manufacturers' recommendations and as previously described (Sun, Fang et al. 2008). C8-PA stimulation of the cells was as described previously (Sun, Fang et al. 2008).

II. 2. 4. Lentivirus-mediated RNAi

All shRNAs were obtained from Sigma-Aldrich in the pLKO.1-puro vector (MISSION® shRNA). Lentivirus packaging and testing were performed as previously described (Yoon and Chen 2008). HEK293 cells were infected with the lentiviruses in growth medium containing 6 μg/ml polybrene, followed by selection in 1.5 μg/ml puromycin for 3-4 days. The scramble and PLD1 TRC shRNA clones were previously described (Sun, Fang et al. 2008). Human FKBP38 shRNA was TRCN0000010595.

II. 2. 5. Protein purification

GST-fusion proteins (GST-mTOR-225, GST-FKBP38, GST-FKBP12) were expressed in *E. coli*, purified using glutathione beads, and cleaved of the GST tag as previously described (Fang, Vilella-Bach et al. 2001; Bai, Ma et al. 2007).

II. 2. 6. *In vitro* binding assays

Purified GST-FKBP38 and mTOR-225 proteins were mixed at 5 μg each and incubated on ice in 500 μl binding buffer (40 mM Tris-Cl, pH7.5, 150 mM NaCl, 2 mM EDTA, 2 mM EGTA, 1 mM DTT) for 15 min. Where applicable, lipid vesicles were pre-incubated with mTOR-225 for 15 min prior to addition of GST-FKBP38. PA vesicles (50% PA + 50% PC) and PC vesicles (100% PC) were made by probe-sonication as previously described (Fang, Vilella-Bach et al. 2001). Glutathione beads were used to pull down GST fusion proteins, and the beads were washed with binding buffer, followed by boiling in SDS samples buffer and Western analysis.

II. 2. 7. Cell lysis, immunoprecipitation, and western analysis

Cells were rinsed once with ice-cold PBS and lysed in ice-cold lysis buffer (40 mM HEPES, pH7.2, 120 mM NaCl, 10 mM pyrophosphate, 50 mM NaF, 10 mM b-glycerophosphate, 2 mM EDTA, 1x Sigma protease inhibitor cocktail, and 0.3% CHAPS). The supernatant after microcentrifugation at 13,000 rpm for 10 min was collected and subjected to immunoprecipitation at 4°C with various antibodies in the lysis buffer. The beads were washed 3 times with lysis buffer, and then boiled in SDS

sample buffer for 5 min. Proteins were resolved on SDS-PAGE and transferred onto PVDF membrane (Millipore), followed by incubation with various antibodies according to the manufacturers' recommendations. Detection of horseradish peroxidase-conjugated secondary antibodies was performed with Western Lightning™ Chemiluminescence Reagent Plus (Perkin Elmer, Inc.). Quantification of Western band intensities was performed by densitometry of X-ray film images using the software Image J.

II. 2. 8. *In vitro* mTOR kinase assays

mTORC1 and mTORC2 were immunoprecipitated using anti-raptor and anti-rictor antibodies, respectively, followed by incubation with protein G agarose beads. The kinase assays were performed following procedures described by Ikenoue et al. (Ikenoue, Hong et al. 2009). mTORC1 kinase assays were carried out at 30 °C for 30 min in 25mM HEPES (pH 7.4), 50 mM KCl, 10 mM $MgCl_2$ and 250 μM ATP, with 100 ng GST-S6K1 as the substrate. mTORC2 kinase assays were carried out at 37 °C for 30 min in 25mM HEPES (pH 7.4), 100 mM potassium acetate, 1 mM $MgCl_2$ and 500 μM ATP, with 250 ng His-Akt as the substrate. Where applicable, PA or PC vesicles, and/or FKBP38 were added to the immunocomplexes 15 min before initiation of the kinase assay by the addition of ATP. Reactions were stopped by the addition of 20 µl SDS sample buffer and boiling.

II. 3. Results

II. 3. 1. PA stimulates mTORC1 kinase activity

To evaluate a potential effect of PA on the kinase activity of mTOR in cells, we examined the phosphorylation of mTOR on Ser2481, an autophosphorylation site that has recently been reported to monitor mTORC-specific catalytic activities (Soliman, Acosta-Jaquez et al. 2009). To avoid potential complications from exogenous PA-derived lysophosphatidic acid (LPA) (Billon-Denis, Tanfin et al. 2008), which would initiate signaling through the membrane-bound LPA receptors, we used a short-chain PA (C8-PA) for delivery into cells, which would not be converted into active LPA (van Corven, van Rijswijk et al. 1992; Fischer, Nusser et al. 2001). mTORC1 and

mTORC2 were isolated from HEK293 cells by immunoprecipitation of raptor and rictor, respectively. As shown in Figure II. 1A, C8-PA treatment of the cells in the absence of any mitogen induced Ser2481 phosphorylation of raptor-associated mTOR; rictor-associated mTOR, on the other hand, displayed a higher basal level of pSer2481 that was not affected by PA stimulation. PA activation of mTORC1 signaling was confirmed by S6K1 phosphorylation on Thr389, whereas phospho-Ser473-Akt, an indicator of mTORC2 signaling, was not detectable upon PA treatment (Fig. II. 1B). These results suggest that PA activates mTORC1, but not mTORC2, kinase activity in cells.

Next, we asked whether PA could directly activate mTORC1 kinase *in vitro*. Previously we had found the FRB domain of mTOR to bind specifically to PA-containing vesicle *in vitro*, and not vesicles of other lipid compositions including PC, phosphatidylethanol, phosphatidylserine and various phosphatidylinositides (Fang, Vilella-Bach et al. 2001). Kinase assays were performed with immunoprecipitated endogenous mTORC1 and bacterially purified GST-S6K1 as a substrate. Vesicles containing 50% 1-palmitoyl-2-oleoyl-PA (PA) and 50% 1-palmitoyl-2-oleoyl-phosphatidylcholine (PC) were added to the kinase reaction, with 100% PC vesicles as a negative control. As shown in Figure II. 2A, PA stimulated the *in vitro* kinase activity of mTORC1 while PC had no effect. Most likely owing to a narrow dynamic range of the *in vitro* assay, the effects of PA vesicles were similar at 100 μM and 200 μM (Fig. II. 2A), and mild at 20-50 μM (data not shown). The kinase activity of mTORC2, assayed with Akt as a substrate, was unaffected by PA vesicles at the same concentrations (Fig. II. 2B). The degrees of S6K1 and Akt phosphorylation were measured by densitometry to quantify the kinase activities (Fig. II. 2A and B, lower panels). These data demonstrate that PA selectively activates mTORC1 kinase *in vitro*.

II. 3. 2. PA disrupts FKBP38-mTOR interaction

To probe into the mechanism by which PA activates mTORC1 kinase, we considered the role of FKBP38 as an endogenous inhibitor of mTORC1 (Bai, Ma et

al. 2007). Because FKBP38 binds mTOR through a region that overlaps with the PA-binding FRB domain (Fang, Vilella-Bach et al. 2001; Bai, Ma et al. 2007), it appeared plausible that PA could compete with FKBP38 for mTOR binding as a mechanism of activating mTORC1. However, although several groups independently demonstrated a role of FKBP38 as a negative regulator of mTORC1 (Bai, Ma et al. 2007; Dunlop, Dodd et al. 2009; Peng, Liang et al. 2010), others challenged this conclusion (Maehama, Tanaka et al. 2008; Wang, Fonseca et al. 2008). Therefore, we deemed it necessary to re-examine the role of FKBP38 in mTORC1 signaling in the Chen laboratory. We found that overexpression of FKBP38 in HEK293 cells inhibited serum-stimulated phosphorylation of both S6K1 and 4EBP1 (Fig. II. 3A), whereas knockdown of endogenous FKBP38 enhanced the phosphorylation of those mTORC1 targets (Fig. II. 3B).

To test the hypothesis that PA competes with FKBP38 for mTOR binding, we first performed *in vitro* binding assays with bacterially expressed and purified mTOR fragment (a.a. 1967-2191; designated mTOR-225) and GST-FKBP38. The specific interaction between mTOR-225 and FKBP38 (Bai, Ma et al. 2007) was confirmed by GST pull-down assays (Fig. II. 4A). Importantly, pre-incubation with PA vesicles, but not PC vesicles, disrupted the interaction between GST-FKBP38 and mTOR-225 in a dose-dependent manner (Fig. II. 4B). Thus, a competition between PA and FKBP38 for binding to the mTOR fragment is evident *in vitro*. It is not feasible to mimic physiological concentrations in the *in vitro* vesicle binding assays, as local concentrations of PA in a cell are not known (but could conceivably be very high).

We also confirmed the interaction between FKBP38 and full-length mTOR by co-IP of epitope-tagged FKBP38 and mTOR (Fig. II. 4C), the latter expressed at a level comparable to endogenous mTOR (data not shown). Moreover, the FKBP38-mTOR interaction was disrupted when cells were exposed to C8-PA (Fig. II. 4C). PLD1 is responsible for the production of PA upstream of mTORC1 (Fang, Park et al. 2003; Sun and Chen 2008). When PLD1 was knocked down, accompanied by diminished S6K1 phosphorylation as expected, an increased amount of mTOR was associated with FKBP38 (Fig. II. 4D). Collectively, these observations strongly suggest that the FKBP38-mTOR interaction is disrupted by PLD1 signaling and PA.

II. 3. 3. PA antagonizes the inhibitory effect of FKBP38 on mTORC1 kinase activity and signaling

Next we asked whether the PA/FKBP38 competition for mTOR binding would manifest into an antagonistic relationship on the regulation of mTORC1 kinase activity. Purified FKBP38 inhibited the *in vitro* kinase activity of mTORC1 in a dose-dependent manner (Fig. II. 5A), consistent with previous reports (Bai, Ma et al. 2007; Dunlop, Dodd et al. 2009). FKBP12 added at the same concentrations did not have any effect (Fig. II. 5A), confirming the specificity of FKBP38 inhibition of mTORC1. Significantly, the presence of PA vesicles, but not PC vesicles, in the reaction rescued kinase activity from FKBP38 inhibition (Fig. II. 5B), suggesting that PA directly antagonizes the inhibitory effect of FKBP38 *in vitro*.

We also examined the relationship between PA and FKBP38 in the context of mTORC1 signaling in cells. As shown in Figure II. 6A, C8-PA stimulation of S6K1 phosphorylation in the absence of any mitogen was inhibited by FKBP38 overexpression. On the other hand, inhibition of serum-activation of S6K1 by overexpressed FKBP38 was reversed by exogenous PA (Fig. II. 6B). We did not observe a reversal of FKBP38 inhibition of mTORC1 signaling with increasing C8-PA concentrations in the absence of any other mitogen (data not shown), possibly due to limited delivery efficiency of exogenous PA. It is also not feasible to estimate or mimic physiological concentrations of PA, as endogenous PA may be highly localized. Nevertheless, our data taken together are fully consistent with the model that PA activates mTORC1 by antagonizing FKBP38 both *in vitro* and in cells.

II. 3. 4. PA is also an allosteric activator of mTORC1 kinase

If removing FKBP38 were the sole mechanism for PA activation of mTORC1, one would expect that, in the absence of FKBP38, PA would not further stimulate mTORC1. To probe into this issue, we knocked down FKBP38. As shown in Figure II. 7A, the level of endogenous FKBP38 was drastically reduced by lentivirus-delivered shRNA, which was accompanied by modestly increased S6K1 and 4EBP1

phosphorylation in serum-starved cells. Interestingly, exogenous C8-PA further stimulated mTORC1 signaling despite the FKBP38 knockdown (Fig. II. 7A). The dramatic degree of stimulation is unlikely to be explained by any residual FKBP38 protein after knockdown. Rather, this data strongly suggests that displacement of FKBP38 alone is insufficient for PA activation of mTORC1 signaling. Nevertheless, this does not contradict the necessity of FKBP38 displacement by PA for the activation.

To assess the role of endogenous PA, we knocked down PLD1. If the predominant role of PA were to remove FKBP38, we would expect that, in the absence of FKBP38, PLD1 would no longer be essential for mTORC1 signaling. However, we found that PLD1 knockdown abolished the ability of FKBP38 knockdown to induce mTORC1 signaling (Fig. II. 7B, compare lane 2 and lane 4). This is consistent with the observation in Figure II. 7A, suggesting that PA is required for mTORC1 activation in addition to removing FKBP38. PLD1 knockdown alone did not have an obvious effect on the *basal* activity of mTORC1 (Fig. II. 7B), as expected (Fang, Park et al. 2003). It was noted that FKBP38 knockdown was less efficient, and the effect on mTORC1 signaling less pronounced, when the cells were transduced by both FKBP38 and PLD1 shRNA lentiviruses (compare Fig. II. 7A and Fig. II. 7B), likely because selection of cells infected by two types of viruses relied on the same drug (puromycin). Nevertheless, this FKBP38 reduction led to reproducible mTORC1 activation that was eliminated by PLD1 knockdown, as clearly shown by the quantitative measurements of S6K1 and 4E-BP1 phosphorylation (Fig. II. 7C).

To further validate the observations above, we carried out in vitro kinase assays with mTORC1 isolated from FKBP38 knockdown cells. As shown in Figure II. 7D, PA vesicles stimulated the kinase activity of FKBP38-deficient mTORC1, supporting the notion that PA has a positive role in the absence of FKBP38. Of note, the immunoprecipitated mTORC1 activity was indistinguishable between FKBP38 knockdown and control cells both in the presence and absence of added PA vesicles (Fig. II. 7D), suggesting that even without knockdown the amount of FKBP38 associated with the mTORC1 complex under our experimental conditions was most likely negligible.

Therefore, in addition to displacing FKBP38, PA also activates mTORC1 through another mechanism. The other known inhibitors of mTORC1 are PRAS40 and DEPTOR, both of which would be absent in the mTORC1 immunoprecipitate here as it was subjected to high salt (500 mM NaCl) wash that removed these two proteins ((Sancak, Thoreen et al. 2007; Peterson, Laplante et al. 2009) and data not shown). The *in vitro* assay system also made it virtually impossible for PA to recruit an activator. Hence, collectively the current observations point to the simplest model that the physical interaction between PA and mTOR exerts an allosteric effect that is required for the kinase activity of mTORC1 after displacement of FKBP38, although the involvement of a third factor (an unknown inhibitor) cannot be formally excluded.

II. 4. Discussion

Our studies have revealed direct activation of the mTORC1 kinase by phosphatidic acid and identified a dual mechanism by which PA activates mTORC1: displacing FKBP38 and exerting an allosteric effect on the catalytic activity (Fig. II. 8). These findings provide answers to the long-standing question of how PA activates mTOR signaling. The new mechanistic insights may facilitate the exploration of the tremendous therapeutic potential of this signaling network.

It is noteworthy that we had previously failed to observe an effect of PA on mTOR catalytic activity (Fang, Vilella-Bach et al. 2001; Chen and Fang 2002). One plausible explanation for the discrepancy may come from the conditions of isolating mTOR for *in vitro* kinase assays. In previous studies we had used Triton X-100 as the detergent in cell lysis prior to mTOR immunoprecipitation, whereas in the current study CHAPS was used and mTORC1 was isolated by raptor pull-down. As reported by Kim et al. (Kim, Sarbassov et al. 2002), the raptor-mTOR interaction would be disrupted by Triton. The loss of raptor may have prevented PA activation of mTORC1.

We had previously reported a mutation in mTOR (R2109A) that had dampened FRB binding to PA *in vitro* and mTOR signaling in cells by ~50% (Fang, Vilella-Bach et al. 2001). This mTOR mutant, however, did not display differential sensitivity to PA compared to wt mTOR in FKBP38 binding (data not shown). It is

possible that limitations in the vesicle binding assay and cellular delivery of C8-PA render insufficient dynamic ranges to discern the partial defect of the R2109A mutant. With the solution structure of the FRB-PA complex (Veverka, Crabbe et al. 2008) as a guide, identification of additional mutations in FRB that drastically disrupt the PA-FRB interaction may be possible. Such mutants would be desirable for future investigations of PA in the regulation of mTORC1.

Although our present data suggest that PA selectively activates mTORC1 and not mTORC2 (Figs. 1 and 2), it has been proposed by Foster and colleagues (Toschi, Lee et al. 2009) that PA is required for the assembly of both mTORC1 and mTORC2. These two conclusions need not be mutually exclusive. In the present studies, we examined PA for its acute effect in stimulating cells and in directly activating mTOR kinase. On the other hand, the effects that Toschi et al. (Toschi, Lee et al. 2009) have observed may stem from a basal level of PA in maintaining the integrity of mTOR complexes prior to activation of the kinases. It will be interesting in future investigations to determine whether the activation of mTORC1 and assembly of mTOR complexes share the same mode of PA-mTOR interaction or represent two molecularly distinct mechanisms of PA action.

The recent controversy surrounding FKBP38's role in regulating mTORC1 prompted us to re-examine this reported endogenous inhibitor, and our results described here clearly support the model that FKBP38 binds and inhibits mTORC1. We and others (Dunlop, Dodd et al. 2009) observed that recombinant FKBP38 inhibited mTORC1 signaling in cells only when it was highly overexpressed, which may explain the absence of FKBP38 effect in similar experiments performed by some groups (Maehama, Tanaka et al. 2008; Wang, Fonseca et al. 2008). The requirement of high levels of recombinant FKBP38 to exert an inhibitory effect on mTORC1 does not necessarily mean the FKBP38 mechanism is an inefficient one; one could envision that endogenous FKBP38 might be highly localized for its mTORC1-regulating function and/or that high concentrations of FKBP38 might be necessary to set a threshold to ensure signaling fidelity. *In vitro*, the inhibitory effect of recombinant FKBP38 on mTORC1 kinase activity was easily detected (Fig. II. 5A), most likely owing to the condition of mTORC1 isolation that led to the dissociation

of endogenous FKBP38. The reported ability of Rheb to bind FKBP38 and displace it from mTOR (Bai, Ma et al. 2007) has also been disputed (Wang, Fonseca et al. 2008; Uhlenbrock, Weiwad et al. 2009). We have not examined the role of Rheb in our studies, as our proposed model of PA action is independent of Rheb-FKBP38 interaction, although it does not exclude the involvement of Rheb.

Displacement of FKBP38 appears to be a simple and effective way for PA to activate the mTOR kinase, and yet, to the best of our knowledge, this is the first example of PA regulating an effector through removing an inhibitor. mTOR also joins a small roster of PA effectors, the enzymatic activities of which are allosterically regulated by PA binding (Stace and Ktistakis 2006). The only other protein kinase that has been reported to be activated by PA through a possible allosteric effect is Fer, a tyrosine kinase that regulates actin polymerization in cell migration (Itoh, Hasegawa et al. 2009). Other than the fact that PA binds at a site N-terminal to the kinase domain, mTOR and Fer do not share any common feature in their PA binding domains. Since PA stimulates mTORC1 activity on an autophosphorylation site but not mTORC2 activity on the same site (Fig. II. 1), the allosteric effect of PA is unlikely to simply confer catalytic activation or substrate specificity of the kinase domain; other components in mTORC1, raptor in particular, most likely play an integral role. Future structural studies will be needed to shed light on the exact mode of allosteric regulation by PA of mTOR, or of any other kinase.

II. 5. Figures

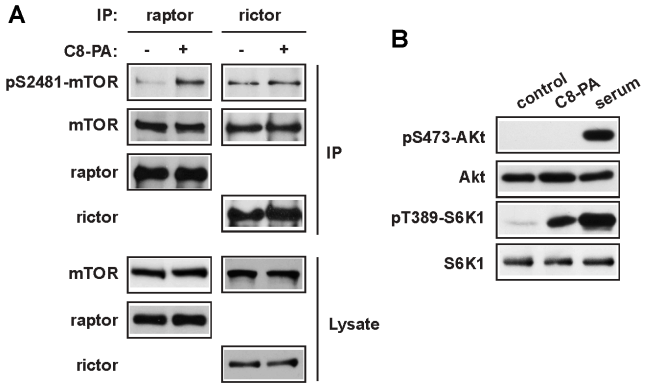

Figure II. 1. PA activates mTORC1 autophosphorylation in cells. (A) HEK293 cells were serum-starved overnight, and then stimulated with 300 μM C8-PA for 30 min. mTORC1 and mTORC2 were immunoprecipitated with anti-raptor and anti-rictor antibodies, respectively, followed by Western blotting. (B) Cells were serum-starved overnight, and then stimulated with 300 μM C8-PA or 20% serum for 30 min followed by cell lysis and Western blotting. (C) Cells were transduced with lentivirus expressing raptor shRNA, serum-starved, and then stimulated with 300 μM PA or 20% serum for 30 min, followed by Western analysis of the cell lysates. Each experiment was performed at least 3 times, and the representative blots are shown.

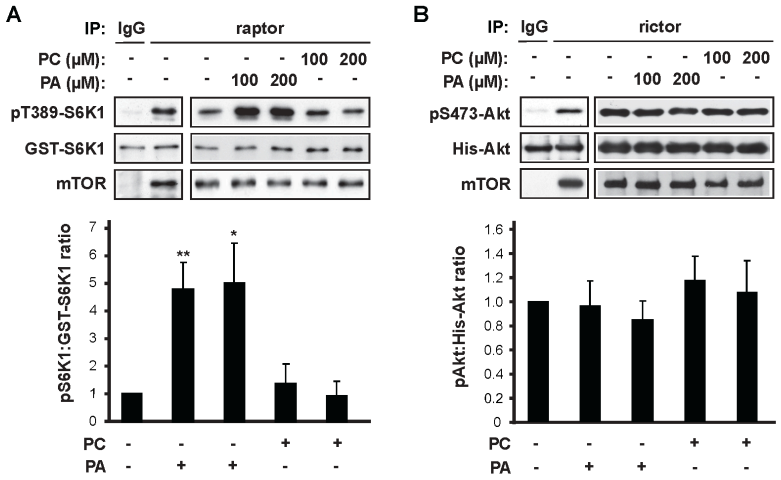

Figure II. 2. PA stimulates mTORC1 kinase activity *in vitro*. (A) Raptor was immunoprecipitated from HEK293 cells and subjected to *in vitro* kinase assays using GST-S6K1 as the substrate. PA or PC vesicles were added at 100 μM and 200 μM prior to kinase assays in the samples indicated. The pS6K1 and GST-S6K1 blots with raptor IP were quantified by densitometry, and the relative ratios of pS6K1 versus GST-S6K1 were calculated with control (no vesicles) designated as 1. (B) Rictor was immunoprecipitated from HEK293 cells and subjected to *in vitro* kinase assays using His-Akt as the substrate. The pAkt and His-Akt blots were quantified as described in (A). The data shown in the graphs are mean ± standard deviation of three independent experiments. Each data point is compared to the control by one-sample *t* test and significantly different data points are indicated: **P*<0.05, ***P*<0.01.

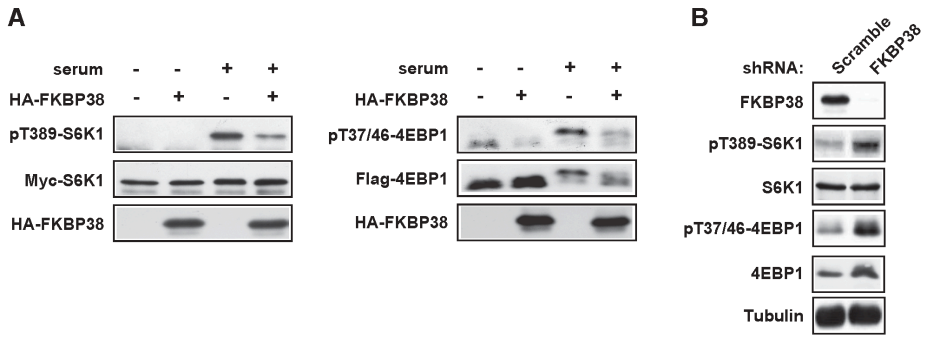

Figure II. 3. FKBP38 is an endogenous inhibitor of mTORC1 signaling. (A) HEK293 cells were transfected with Myc-S6K1 (left panels) or Flag-4EBP1 (right panels) with or without HA-FKBP38, serum starved, and then stimulated with 10% serum for 30 min, followed by Western analysis of cell lysates. Note that the phosphorylation state of 4EBP1 was reflected by band-shift on Flag-4EBP1 blot in addition to phospho-specific antibody recognition. (B) Cells were transduced with lentivirus expressing FKBP38 shRNA or a hairpin of scrambled sequence as control, serum-starved, and then lysed for Western analysis.

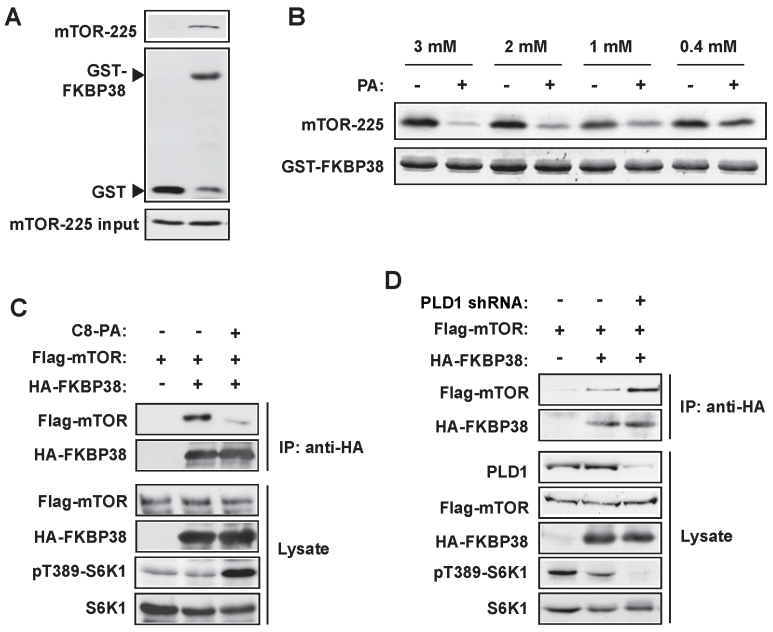

Figure II. 4. PA disrupts FKBP38-mTOR interaction. (A) GST pull-down assays were performed with purified mTOR-225 and GST-FKBP38, with GST as a negative control. Western blots are shown. Note that some free GST was present in the GST-FKBP38 protein preparation. (B) GST-FKBP38 was pre-incubated with varying concentrations of PA (+) or PC (-) vesicles prior to addition of purified mTOR-255 and subsequent pull-down assays. (C) HEK293 cells were co-transfected with HA-FKBP38 and Flag-mTOR, followed by serum-starvation and stimulation with 300 μM C8-PA for 30 min. HA-FKBP38 was immunoprecipitated, followed by Western analysis. (D) Cells were transduced with lentivirus expressing PLD1 shRNA, and then co-transfected with HA-FKBP38 and Flag-mTOR, followed by IP of HA-FKBP38 and subsequent Western analysis. Each experiment was performed at least 3 times, and the representative blots are shown.

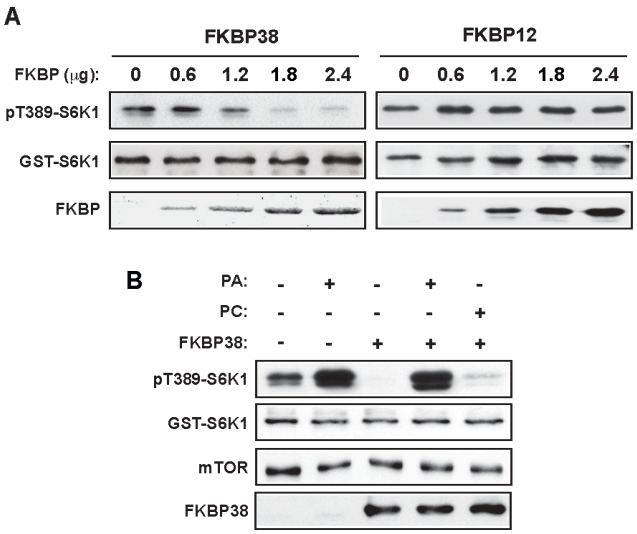

Figure II. 5. PA antagonizes FKBP38 inhibition of mTORC1 kinase activity *in vitro*. mTORC1 was immunoprecipitated with anti-raptor antibody from HEK293 cells and subjected to *in vitro* kinase assays using GST-S6K1 as a substrate. (A) FKBP38 and FKBP12 were added at increasing amounts as indicated prior to kinase assays. (B) PA or PC vesicles at 100 μM were added together with FKBP38 prior to kinase assays. Each experiment was performed at least 3 times, and the representative Western blots (or Coomassie Blue stain for FKBP38 in A) are shown.

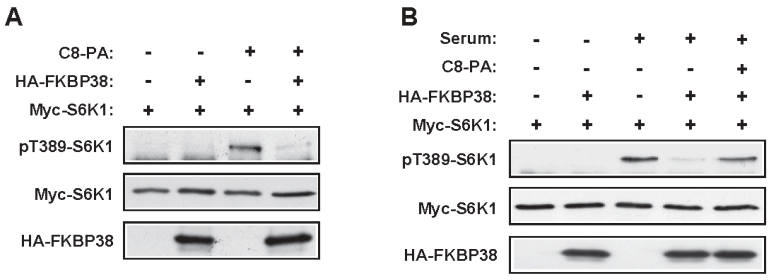

Figure II. 6. PA and FKBP38 antagonize each other in the regulation of mTORC1 signaling in cells. (A) HEK293 cells were co-transfected with Myc-S6K1 and HA-FKBP38, serum-starved, and then stimulated with 300 μM C8-PA, followed by Western analysis of cell lysates. (B) Cells were transfected and starved as in (A), and stimulated with 10% serum with or without C8-PA, followed by Western analysis of cell lysates. Each experiment was performed at least 3 times, and the representative blots are shown.

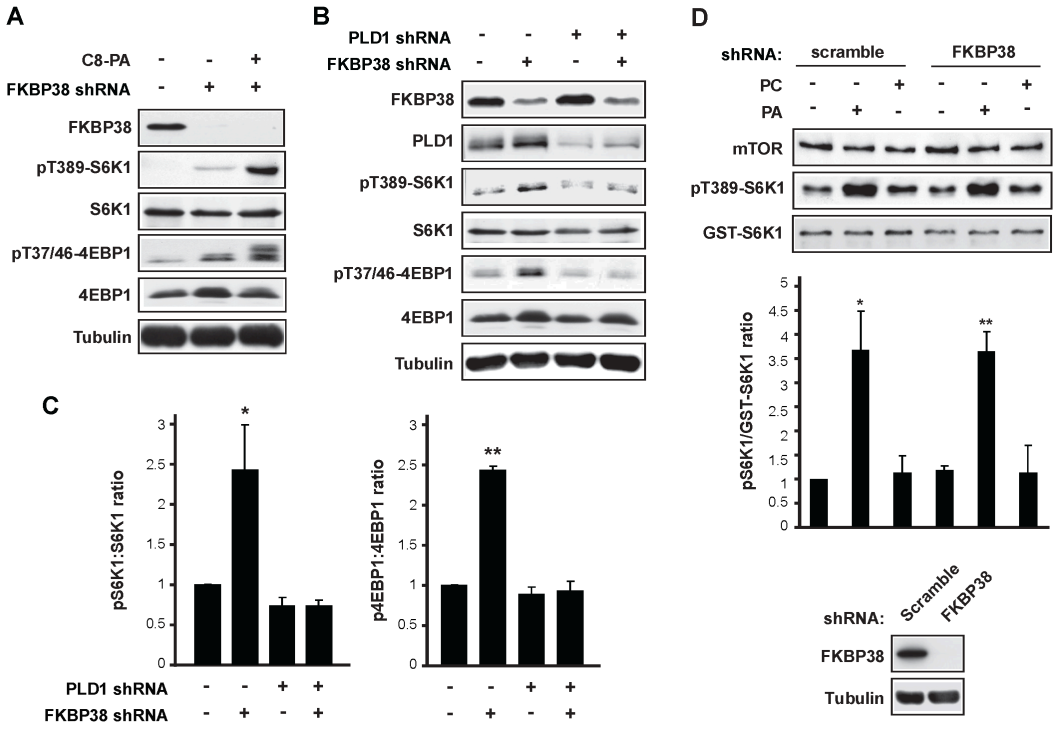

Figure II. 7. PA activates mTORC1 in the absence of FKBP38. (A) HEK293 cells were transduced with lentivirus expressing FKBP38 shRNA, serum-starved, and then stimulated with 300 μM C8-PA, followed by Western analysis of lysates. (B) Cells were transduced with lentiviruses expressing shRNA for FKBP38, or PLD1, or both, followed by serum starvation and then Western analysis. (C) The Western results represented by blots in (B) were quantified by densitometry, and the relative ratios of pS6K1 versus S6K1 and p4EBP1 versus 4EBP1 were calculated with control (no shRNA) designated as 1. (D) mTORC1 was immunoprecipitated by anti-raptor from cells expressing FKBP38 shRNA or a hairpin of scrambled sequence as control, and subjected to *in vitro* kinase assays with or without PA or PC vesicles at 100 μM. The Western results were quantified by densitometry, and the relative ratios of pS6K1 versus GST-S6K1 were calculated with control (no vesicles) designated as 1. The data shown are mean ± standard deviation or representative blots of three independent experiments. Each data point is compared to the control by one-sample *t* test and significantly different data points are indicated: **P*<0.05, ***P*<0.01.

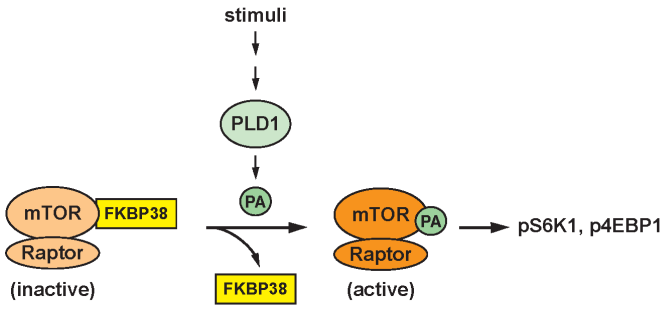

Figure II. 8. A proposed model for PA activation of mTORC1. FKBP38 binds and inhibits mTORC1. Upon stimulation of PLD1, PA is produced, which binds mTOR at FKBP38-binding site and displaces FKBP38. The physical interaction of PA with mTOR also allosterically activates the kinase.

II. 6. References

Avruch, J., X. Long, et al. (2009). "Amino acid regulation of TOR complex 1." Am J Physiol Endocrinol Metab. 296(4): E592-602. Epub 2008 Sep 2002.

Bai, X., D. Ma, et al. (2007). "Rheb activates mTOR by antagonizing its endogenous inhibitor, FKBP38." Science 318(5852): 977-980.

Billon-Denis, E., Z. Tanfin, et al. (2008). "Role of lysophosphatidic acid in the regulation of uterine leiomyoma cell proliferation by phospholipase D and autotaxin." J Lipid Res. 49(2): 295-307. Epub 2007 Nov 2016.

Chen, J. and Y. Fang (2002). "A novel pathway regulating the mammalian target of rapamycin (mTOR) signaling." Biochem Pharmacol 64(7): 1071.

Dunlop, E. A., K. M. Dodd, et al. (2009). "Mammalian target of rapamycin complex 1-mediated phosphorylation of eukaryotic initiation factor 4E-binding protein 1 requires multiple protein-protein interactions for substrate recognition." Cell Signal. 21(7): 1073-1084. Epub 2009 Mar 1079.

Facchinetti, V., W. Ouyang, et al. (2008). "The mammalian target of rapamycin complex 2 controls folding and stability of Akt and protein kinase C." Embo J 19: 19.

Fang, Y., I. H. Park, et al. (2003). "PLD1 regulates mTOR signaling and mediates Cdc42 activation of S6K1." Curr Biol 13(23): 2037-2044.

Fang, Y., M. Vilella-Bach, et al. (2001). "Phosphatidic acid-mediated mitogenic activation of mTOR signaling." Science 294(5548): 1942-1945.

Fingar, D. C. and J. Blenis (2004). "Target of rapamycin (TOR): an integrator of nutrient and growth factor signals and coordinator of cell growth and cell cycle progression." Oncogene 23(18): 3151-3171.

Fischer, D. J., N. Nusser, et al. (2001). "Short-chain phosphatidates are subtype-selective antagonists of lysophosphatidic acid receptors." Mol Pharmacol. 60(4): 776-784.

Foster, D. A. (2007). "Regulation of mTOR by phosphatidic acid?" Cancer Res. 67(1): 1-4.

Frohman, M. A., T. C. Sung, et al. (1999). "Mammalian phospholipase D structure and regulation." Biochim Biophys Acta 1439(2): 175-186.

Guertin, D. A. and D. M. Sabatini (2007). "Defining the role of mTOR in cancer." Cancer Cell. 12(1): 9-22.

Ikenoue, T., S. Hong, et al. (2009). "Monitoring mammalian target of rapamycin (mTOR) activity." Methods Enzymol. 452: 165-180.

Ikenoue, T., K. Inoki, et al. (2008). "Essential function of TORC2 in PKC and Akt turn motif phosphorylation, maturation and signalling." Embo J 19: 19.

Itoh, T., J. Hasegawa, et al. (2009). "The tyrosine kinase Fer is a downstream target of the PLD-PA pathway that regulates cell migration." Sci Signal. 2(87): ra52.

Kim, D. H., D. D. Sarbassov, et al. (2002). "mTOR interacts with raptor to form a nutrient-sensitive complex that signals to the cell growth machinery." Cell 110(2): 163-175.

Kim, J. E. and J. Chen (2000). "Cytoplasmic-nuclear shuttling of FKBP12-rapamycin-associated protein is involved in rapamycin-sensitive signaling and translation initiation." Proc Natl Acad Sci U S A 97(26): 14340-14345.

Li, Y., M. N. Corradetti, et al. (2004). "TSC2: filling the GAP in the mTOR signaling pathway." Trends Biochem Sci 29(1): 32-38.

Long, X., Y. Lin, et al. (2005). "Rheb Binds and Regulates the mTOR Kinase." Curr Biol 15(8): 702-713.

Ma, X. M. and J. Blenis (2009). "Molecular mechanisms of mTOR-mediated translational control." Nature Reviews Molecular Cell Biology 10(5): 307-318.

Maehama, T., M. Tanaka, et al. (2008). "RalA functions as an indispensable signal mediator for the nutrient-sensing system." J Biol Chem. 283(50): 35053-35059. Epub 32008 Oct 35023.

Manning, B. D. and L. C. Cantley (2003). "Rheb fills a GAP between TSC and TOR." Trends Biochem Sci 28(11): 573-576.

Martin, D. E. and M. N. Hall (2005). "The expanding TOR signaling network." Curr Opin Cell Biol. 17(2): 158-166.

Peng, L., D. Liang, et al. (2010). "Hepatitis C virus NS5A activates the mammalian target of rapamycin (mTOR) pathway, contributing to cell survival by disrupting the interaction between FK506-binding protein 38 (FKBP38) and mTOR." J Biol Chem 285(27): 20870-20881. Epub 22010 May 20873.

Peterson, T. R., M. Laplante, et al. (2009). "DEPTOR Is an mTOR Inhibitor Frequently Overexpressed in Multiple Myeloma Cells and Required for Their Survival." Cell 13: 13.

Sancak, Y., C. C. Thoreen, et al. (2007). "PRAS40 is an insulin-regulated inhibitor of the mTORC1 protein kinase." Mol Cell. 25(6): 903-915.

Sarbassov, D. D., S. M. Ali, et al. (2005). "Growing roles for the mTOR pathway." Curr Opin Cell Biol 17(6): 596-603.

Soliman, G. A., H. A. Acosta-Jaquez, et al. (2009). "mTOR S2481 autophosphorylation monitors mTORC-specific catalytic activity and clarifies rapamycin mechanism of action." J Biol Chem 18: 18.

Stace, C. L. and N. T. Ktistakis (2006). "Phosphatidic acid- and phosphatidylserine-binding proteins." Biochim Biophys Acta. 1761(8): 913-926. Epub 2006 Apr 2003.

Sun, Y. and J. Chen (2008). "mTOR signaling: PLD takes center stage." Cell Cycle. 7(20): 3118-3123. Epub 2008 Oct 3127.

Sun, Y., Y. Fang, et al. (2008). "Phospholipase D1 is an effector of Rheb in the mTOR pathway." Proc Natl Acad Sci U S A 105: 8286.

Toschi, A., E. Lee, et al. (2009). "Regulation of mTORC1 and mTORC2 Complex Assembly by Phosphatidic Acid - a Competition with Rapamycin." Mol Cell Biol 29(6): 1411-1420.

Uhlenbrock, K., M. Weiwad, et al. (2009). "Reassessment of the role of FKBP38 in the Rheb/mTORC1 pathway." FEBS Lett. 583(6): 965-970. Epub 2009 Feb 2015.

van Corven, E. J., A. van Rijswijk, et al. (1992). "Mitogenic action of lysophosphatidic acid and phosphatidic acid on fibroblasts. Dependence on acyl-chain length and inhibition by suramin." Biochem J. 281(Pt 1): 163-169.

Veverka, V., T. Crabbe, et al. (2008). "Structural characterization of the interaction of mTOR with phosphatidic acid and a novel class of inhibitor: compelling evidence for a central role of the FRB domain in small molecule-mediated regulation of mTOR." Oncogene. 27(5): 585-595. Epub 2007 Aug 2006.

Vilella-Bach, M., P. Nuzzi, et al. (1999). "The FKBP12-rapamycin-binding domain is required for FKBP12-rapamycin- associated protein kinase activity and G1 progression." J Biol Chem 274(7): 4266-4272.

Wang, X., B. D. Fonseca, et al. (2008). "Re-evaluating the roles of proposed modulators of mammalian target of rapamycin complex 1 (mTORC1) signaling." J Biol Chem 1: 1.

Yoon, M. S. and J. Chen (2008). "PLD regulates myoblast differentiation through the mTOR-IGF2 pathway." J Cell Sci. 121(Pt 3): 282-289.

CHAPTER III

Stoichiometry and assembly of mTOR complexes revealed by single-molecule pulldown[1]

III. 1. Introduction

The mammalian target of rapamycin (mTOR) is a master regulator of crucial cellular and developmental processes. As a serine/threonine protein kinase belonging to the phosphatidylinositol-3-kinase (PI3K)-related kinase family, mTOR integrates the sensing of nutrients, growth factors, oxygen, energy, and different types of stress to regulate a myriad of biological processes such as cell growth, proliferation, differentiation, and metabolism (Laplante and Sabatini 2012). mTOR functions as part of at least two biochemically and functionally distinct complexes—mTORC1 and mTORC2 (Laplante and Sabatini 2009). mTORC1, better characterized of the two complexes, is the rapamycin-sensitive complex, composed of the proteins raptor and mLST8, and it is regulated by the inhibitory proteins PRAS40 and DEPTOR (Laplante and Sabatini 2009; Peterson, Laplante et al. 2009). mTORC1 is activated by nutrients (such as amino acids), growth factors, and cellular energy among other stimuli (Laplante and Sabatini 2009; Laplante and Sabatini 2012). mTORC2 contains rictor, mLST8, and mSin, as well as the negative regulator DEPTOR (Laplante and Sabatini 2009; Peterson, Laplante et al. 2009).

PI3K-related kinases (PIKKs) such as ataxia telangiectasia mutated (ATM), ATM and Rad3-related protein (ATR), and DNA-dependent protein kinase (DNA-PK) are known to oligomerize (Bakkenist and Kastan 2003; Ball and Cortez 2005; Spagnolo, Rivera-Calzada et al. 2006). Biochemical and genetic analyses have identified self-association of mTOR and its orthologs in yeast and *Drosophila* (Wullschleger, Loewith et al. 2005; Takahara, Hara et al. 2006; Wang, Rhodes et al. 2006; Zhang, Billington et al. 2006). A cryoelectron microscopy (cryo-EM) study revealed that mTORC1 self-associates into a dimeric structure (Yip, Murata et al. 2010). Oligomerization of

---

[1]This chapter appeared in its entirety in Proceedings of the National Academy of Sciences 111 (2014), pages 17833-38 by Ankur jain*, **Edwin Arauz***, Vasudha Aggarwal, Nikita Ikon, Jie Chen, and Taekjip Ha. (*Co-first authors)

mTORC1 has been reported to be sensitive to nutrient status based on biochemical analyses of recombinant proteins (Takahara, Hara et al. 2006; Kim, Hoffman et al. 2013). Consensus is lacking on the oligomeric state of mTORC2, which has been proposed to be monomeric, dimeric, or multimeric (Wullschleger, Loewith et al. 2005; Frias, Thoreen et al. 2006; Takahara, Hara et al. 2006; Tao, Barker et al. 2010). High-resolution structural analysis of mTORC2 has not been possible thus far, likely owing to its large size and multiplicity of interaction partners.

Ensemble biochemical methods have inherent limitations in analyzing multicomponent heterogeneous protein assemblies. These methods do not directly reveal the stoichiometry of interaction and offer low-resolution estimates of the sizes of protein complexes. Additionally, the lengthy procedures often associated with biochemical characterization may lead to loss or alteration of physiological protein complexes. We recently reported a single-molecule pulldown (SiMPull) technology that combines the principles of conventional pulldown assays with single-molecule fluorescence microscopy (Jain, Liu et al. 2011). In SiMPull, protein complexes are pulled down from freshly lysed cells directly onto chambers for single-molecule fluorescence microscopy. When proteins are stoichiometrically labeled for example using fluorescent protein tags, SiMPull can reveal the stoichiometry of the protein complexes via single-molecule fluorescence photobleaching step analysis (Jain, Liu et al. 2011).

We have used SiMPull to investigate the oligomeric assembly of mTORCs. Upon validating our approach by demonstrating dimeric assembly of mTORC1, we find that mTORC2 is also dimeric and contains two molecules of mTOR and rictor per complex. Individual mTORC components are predominantly monomeric, but under physiological conditions there is no evidence of monomeric interaction between mTOR and raptor or rictor. Multicolor imaging of individual complexes revealed that although the two complexes are predominantly distinct, small fractions of mTORC1 and mTORC2 components coexist in the same complex. Physiological perturbations that abrogate mTOR signaling had no effect on the stoichiometry of mTOR complexes, indicating that inhibition of mTOR signaling can be achieved without requiring disassembly of mTOR complexes or changing their oligomeric state. On the other hand, treatment with rapamycin led to transient mTOR–raptor complexes containing one mTOR before

complete disassembly of the interaction, whereas mTORC2 stoichiometry was unaffected.

III. 2. Materials and methods

III. 2. 1. Antibodies and other reagents

All antibodies used were obtained from commercial sources as follows: anti-Flag and biotinylated anti-Flag M2 from Sigma-Aldrich; anti-Myc (9E10.2) and anti-HA (16B12) from Covance or Abcam (ab26228); anti-GFP from Roche and Rockland Immunochemicals; anti-DEPTOR from Novus Biologicals; and rictor, raptor, mLST8, and mTOR antibodies from Cell Signaling Technology. Raptor and rictor antibodies for immunoprecipitation were from Bethyl Laboratories, and mTOR antibody (N-19) for immunoprecipitation was from Santa Cruz Biotechnology. All secondary antibodies for Western blotting and SiMPull were from Jackson ImunoResearch Labs. Rapamycin was from Calbiochem, EZview Red anti-HA beads and anti-Flag M2 beads from Sigma, NeutrAvidin from ThermoFisher, dithiobis(succcinimidyl propionate) (DSP) was from Pierce, and BSA from New England Biolabs.

III. 2. 2. Plasmids

Plasmids pRK5–HA–raptor (Addgene plasmid 8513) (Kim, Sarbassov et al. 2002), pRK5–HA–mLST8 (Addgene plasmid 1865) (2) and pRK5– myc–rictor (Addgene plasmid 1860) (Sarbassov, Ali et al. 2004) were obtained from Addgene. pCDNA–Flag–mTOR has been described previously (Vilella-Bach, Nuzzi et al. 1999). YFP–raptor was constructed by inserting monomeric eYFP (A206K) cDNA into pRK5–HA–raptor between the HA tag and raptor sequence. YFP–rictor was constructed by replacing the raptor cDNA in YFP–raptor with rictor cDNA from pRK5–myc– rictor. pCDNA–mSin1–HA was constructed by cutting mSin1.1– HA from pMSCV–mSin1.1–HA (Addgene plasmid 12582) (Frias, Thoreen et al. 2006) using BglII and EcoRI, and inserted into pCDNA3 cut with BamHI and EcoRI. YFP–mTOR was created by inserting mTOR cDNA into the peYFP–C1 plasmid (Clontech). YFP–PRAS40 was constructed by replacing the raptor cDNA in YFP–raptor with PRAS40 cDNA from pRK5–HA–PRAS40 (Addgene plasmid 15481) (Vander Haar, Lee et al. 2007). YFP–DEPTOR was

constructed by replacing the raptor cDNA in YFP–raptor with DEPTOR cDNA from pRK5– Flag–DEPTOR (Addgene plasmid 21334) (Peterson, Laplante et al. 2009). mCherry–raptor was constructed by replacing YFP cDNA in YFP–raptor with mCherry cDNA from pmCherry–C1 (Clontech).

III. 2. 3. Cell culture and transfection

HEK293 cells were grown in DMEM containing 10% (vol/vol) FBS at 37 °C with 5% (vol/vol) CO_2. All transfection experiments were performed when cells were 60–70% confluent in 6-cm plates. Transfection of plasmids was carried out using PolyFect (Qiagen) following the manufacturer's recommendations. One day after transfection, cells (3.5×10^6) were lysed in 500 μL of ice-cold lysis buffer (40 mM Hepes, pH 7.5, 120 mM NaCl, 10 mM pyrophosphate, 10 mM β-glycerophosphate, 2 mM EDTA, 1× protease inhibitor mixture, 0.3% CHAPS; designated "CHAPS buffer") and analyzed by various assays. To establish the YFP–mTOR stable cell line, HEK293 cells were transfected with the YFP–mTOR plasmid, plated at low density for single-clone colonies to form, and selected in 500 μg/mL of G418. A cell clone expressing YFP–mTOR at a level comparable to that of endogenous mTOR was chosen. Endogenous mTOR was then knocked down by lentivirus-delivered shRNA (Addgene plasmid 1856) (Sarbassov, Guertin et al. 2005) as previously described (Yoon, Du et al. 2011), and selected by 1 μg/mL of puromycin. For insulin stimulation, cells were cultured in serum-free medium for 24 h, followed by treatment with 100 nM insulin for 30 min. For glucose/glutamine, amino acids, or leucine stimulation, cells were cultured in glucose/ glutamine-free medium for 12 h, amino-acid-free medium for 2 h, or leucine-free medium for 1 h, followed by restimulation with glucose/glutamine for 1 h, amino acids for 30 min, or leucine for 15 min, respectively.

III. 2. 4. Immunoprecipitation and in vitro kinase assay

Cells were rinsed once with ice-cold PBS and lysed in ice-cold CHAPS buffer. The lysates were cleared by centrifugation at 10,000 × g for 10 min, and then subjected to immunoprecipitation at 4 °C with anti-HA beads or anti-Flag M2 beads for 2 h. For GFP or mTOR immunoprecipitation, anti-GFP or anti-mTOR (N-19) antibody was incubated

with the cell lysates for 2 h, followed by incubation with protein G beads for 1 h. The beads were washed three times with lysis buffer and then boiled in 2× SDS sample buffer for 5 min. Samples were analyzed by Western blotting. mTOR kinase assays were performed as previously described (Yoon, Du et al. 2011). mTORC1 kinase assays were carried out at 30 °C for 30 min in 25 mM Hepes (pH 7.4), 50 mM KCl, 10 mM $MgCl_2$ and 250 μM ATP, with 100 ng GST–S6K1 as the substrate. mTORC2 kinase assays were carried out at 37 °C for 30 min in 25 mM Hepes (pH 7.4), 100 mM potassium acetate, 1 mM $MgCl_2$, and 500 μM ATP, with 250 ng His–Akt as the substrate.

III. 2. 5. Western blot analysis

Cells were lysed in either CHAPS buffer or a buffer containing 20 mM Tris·HCl, pH 7.5, 0.1 mM Na_3VO_4, 25 mM NaF, 25 mM glycerophosphate, 2 mM EGTA, 2 mM EDTA, 1 mM DTT, 0.5 mM phenylmethylsulfonyl fluoride, 1× protease inhibitor mixture (Sigma-Aldrich), 0.3% Triton X-100. The lysates were cleared by centrifugation at 10,000 × g, then mixed with 2× SDS sample buffer and boiled for 5 min. Proteins were resolved on SDS/PAGE and transferred onto PVDF membrane (Millipore), followed by incubation with various antibodies according to the manufacturer's recommendations. Detection of horseradish peroxidase-conjugated secondary antibodies was performed with Western Lightning Chemiluminescence Reagent Plus (Perkin-Elmer). Results were developed on X-ray films and scanned with an Epson scanner (Perfection 2400).

III. 2. 6. In-cell cross-linking

Chemical cross-linking was performed as described by Sancak et al. (9) Briefly, cells were grown in 6-cm plates and incubated with 3 mL of fresh culture media containing 1 mg/mL DSP (2.5 mM) for 10 min at 37 °C, and 5% CO2. DSP was prepared fresh as a stock solution of 250 mg/mL in DMSO. After the incubation time, DSP was quenched by adding Tris·HCl (pH 8.0) to a final concentration of 100 mM in fresh cell culture medium. After an additional 10-min incubation at 37 °C, 5% CO_2 cells were washed on ice twice with cold PBS and lysed in 500 μL of lysis buffer (with CHAPS or Triton; see below). Cell lysates were diluted 50-fold and immediately infused into chambers for SiMPull analysis.

III. 2. 7. Single-molecule imaging and spot counting

Cells (3.5×10^6) growing in 6-cm plates were lysed in ~500 μL CHAPS buffer or Triton buffer (40 mM Hepes, pH 7.5, 120 mM NaCl, 10 mM pyrophosphate, 10 mM β-glycerophosphate, 2 mM EDTA, 1× protease inhibitor mixture, 0.3% Triton) to yield a final lysate concentration of 3.5 mg/mL (Bradford assay). For cell mixing experiments, cells were scraped in CHAPS buffer, mixed at 1:1 ratio, and then incubated on ice for 15 min. Alternatively, cells were trypsinized and resuspended in PBS, mixed at 1:1 ratio, and then pelleted, followed by lysis in CHAPS buffer. Lysates were cleared by centrifugation at 10,000 × g for 10 min and diluted 20- to 100-fold (in most cases 50-fold) to obtain a surface density optimal for single-molecule analysis (~300 molecules in 2,500 μm^2 imaging area). Dilutions were made either in detergent-free lysis buffer or 20 mM Tris, pH 8.0, 50 mM NaCl; similar results were obtained in both cases. A prism-type total internal reflection fluorescence microscope was used to acquire single-molecule data. Quartz slides were passivated with 200 mg/mL methoxy polyethylene glycol (PEG) containing 2.5% (wt/wt) biotinylated PEG. YFP- and mCherry-tagged proteins were excited at 488 nm and 568 nm, respectively. Band pass filters (HQ 535/30, Chroma Technology for YFP and BL 607/36, Semrock for mCherry) were used to collect the emitted fluorescence signal. All experiments were performed at room temperature (22–25 °C) unless specified. Mean spot count per image (imaging area 2,500 μm^2) and SD were calculated from images taken from 20 or more different regions.

III. 2. 8. Photobleaching analysis and single-molecule colocalization

Analysis were performed as previously reported (Jain, Liu et al. 2011; Jain, Liu et al. 2012). Briefly, single-molecule fluorescence time traces of surface immobilized YFP-tagged proteins were manually scored for the number of bleaching steps. To avoid false colocalization, samples were immobilized at an optimal surface density (~300 molecules in 2,500 μm^2 imaging area) by adjusting the dilution factor for each lysate. The fluorescence trace of each molecule was classified as having one to four bleaching steps or was discarded if no clean bleaching steps could be identified. At least 400 molecules were evaluated for each experiment; the total number of molecules successfully scored as bleaching in one to four steps (N) is depicted in the figures. The intensity of molecules

scored as bleaching in one and two steps was plotted to verify scoring: on average we expect the fraction of molecules bleaching in two steps to be twice as bright as the molecules bleaching in one step. The intensity of discarded molecules was also plotted to ensure unbiased scoring as observed via lack of enrichment of any specific intensities. To convert the photobleaching step distribution to monomer/dimer fraction, the percentage of molecules bleaching in two steps was compared with the calibration experiment in Figure III. 1I. This conversion was performed only when >90% of the molecules bleached in one or two photobleaching steps. For single-molecule colocalization, two separate images were acquired imaging YFP or mCherry in the same region of interest. Positions of YFP and mCherry molecules were determined to half-pixel accuracy by fitting a Gaussian point spread function. Molecules lying within 1-pixel distance (pixel size, ~150 nm) were said to be colocalized. For determining false colocalization by chance, two different regions were imaged and similar analysis was performed; colocalization by chance was observed to be ~1%.

III. 2. 9. Statistical analysis

All data are presented as mean ± SD, or representative images, of at least three sets of independent experiments. Whenever necessary, statistical significance of the data was analyzed by performing one-sample or paired *t* tests.

III. 3. Results

III. 3. 1. Assay validation and mTORC1 stoichiometry

To study mTOR complexes by SiMPull, we deemed it important to establish a system where a fluorescently tagged mTOR can incorporate into endogenous complexes. To that end, we established a cell line stably expressing YFP–mTOR in which the endogenous mTOR was silenced by short hairpin RNA (Fig. III. 1*A*, henceforth called "YFP–mTOR stable cell line"). The YFP–mTOR protein associated with endogenous raptor and rictor (Fig. III. 1*A*). More importantly, the cell line faithfully recapitulated known regulations of mTOR signaling, such as insulin- and serum-stimulated phosphorylation of mTORC1 targets S6K1 and 4E-BP1, and mTORC2 target Akt, as well as amino acid dependence of S6K1 and 4E-BP1 phosphorylation (Fig. III. 1*B* and

Fig. III. 2*A*). When cell lysates from this line were applied to single-molecule imaging chambers coated with an antibody against raptor, YFP–mTOR fluorescence spots were observed, well above the background level of fluorescence seen in the control channel without the antibody (Fig. III. 1 *C* and *D*), illustrating specific pulldown of mTOR in complex with raptor, or mTORC1.

To assess the sensitivity of SiMPull, we compared detection of YFP–mTOR by Western blotting and by SiMPull with cell lysates at the same concentrations. Remarkably, even at 1,000-fold dilution of the lysates SiMPull detected YFP–mTOR specifically (Fig. III. 3*A*), whereas at 100-fold dilution of the same lysates, there was no longer any signal on Western blots (Fig. III. 3*B*). Furthermore, in SiMPull, we were able to detect YFP–mTOR pulled down via endogenous raptor using a 100-fold dilution of the lysate (Fig. III. 3 *C* and *D*), whereas no signal was detected in conventional coimmunoprecipitation using the same dilution of lysate and raptor antibody (Fig. III. 3*E*); SiMPull required only 50 μL of the extract as opposed to 500 μL used for the corresponding coimmunoprecipitation. Hence, the SiMPull method is highly sensitive compared with conventional biochemical methods.

We then analyzed the fluorescence time trajectories of YFP–mTOR pulled down with raptor. Most molecules (96%) bleached in either one or two steps, indicating that mTORC1 contains one or two molecules of fluorescently active YFP–mTOR (Fig. III. 1*E*). Nearly 60% of the molecules exhibited two-step bleaching, whereas 36% bleached in a single step. The molecules bleaching in two steps were nearly twice as bright as one-step bleachers on average, indicating a reliable classification based on photobleaching steps (Fig. III. 1*E*). Previous studies have determined that fluorescent proteins may not all mature to completion and the fraction of fluorescently active YFP is ~75% (Ulbrich and Isacoff 2007; Jain, Liu et al. 2011). In a calibration experiment, photobleaching step distribution of monomeric and dimeric YFP or a mixture of the two proteins was measured, which revealed that the fraction of two-step photobleaching spots is linearly proportional to the fraction of dimeric YFP included (Fig. III. 1 *H* and *I*). A comparison of the observed photobleaching step distribution of YFP–mTOR in mTORC1 to the calibration data suggested that nearly all mTORC1 complexes (>95%) contain two copies of YFP–mTOR, assuming the maturation level of YFP for all experiments is the same.

We also transiently coexpressed YFP–mTOR and HA–raptor, which assembled into functional mTORC1 complexes (Fig. III. 2*B*). Single-molecule fluorescence photobleaching analysis for YFP–mTOR pulled down with HA–raptor revealed that the complexes each contained two copies of YFP–mTOR (Fig. III. 4 *A* and *B*). Similarly, when YFP–raptor and Flag–mTOR were coexpressed (Fig. III. S1 *C* and *D*), two copies of YFP–raptor were found in each mTOR–raptor complex (Fig. III. 1 *F* and *G*). Additionally, the mTORC1 inhibitors PRAS40 and DEPTOR were also present in two copies per mTORC1 (Figs. 2 *E–G* and 4 *C–F*).

To confirm that the complexes captured via SiMPull represent physiological state of mTORC1 and are not assembled/disassembled upon cell lysis, we followed the strategy of Riley et al. (Riley, Yario et al. 2012) and mixed lysates from cells expressing YFP–raptor and Flag–mTOR separately, and compared them to lysates of cells coexpressing the same proteins at similar expression levels (Fig. III. 4*G*). At least 10-fold more mTORC1 complexes were detected in the lysates from cotransfected cells than the mixed lysates (Fig. III. 4*H*). Similar results were obtained when intact cells were mixed before lysis (Fig. III. 4*I*). Thus, postlysis association of mTORC1 components does not significantly contribute to the complexes detected here via SiMPull.

SiMPull requires dilution of cell lysates to achieve low pulldown density suitable for single-molecule analysis, which could lead to loss of weakly associated physiological complexes. To address this issue, we treated YFP–mTOR-expressing cells with the cross-linker dithiobis(succinimidylpropionate) (DSP) before cell lysis. Lysis of cells using a Triton X-100–containing buffer disrupted mTORC1 complexes as expected (Kim, Sarbassov et al. 2002), whereas DSP cross-linking before cell lysis preserved the complex under the same lysis condition (Fig. III. 5 *A* and *B*), validating our cross-linking conditions. Importantly, cross-linked mTORC1 complexes exhibited a photobleaching step distribution corresponding to that of a dimer (Fig. III. 5*C*), suggesting that the physiological complexes are intact during SiMPull analysis without cross-linking. In summary, we find that mTORC1 is dimeric, containing two copies of each component. These findings are consistent with the previous cryo-EM data (Yip, Murata et al. 2010), thus validating our experimental system for analysis of mTOR complexes by SiMPull.

III. 3. 2. mTORC2 is dimeric

mTORC2 assembly requires mSin and mLST8 (Frias, Thoreen et al. 2006; Guertin, Stevens et al. 2006) in addition to mTOR and rictor, but the oligomeric state of mTORC2 is under debate (Wullschleger, Loewith et al. 2005; Frias, Thoreen et al. 2006; Takahara, Hara et al. 2006; Tao, Barker et al. 2010). When all four core components of mTORC2 (mTOR, rictor, mSin, and mLST8) were coexpressed, each component self-associated as indicated by coimmunoprecipitation of the recombinant protein with two different tags (Fig. III. 6*A* and Fig. III. 7*A*), suggesting that assembled mTORC2 is oligomeric. To determine the oligomeric state of mTOR in mTORC2, we captured mTORC2 complexes from the YFP–mTOR stable cell line on SiMPull surfaces using an antibody against endogenous rictor (Fig. III. 6*B*). Intriguingly, once again we observed a photobleaching pattern characteristic for dimeric YFP–mTOR (Fig. III. 6*C*). Similar results were obtained when YFP–mTOR was coexpressed with recombinant mTORC2 components (Fig. III. 8 *A* and *B*), which also assembled into functional mTORC2 (Fig. III. 7 *B* and *C*).

Next, we probed the stoichiometry of rictor in mTORC2. YFP–rictor was coexpressed with Flag–mTOR, mSin–HA and HA–mLST8, and the assembly of mTORC2 was verified by ensemble pulldown (Fig. III. 7 *D* and *E*). Upon single-molecule pulldown of mTORC2 via Flag–mTOR (Fig. III. 6*D*), we observed YFP–rictor photobleaching consistent with two copies of rictor per mTORC2 (Fig. III. 6*E*). Furthermore, YFP–DEPTOR in mTORC2 was found to display photobleaching distribution that corresponded to a mixture of monomers and dimers (~60% dimer) (Fig. III. 8 *C* and *D*), indicating that each mTORC2 can harbor up to two copies of DEPTOR.

Once again, cell mixing (Fig. III. 8 *E* and *F*) and DSP cross-linking (Fig. III. 8 *G* and *H*) experiments were performed, the results of which confirmed that the dimeric stoichiometry most likely reflects physiological assembly of mTORC2 in live cells. In conclusion, our results unequivocally reveal mTORC2 as a dimer, in which each subunit is present in two copies.

III. 3. 3. mTORC1 and mTORC2 are mostly distinct but cocomplexes exist

Biochemical characterizations so far suggest that mTORC1 and mTORC2 are mutually exclusive, but functional cross-talk between these two complexes at multiple levels is increasingly apparent (Dibble, Asara et al. 2009; Huang and Manning 2009; Julien, Carriere et al. 2010). Even a small fraction of mTORC1/mTORC2 cocomplex could be functionally significant, but may have escaped detection by conventional biochemical methods. Multicolor SiMPull should allow direct visualization of such hybrid complexes, if any. As a positive control, we coexpressed Flag–mTOR, mCherry–raptor, and YFP–PRAS40. Upon capturing Flag–mTOR, we observed both mCherry–raptor and YFP–PRAS40 fluorescence spots (Fig. III. 9*A*); ~49% of YFP–PRAS40 spots colocalized with mCherry–raptor, indicating their coexistence in the same complexes. Incomplete colocalization between the two likely arises from incomplete chromophore maturation (~40% for mCherry and ~75% for YFP) (Ulbrich and Isacoff 2008; Dunne, Fernandes et al. 2009) and the participation of endogenous untagged proteins.

Next, we coexpressed mCherry–raptor and YFP–rictor together with Flag–mTOR, mLST8, and mSin. An anti-Flag antibody captured both mTORC1 and mTORC2 as visualized by mCherry and YFP fluorescent spots, respectively, and about 7% of mCherry–raptor spots reproducibly colocalized with YFP–rictor (Fig. III. 9*B*). Taken into consideration the incomplete chromophore maturation mentioned above, it is likely that the true fraction of the mTORC1/mTORC2 cocomplex is higher than 7%. Under these experimental conditions, the colocalization by chance was ~1% (Fig. III. 10*A*). Additionally, when YFP instead of YFP–rictor was expressed, only a background level of YFP fluorescent spots was observed upon Flag–mTOR pulldown, and these spots did not colocalize with mCherry–raptor (Fig. III. 10*B*). Importantly, raptor coexpression did not alter mTORC2 stoichiometry, as rictor was still present in two copies (Fig. III. 10*C*).

To verify that the hybrid complex was not an artifact of cell lysis, we performed cell mixing experiments. mTORC1 components (Flag–mTOR and mCherry–raptor) and mTORC2 components (Flag–mTOR, YFP–rictor, mSin–HA, and HA–mLST8) were expressed in two separate pools of cells, which were mixed during lysis (Fig. III. 10 *D*–*F*). After accounting for false colocalization by chance, only 2% colocalization between

mCherry–raptor and YFP–rictor was observed from mixed lysates. Therefore, although the two mTOR complexes are predominantly distinct, hybrid mTOR complexes containing both raptor and rictor or higher order assemblies of mTORC1/mTORC2 exist, albeit at a low level.

III. 3. 4. mTORC1 and mTORC2 components are monomeric

Because both mTORC1 and mTORC2 are dimeric, we asked if mTOR or other core components could self-dimerize. To that end, each component tagged with YFP was individually expressed. When YFP–mTOR was captured using an anti-mTOR antibody, nearly 75% of the molecules bleached in a single step, whereas 20% bleached in two steps, indicating that a majority of overexpressed mTOR was monomeric (Fig. III. 11*A*). Furthermore, when YFP–mTOR and HA–mLST8 were coexpressed and the mTOR–mLST8 subcomplexes were captured through the HA tag, a photobleaching step distribution characteristic of monomers was observed for YFP–mTOR (Fig. III. 11*B*). Similar analysis for HA–YFP–raptor and HA–YFP–rictor, pulled down through the HA tag, also revealed monomeric distributions (Fig. III. 11 *C* and *D*). In addition, YFP–PRAS40 bound to raptor was monomeric (Fig. III. 12 *A* and *B*). The observed small fractions of dimer may arise due to incorporation of YFP-tagged proteins in endogenous mTOR complexes. Taken together, our results show that although both mTORC1 and mTORC2 are exclusively dimeric, individual mTORC components and subcomplexes are predominantly monomeric. Thus, no single mTORC subunit serves as a dimerizing component.

III. 3. 5. mTORC stoichiometry is unchanged under various physiological conditions

Next we asked if the oligomerization of mTOR complexes was affected by upstream signals or physiological conditions known to regulate mTOR signaling, including growth factors, nutrient availability, and cellular energy levels. To examine the effect of energy sufficiency, we starved the YFP–mTOR stable cells of glucose and glutamine, which leads to energy depletion and inhibition of mTORC1 signaling (Kim, Hoffman et al. 2013), and briefly (1 h) restimulated them with growth medium containing glucose and glutamine. As shown in Fig. III. 13*A*, a nearly equal number of mTORC1

complexes pulled down through endogenous raptor were detected by SiMPull, with similar photobleaching step distribution, under starvation and stimulation conditions. Similarly, neither amino acids (Fig. III. 13*B*) nor leucine (Fig. III. 12 *C* and *D*) stimulation had any effect on the number or stoichiometry of mTORC1. In addition, insulin stimulation did not affect mTORC1 (Fig. III. 13*C*) or mTORC2 assembly (Fig. III. 13*D*). The starvation and stimulation conditions impacted mTOR signaling as expected (Fig. III. 1*B* and Fig. III. 2*A*). These observations directly establish that inhibition of mTOR activity by energy stress or nutrient- or growth-factor depletion can be achieved without disassembly of the mTOR complexes.

III. 3. 6. Effect of rapamycin on mTOR complexes

Several models have been proposed for the mechanism by which rapamycin inhibits mTOR. For example, rapamycin may limit substrate access to the kinase domain (McMahon, Choi et al. 2002; Yang, Rudge et al. 2013), may induce raptor dissociation from mTOR (Kim, Sarbassov et al. 2002; Oshiro, Yoshino et al. 2004; Yip, Murata et al. 2010), or displace a key regulator (Fang, Vilella-Bach et al. 2001). We investigated the effect of rapamycin on the stoichiometry of mTOR complexes. As reported (Sarbassov, Ali et al. 2006), short-term treatment of cells with rapamycin dissociated raptor from mTOR and inhibited mTORC1 signaling, whereas on prolonged treatment, mTORC2 assembly was also affected (Fig. III. 14 *A* and *B*). When YFP–mTOR stable cells were treated with increasing concentrations of rapamycin (2–100 nM) for 30 min and mTORC1 complexes were captured from cell lysates through endogenous raptor, the number of YFP–mTOR pulled down decreased with increasing rapamycin dose (Fig. III. 15*A*): treatment with 2 nM of rapamycin led to reduction by 56%, and a maximal reduction of ~90% was reached by 10 nM and 100 nM rapamycin (Fig. III. 15*C*). The residual mTORC1 appeared to be resistant to rapamycin, consistent with previously reported observations (Kim, Sarbassov et al. 2002). Thus, acute rapamycin treatment at low dose disrupted the interaction between mTOR and raptor.

Additionally, we found that the fraction of dimers decreased as the rapamycin dose was increased. At 2 nM of rapamycin, about 47% of the molecules bleached in two steps, whereas at 100 nM, only 29% of the molecules exhibited two-step bleaching (Fig.

III. 15*B*). The photobleaching analysis was performed at similar surface densities of the complexes (~0.1 molecules·μm^{-2}), precluding any artifacts due to differences in the immobilization density. This observation of transient monomeric mTOR–raptor complexes indicates that rapamycin disrupts mTORC1 in at least two steps, displacing one mTOR (or mTOR–raptor monomeric subcomplex) at a time. Consistent with these results, mTOR bound to FKBP12–rapamycin is monomeric, as indicated by the single-step photobleaching exhibited by YFP–mTOR pulled down via surface immobilized FKBP12–rapamycin (Fig. III. 12 *E* and *F*). The reduction in mTORC1 signaling activity (pS6K1) corresponded with the loss of intact dimeric mTORC1 complexes (Fig. III. 15*C*), implying that disruption of mTORC1 dimeric architecture contributes significantly to rapamycin-induced abrogation of mTORC1 signaling.

Next, we investigated the effect of prolonged rapamycin treatment on mTORC2 assembly by capturing endogenous rictor from YFP–mTOR cell lysates. The number of mTORC2 complexes decreased by 40% upon 6-h treatment with 100 nM of rapamycin and was reduced by 79% after 24 h (Fig. III. 15*D*). Interestingly, in contrast to the transient mTORC1 monomers, mTORC2 remained a dimer at all time points (Fig. III. 15*E*). Rapamycin treatment did not affect mTOR expression levels (Fig. III. 14 *C* and *D*), whereas the amount of mTORC1 decreased (Fig. III. 14*E*). Thus, our results suggest that rapamycin does not directly affect mTORC2 stoichiometry. Instead, rapamycin may sequester free mTOR and subsequently impair mTORC2 assembly over time.

III. 4. Discussion

Using SiMPull we have determined the stoichiometry and assembly of mTOR complexes captured from whole cell lysates. In addition to confirming the dimeric structure of mTORC1 as previously revealed by cryo-EM studies, we find that mTORC2 assembles into a dimer, with two copies of each subunit. Interestingly, all individual subunits of mTORCs including mTOR, when expressed alone, are monomeric. This excludes a commonly presumed role of the HEAT repeats in mediating mTOR self-association. Interaction between mTOR and raptor alone is sufficient to form mTORC1 dimers, but mTORC2 assembly and dimerization require coexpression of mSin and mLST8 in addition to mTOR and rictor. Under physiological conditions, there is no

evidence of monomeric interaction between mTOR and raptor or mTOR and rictor. Hence, we propose a model for mTORC assembly where the interaction between monomeric subunits is unstable; assembly requires multiple subunits to accumulate at high local concentrations (Fig. III. 15*F*), which may be facilitated by membrane localization, subcellular compartmentalization, or scaffolding proteins. The small but significant fraction of mTORC1–mTORC2 cocomplex revealed by SiMPull suggests a potential physical cross-talk between the two complexes that may have evaded detection by conventional biochemical methods. Future investigation examining the biological function of this cocomplex is warranted.

Of significance, our SiMPull assays have captured the existence of monomeric mTORC1 (mTOR–raptor complex) upon acute rapamycin treatment, before complete disruption of the mTOR–raptor interaction (Fig. III. 15*F*). The capture of this intermediate state of mTORC1, which was not detected by cryo-EM analysis (Yip, Murata et al. 2010), further attests to the exquisite sensitivity of the SiMPull method. We also provide direct evidence that cellular stress conditions that abrogate mTORC1- or mTORC2-mediated signaling do not alter the number or oligomerization state of mTOR complexes, indicating that effective inhibition of mTOR signaling can be achieved without disassembling mTOR complexes. Of note, Kim et al. recently reported that glucose and glutamine deprivation results in monomeric mTORC1 (Kim, Hoffman et al. 2013), which is not observed in our SiMPull assays. Again, direct experimentation with fresh cell lysates containing near-endogenous proteins, without any additional manipulation such as those required for conventional coimmunoprecipitation, may be advantageous in capturing physiologically relevant protein complexes. Dimerization of other PIKKs such as ATM and DNA-PK play important roles in the regulation of their activities (Bakkenist and Kastan 2003; Spagnolo, Rivera-Calzada et al. 2006). Our data reveals differences in assembly mode and regulation of mTOR compared with these members of the PIKK family.

Over 75% of the proteins in a cell can oligomerize (Goodsell and Olson 2000). SiMPull is a powerful method to investigate oligomeric protein assemblies. This method provides direct and quantitative readout of the assembly state of the proteins, expressed at endogenous levels directly in their native context. Proteins are captured from freshly

lysed cells and probed at single-molecule resolution without requiring removal of other proteins, minimizing loss of interactions due to stringent wash steps associated with conventional immunoprecipitation. SiMPull worked wherever ensemble immunoprecipitation worked across the variety of constructs and samples tested in this study, highlighting the versatility of the assay. By performing SiMPull and biochemical analysis on the same samples, we were able to correlate the complex architecture with its functional activity. The advent of genetic engineering at endogenous loci and developments in short genetically encoded fluorescent tags should enable powerful applications of this technology to near-endogenous systems.

III. 5. Figures

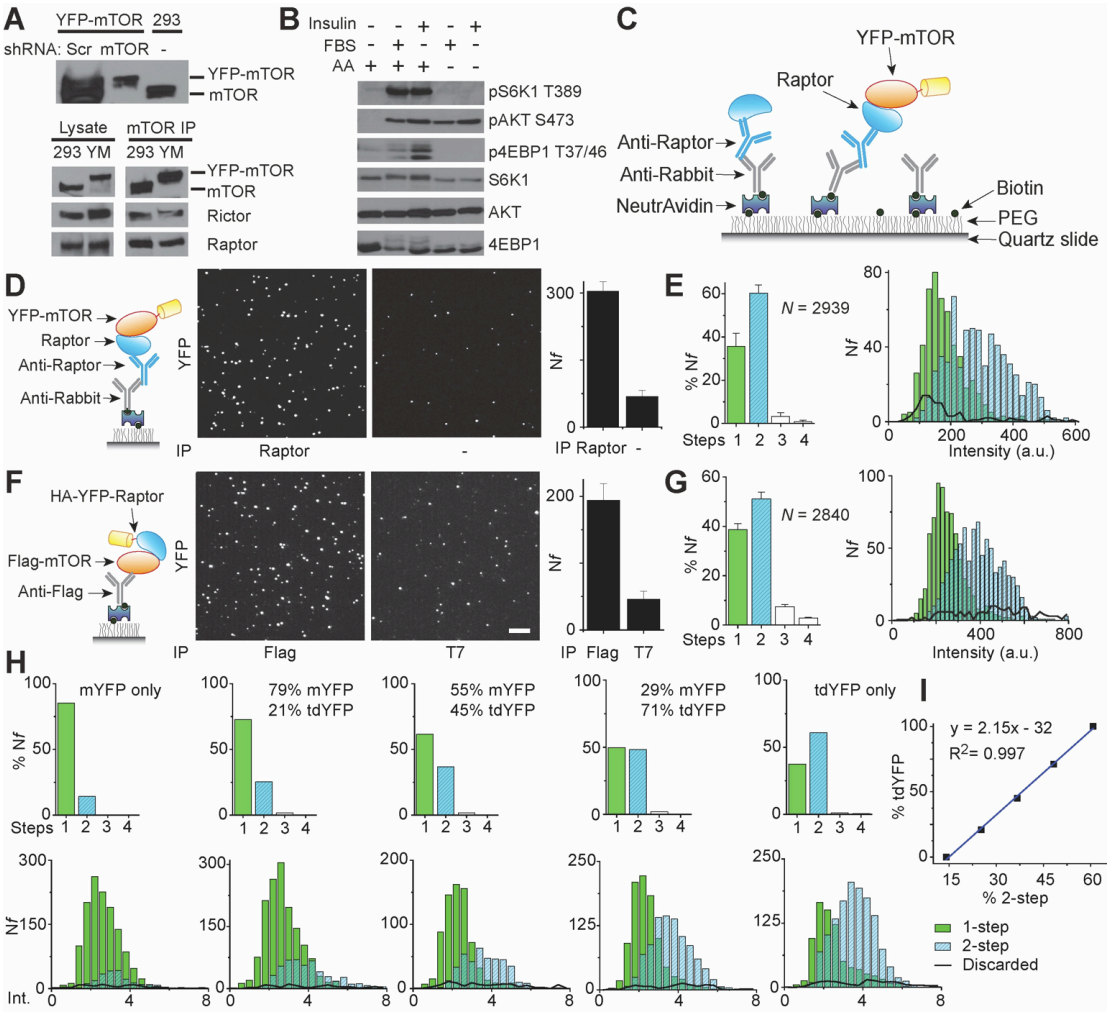

Figure III. 1. mTORC1 is dimeric. (A) Expression of mTOR in the YFP-mTOR stable cells (YM) (upper panels) and interaction with raptor and rictor assessed by co-IP (lower panels) are shown. Scr: scramble. (B) YM cells were stimulated with insulin, serum, or amino acids (AA). (C) Schematic depiction of mTORC1 SiMPull. (D) Endogenous raptor was pulled down from YM cells, followed by SiMPull analysis. Shown are schematic diagram (left), representative YFP fluorescence images (center), and average number of molecules per imaging area (N*f*). (E) Distribution of fluorescence photobleaching steps (left) and corresponding intensity (a.u.: arbitrary units) distribution (right) for samples described in (D). *N*, total number of molecules analyzed. (F) Flag-mTOR and HA-YFP-raptor were co-expressed and Flag-mTOR was pulled down, followed by analyses similar to those in (D). (G) Same analyses as in (E) for samples described in (F). Scale bar: 5 μm. (H) Monomeric YFP (mYFP) and tandem dimeric YFP (tdYFP) were mixed in the ratios as indicated and single molecule fluorescence time-trajectories were analyzed. Top: number of fluorescence photobleaching steps. Bottom: intensity (Int., arbitrary units) of

Figure III. 1 (Cont.)
molecules exhibiting 1 or 2 photobleaching steps. (I) Observed fraction of two-step bleaching events changes linearly with the fraction of tdYFP.

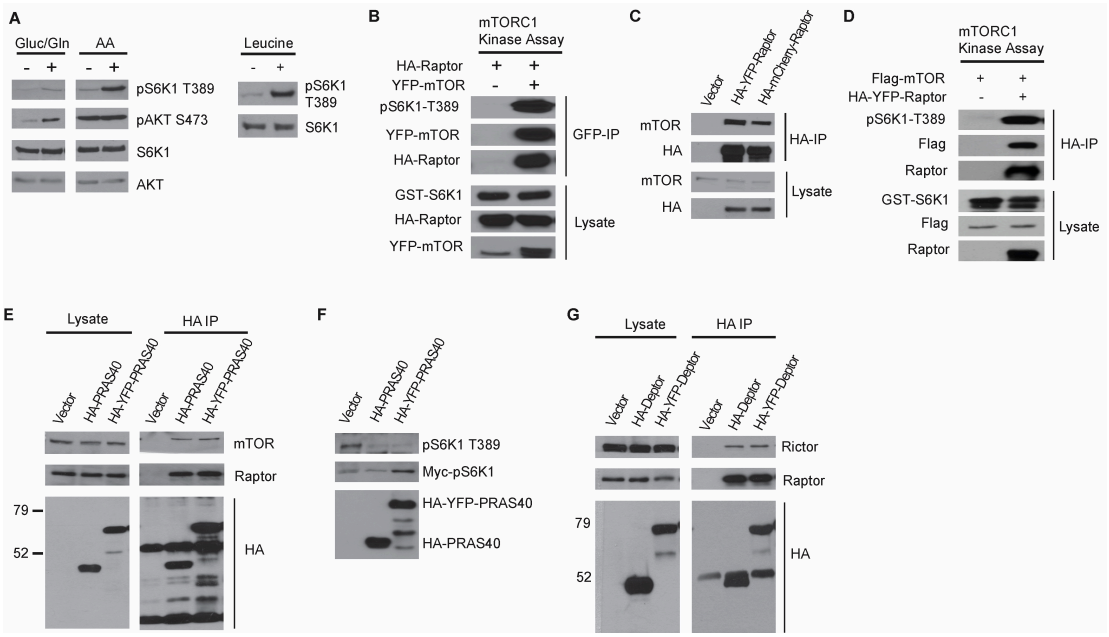

Figure III. 2. Characterization of fluorescent protein-tagged mTORC1 subunits. (A) YFP-mTOR stable cells were deprived of glucose/glutamine for 12 h, amino acids for 2 h, or leucine for 1 h, and then restimulated by complete growth medium for 1h (glucose/glutamine), 30 min (amino acids), or 15 min (leucine). (B) HA-raptor and YFP-mTOR were co-expressed in HEK293 cells and YFP immunoprecipitates from cell lysates were subjected to mTORC1 kinase assay using GST-S6K1 as substrate. (C) Empty vector, YFP-raptor or mCherry-raptor was transfected into HEK293 cells. Cell lysates were subjected to HA immunoprecipitation followed by Western blotting. (D) HA-YFP-raptor and Flag-mTOR were co-expressed in HEK293 cells and HA immunoprecipitates from cell lysates were subjected to mTORC1 kinase assay. (E) HA-PRAS40 or HA-YFP-PRAS40 were transiently expressed in HEK293 cells and cell lysates were subjected to HA immunoprecipitation. Endogenous mTOR and raptor were detected by Western blotting. (F) Empty vector, HA-PRAS40, or HA-YFP-PRAS40 were co-expressed with myc-S6K1 in HEK293 cells. pT389-S6K1, myc-S6K1, and PRAS40 were detected by Western blotting. (G) HA-DEPTOR or HA-YFP-DEPTOR were transiently expressed in HEK293 cells and cell lysates were subjected to HA immunoprecipitation. Endogenous rictor and raptor were detected by Western blotting.

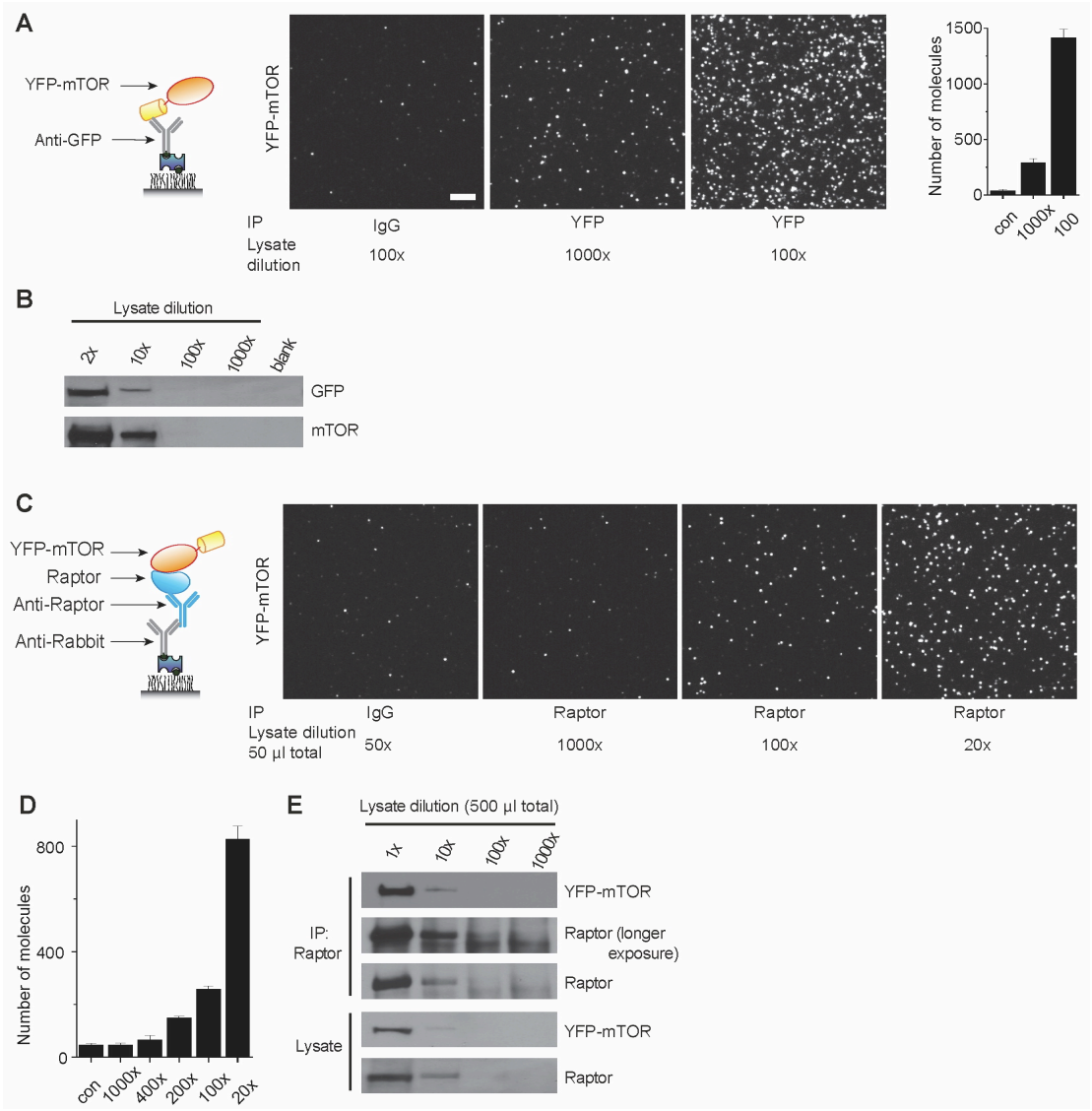

Figure III. 3. Comparison of sensitivity of SiMPull and Western blotting (WB).
(A, B) Comparison of SiMPull with WB. Lysate from YFP-mTOR cells was diluted as indicated. In SiMPull, YFP-mTOR was captured using an antibody against GFP. WB was performed using the same anti-GFP antibody, or an antibody against mTOR.
(C-E) Comparison of SiMPull with co-immunoprecipitation. (C, D) Lysate from YFP-mTOR cell line was diluted as indicated and applied to SiMPull chambers coated with an antibody against raptor. (E) Conventional immunoprecipitation for raptor using various dilutions of YFP-mTOR expressing cells, followed by WB for mTOR and raptor.

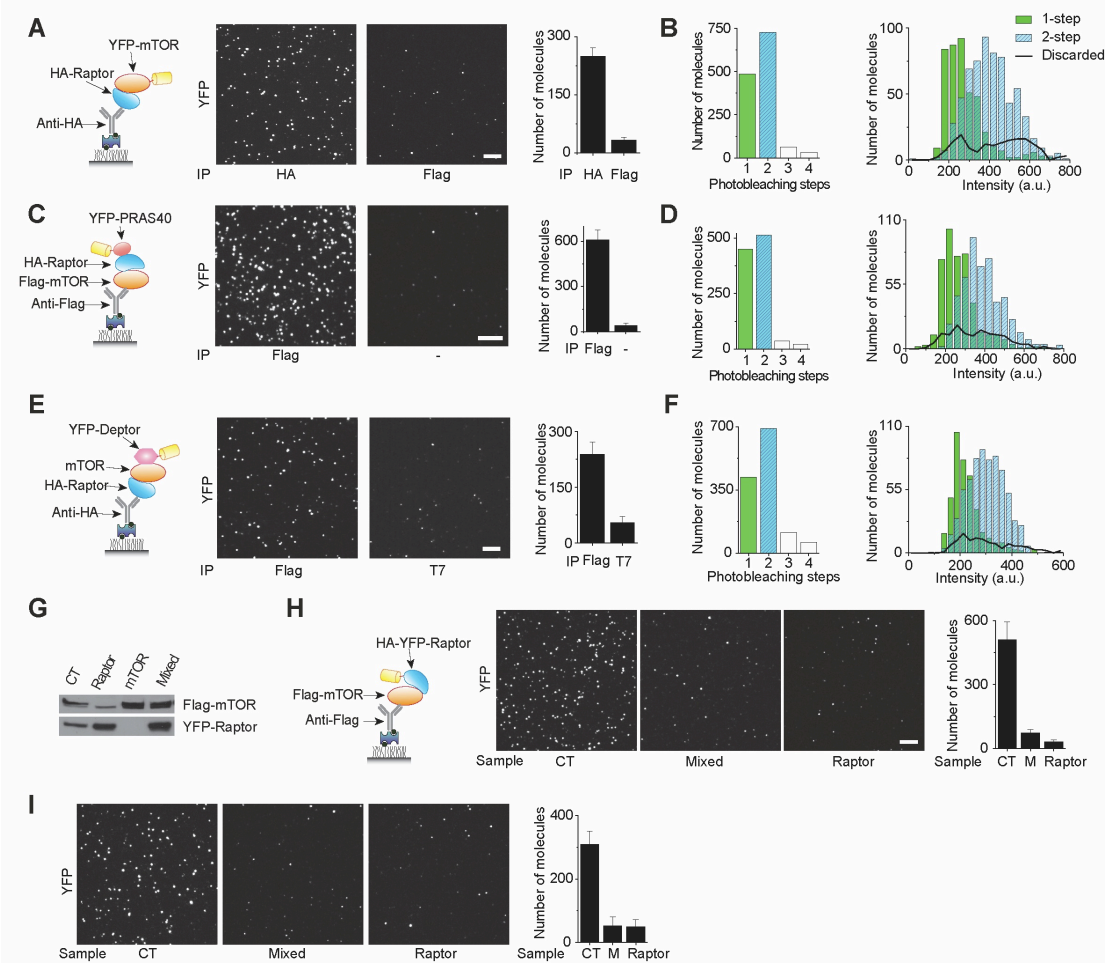

Figure III. 4. mTORC1 is dimeric. Epitope-tagged mTORC1 components were transiently expressed and captured on single-molecule imaging chambers as depicted in schematics (A, C, E left). (A,B) YFP-raptor and mTOR formed dimers when co-expressed. (C, D) PRAS40 when pulled down via mTOR was dimeric. (E, F) DEPTOR associated with mTORC1 was dimeric. (G) YFP-Raptor and Flag-mTOR were co-transfected (CT), or transfected separately (Raptor, mTOR). For Mixed, lysates expressing mTOR and raptor separately were mixed at a 1:1 ratio. Expression levels in these lysates were analyzed by Western blotting. (H) SiMPull analysis of mTOR-Raptor interaction in lysates in (G). (I) Cells were transfected as in (G&H). For Mixed, cells were trypsinized and mixed at 1:1 raito, followed by lysis. SiMPull analysis was performed as in (H). Error bars depict standard deviation of the mean across 20 or more imaging areas. Scale bars: 5μm.

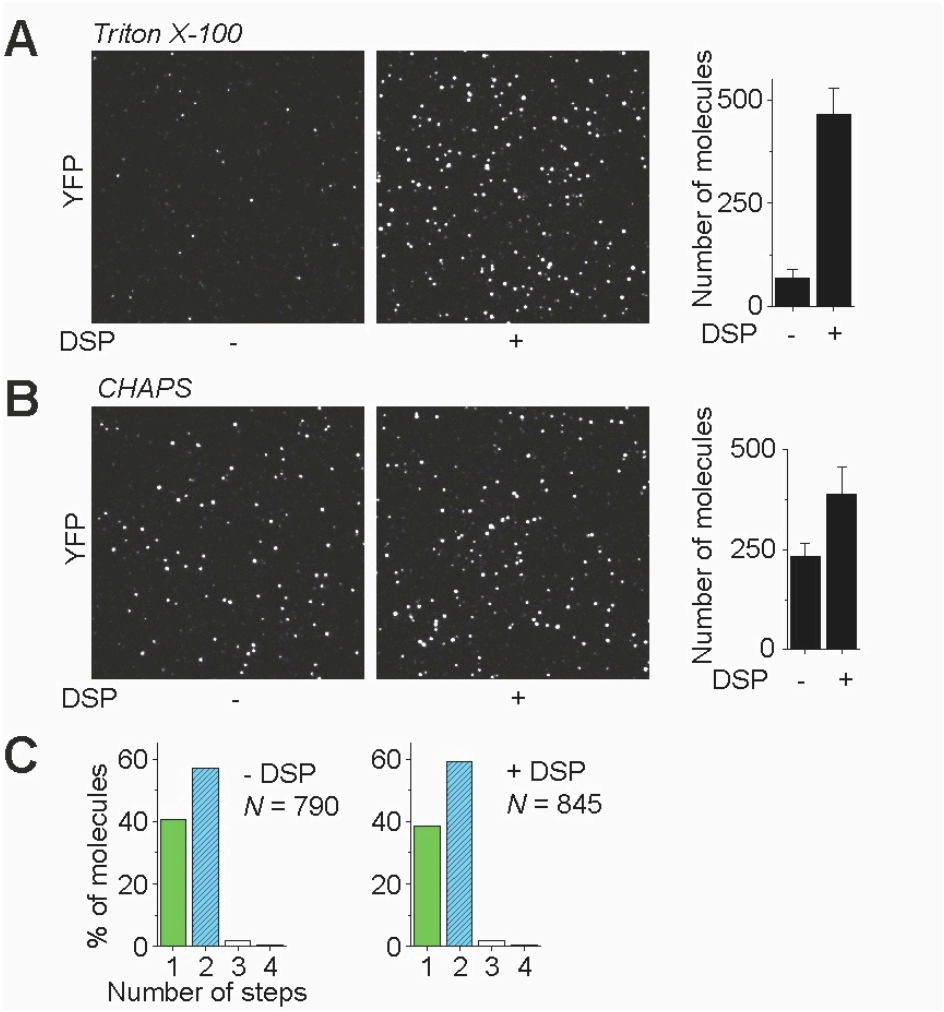

Figure III. 5. mTORC1 crosslinking assay. (A-B) YFP-mTOR stable cells were lysed in buffer containing 1% Triton X-100 or 0.3% CHAPS. For crosslinking, cells were treated with DSP crosslinker prior to cell lysis. mTORC1 was pulled down using anti-raptor antibody. (C) Fluorescence photobleaching step distribution for YFP-mTOR in mTORC1, for cells lysed in 0.3% CHAPS without or with DSP. Error bars depict standard deviation of the mean over > 20 images. Scale bar: 5 μm.

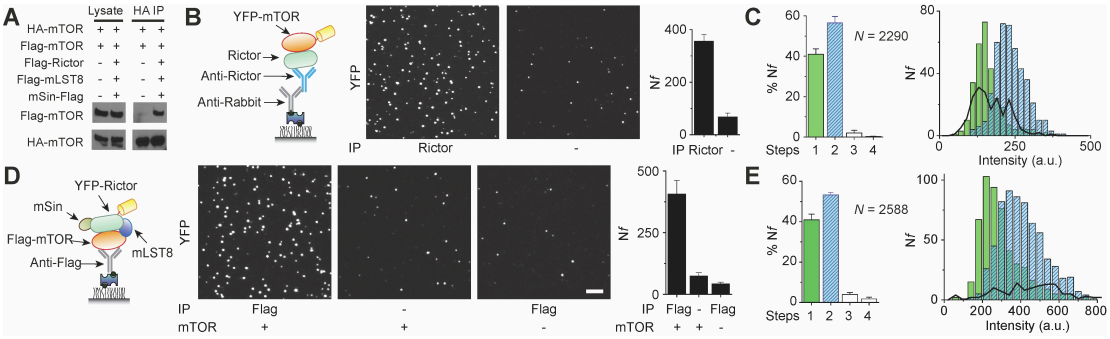

Figure III. 6. mTORC2 is dimeric. (A) mTOR oligomerizes in mTORC2 shown by co-IP. (B, C) SiMPull for endogenous rictor from YM cells and analysis similar to Fig. III. 1D and E. (D, E) YFP-rictor was co-expressed with Flag-mTOR, mSin and mLST8, and Flag-mTOR was pulled down. SiMPull data are presented as in (B, C). Scale bar: 5 μm.

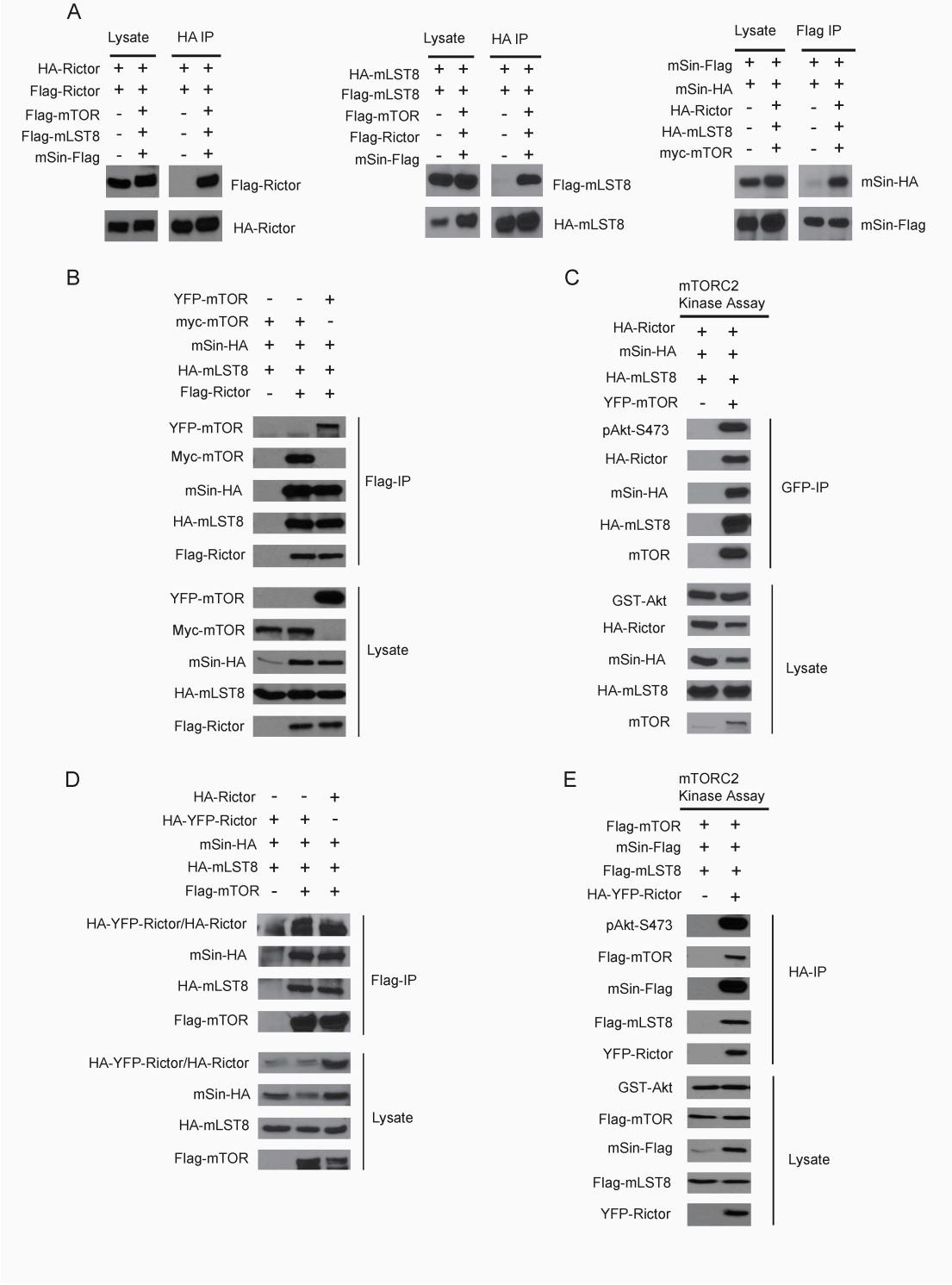

Figure III. 7. mTORC2 oligomerization and incorporation of fluorescently labeled subunits. (A) Recombinant proteins were transiently expressed in HEK293 cells as indicated, followed by Flag or HA immunoprecipitation and Western blotting. (B) Recombinant proteins were transiently expressed in HEK293 cells as indicated, followed by Flag immunoprecipitation and Western blotting. (C) Recombinant proteins

Figure III. 7 (Cont.)
were transiently expressed in HEK293 cells as indicated, followed by GFP immunoprecipitation and in vitro mTORC2 kinase assays using Akt as a substrate. (D) Recombinant proteins were transiently expressed in HEK293 cells as indicated, followed by Flag immunoprecipitation and Western blotting. (E) Recombinant proteins were transiently expressed in HEK293 cells as indicated, followed by HA immunoprecipitation and in vitro mTORC2 kinase assay using Akt as a substrate.

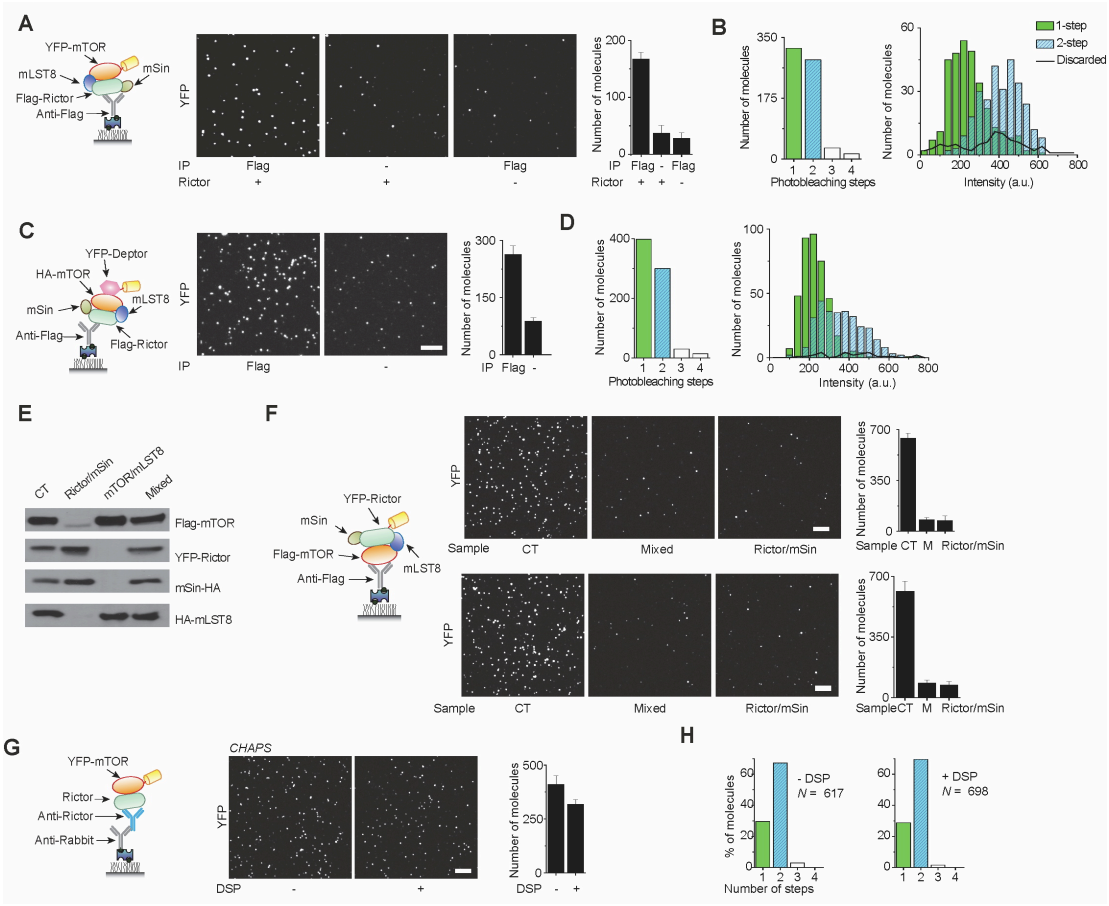

Figure III. 8. mTORC2 is dimeric. (A) YFP-mTOR was co-expressed with mSin-HA, HA-mLST8 and Flag-rictor. mTORC2 complexes were captured on SiMPull using Flag antibody. (B) Fluorescence photobleaching step distribution (left) and intensity of scored molecules (right) for YFP-mTOR in mTORC2. (C) YFP-DEPTOR was co-expressed with core mTORC2 components in HEK293 cells, and was pulled down via Flag-rictor (D) Fluorescence photobleaching step distribution (left) and intensity of scored molecules (right) for YFP-DEPTOR in mTORC2. (E) mTORC2 subunits were co-transfected (CT) or transfected separately (Rictor/mSin and mTOR/mLST8) followed by lysate mixing at 1:1 ratio (Mixed). Expression levels were analyzed by Western blotting. (F) mTORC2 from CT, Mixed, and Rictor/mSin lysates was capture using Flag antibody. Upper panels: for Mixed, lysates were mixed at a 1:1 ratio. Lower panels: for Mixed, cells were trypsinized and mixed at 1:1 ratio, followed by lysis. (G) YFP-mTOR stable cells were lysed in CHAPS buffer. Some cells were incubated with DSP crosslinker prior to cell lysis. mTORC2 as pulled down using anti-Rictor antibody. (H) Fluorescence photobleaching step distribution was analyzed for samples in (G). Scale bar: 5 μm.

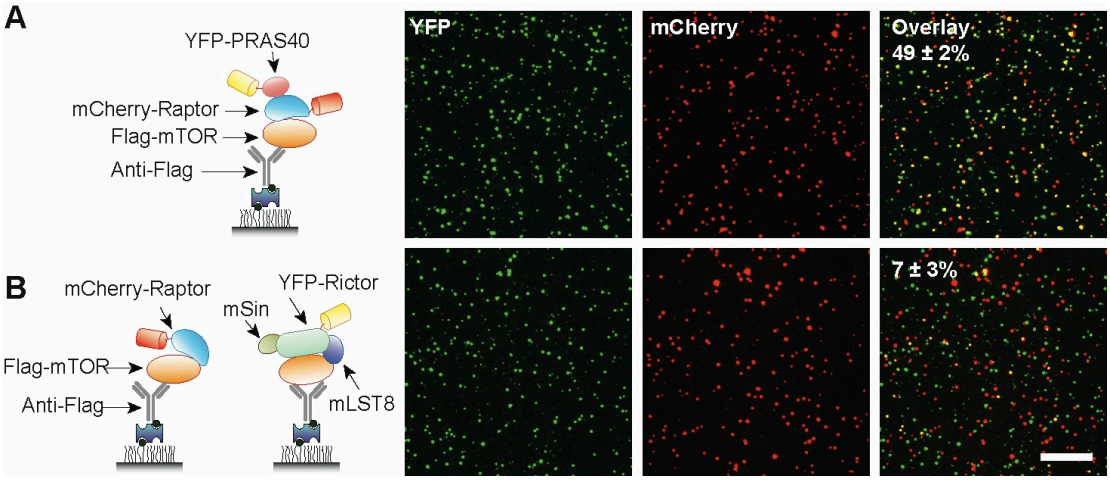

Figure III. 9. mTORC1 and mTORC2 co-localization. (A) Flag-mTOR co-captures YFP-PRAS40 (left) and mCherry-raptor (center). Overlay of the two images (right) showed 49 ± 2% co-localization. (B) Flag-mTOR, mCherry-raptor, YFP-rictor, HA-mLST8 and mSin-HA were co-expressed. Flag-mTOR was pulled down, and YFP (rictor, left) and mCherry (raptor, center) were imaged. Overlay of the two images (right) showed 7 ± 3% co-localization across 6 independent experiments. Scale bar: 10 μm.

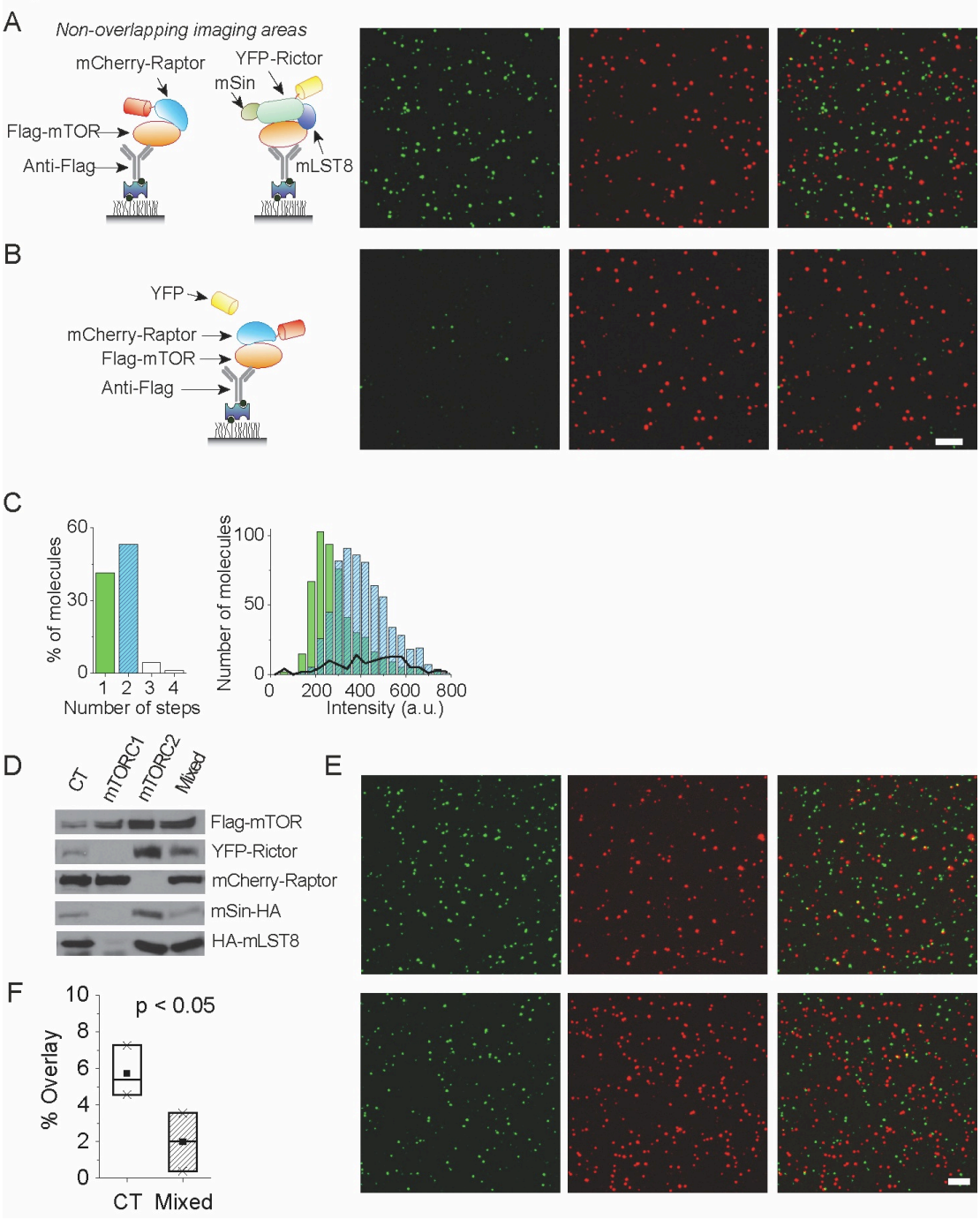

Figure III. 10. Two-color SiMPull for mTORC1 and mTORC2. (A) mCherry-raptor and YFP-rictor were co-expressed with Flag-mTOR, mSin-HA and HA-mLST8. Flag-mTOR is captured using a surface immobilized Flag antibody. Two different imaging areas were visualized for YFP and mCherry to estimate the overlap by chance. The observed overlap was ~1% across 23 imaging areas over 4 independent experiments. (B) mCherry-raptor, YFP, Flag-mTOR, mSin-HA and HA-mLST8 were co-expressed. Flag-mTOR is captured using a surface immobilized Flag antibody. A background level of fluorescence was observed in the YFP channel and these fluorescent spots did not

Figure III. 10 (Cont.)
colocalize with mCherry (0% overlap). (C) Fluorescence photobleaching step distribution for YFP-rictor from (A). (D) Expression levels of mTORC components when mTORC1 and mTORC2 were expressed together, separately, or when lysates mixed at 1:1 ratio. (E) Top panel, colocalization of mTORC1 and mTORC2 when co-transfected in the same cells. Lower panel, colocalization of mTORC1 and mTORC2 when cell lysates are mixed. On capturing Flag-mTOR, YFP-rictor (left), mCherry-raptor (center), and overlapping spots (right) were observed. (F) The box plot shows distribution of overlay percentage from three independent experiments (N = 15 images) calculated after subtracting the false co-localization. Mean is shown as square marker and median as center line. Scale bar: 5 μm.

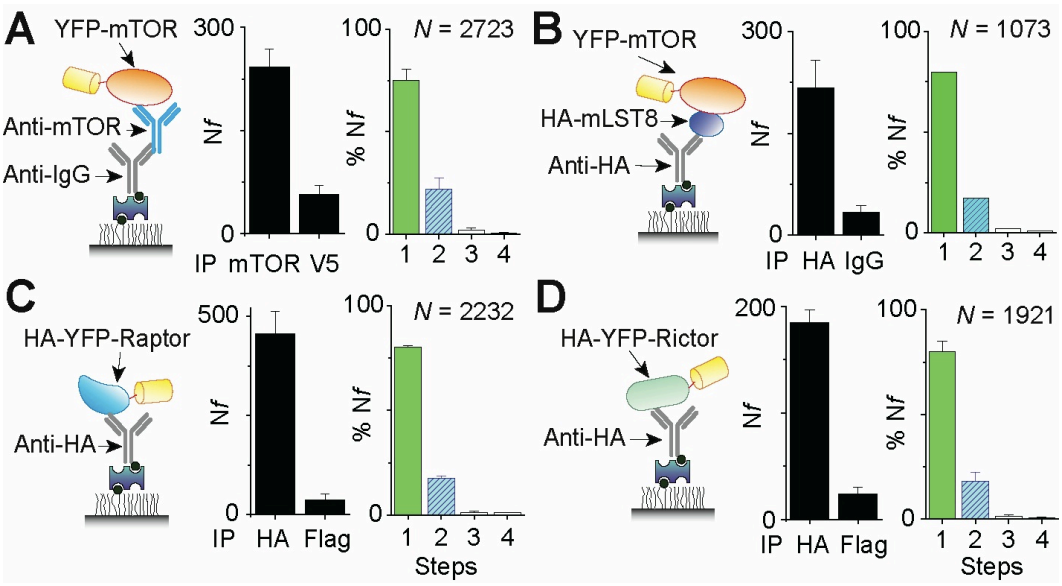

Figure III. 11. mTORC components are monomeric. (A) YFP-mTOR, (B) YFP-mTOR and HA-mLST8, (C) HA-YFP-raptor or (D) HA-YFP-rictor were expressed in HEK293 cells, and captured on SiMPull surfaces as depicted (diagrams on left). The number of molecules observed per imaging area (center), and the distribution of fluorescence photobleaching steps (right) are shown.

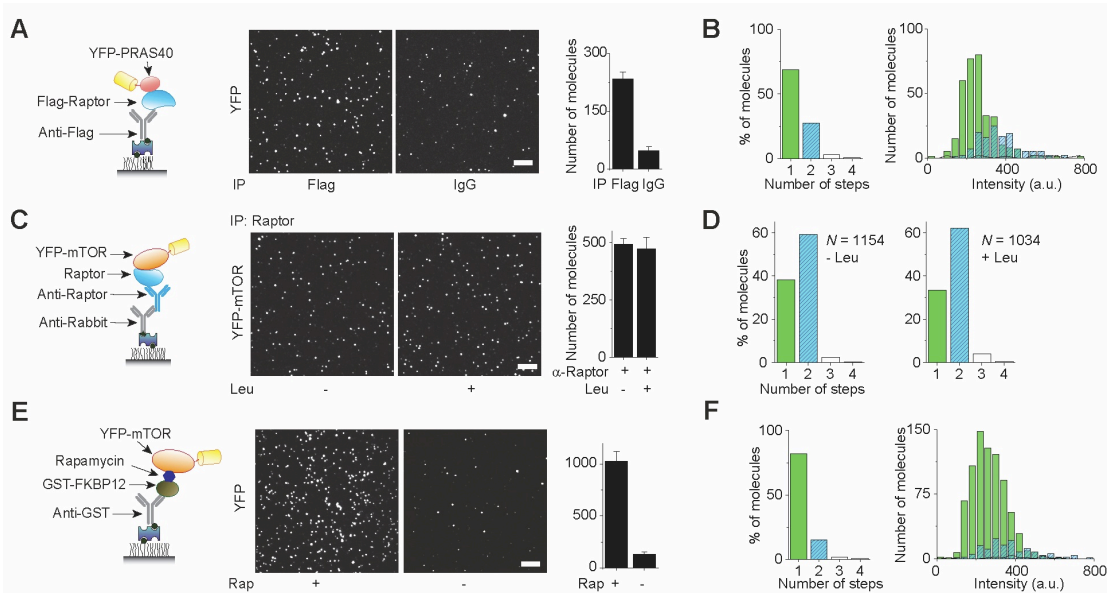

Figure III. 12. mTOR sub-complexes are monomeric. (A) YFP-PRAS40 and Flag-raptor were coexpressed and SiMPull was performed with Flag antibody. (B) YFP-PRAS40 bound to raptor was monomeric as indicated by photobleaching step distribution. (C) YFP-mTOR stable cells were starved (-) leucine (Leu) for 1 h followed by re-stimulation (+) with leucine for 15 min. mTORC1 was pulled down via endogenous raptor followed by SiMPull analysis. (D) mTORC1 dimeric stoichiometry did not change upon leucine stimulation. (E) Lysate from YFP-mTOR stable cells was applied to SiMPull chambers coated with purified FKBP12 with or without rapamycin. YFP-mTOR was captured via FKBP12 in the presence of rapamycin. (F) YFP-mTOR bound to FKBP12-rapamycin was monomeric as indicated by photobleaching step distribution. Scale bars: 5 μm.

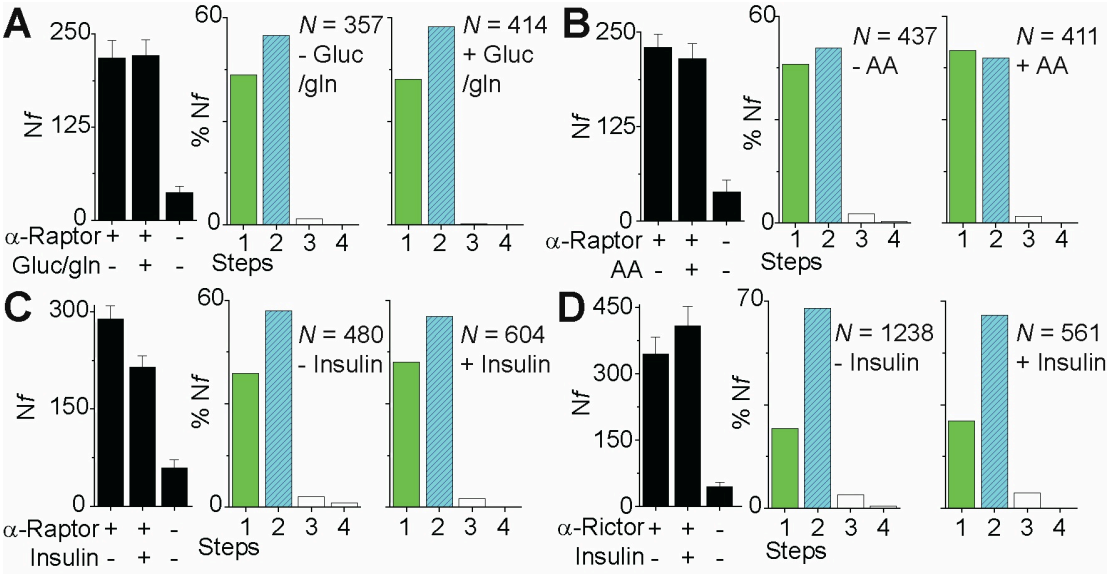

Figure III. 13. Effect of physiological stimulations on mTORCs. YFP-mTOR stable cells were starved (-) of (A) glucose and glutamine (Gluc/gln) for 12 h, (B) amino acids (AA) for 2 h or (C, D) serum for 24 h, followed by re-stimulation (+) with glucose/glutamine for 1 h, amino acids for 30 min, or 100 nM insulin for 30 min, respectively. mTORC1 (A-C) or mTORC2 (D) was pulled down via endogenous raptor or rictor, respectively, followed by SiMPull analysis.

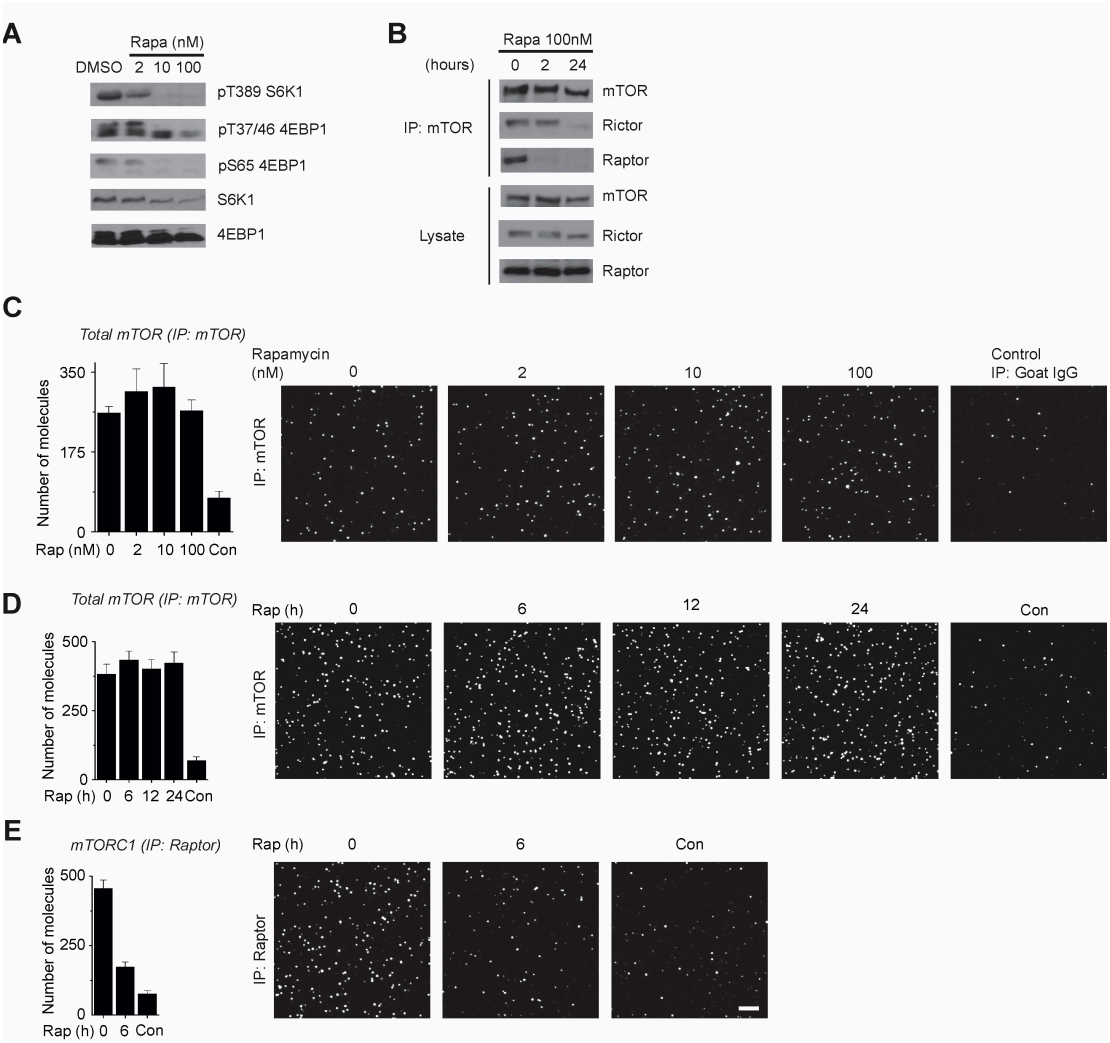

Figure III. 14. Effect of rapamycin on mTOR complexes. (A) HEK293 cells were treated with 2, 10 or 100 nM rapamycin for 30 min. Cell lysates were analyzed by Western blotting with the indicated antibodies. (B) Cells were treated with 100 nM rapamycin for 0, 2, and 24 h. Cell lysates were subjected to mTOR immunoprecipitation, and analyzed by Western blotting. (C) YFP-mTOR stable cells were treated with various doses of rapamycin for 30 min, and SiMPull was performed with an antibody against endogenous mTOR. (D) YFP-mTOR stable cells were treated with 100 nM rapamycin for various lengths of time, and SiMPull was performed with an antibody against endogenous mTOR. (E) Cells were treated as in (D), and SiMPull was performed with an antibody against endogenous raptor. Error bars in (C-E) represent standard deviation of the mean across 20 or more imaging areas. Scale bar: 5 μm.

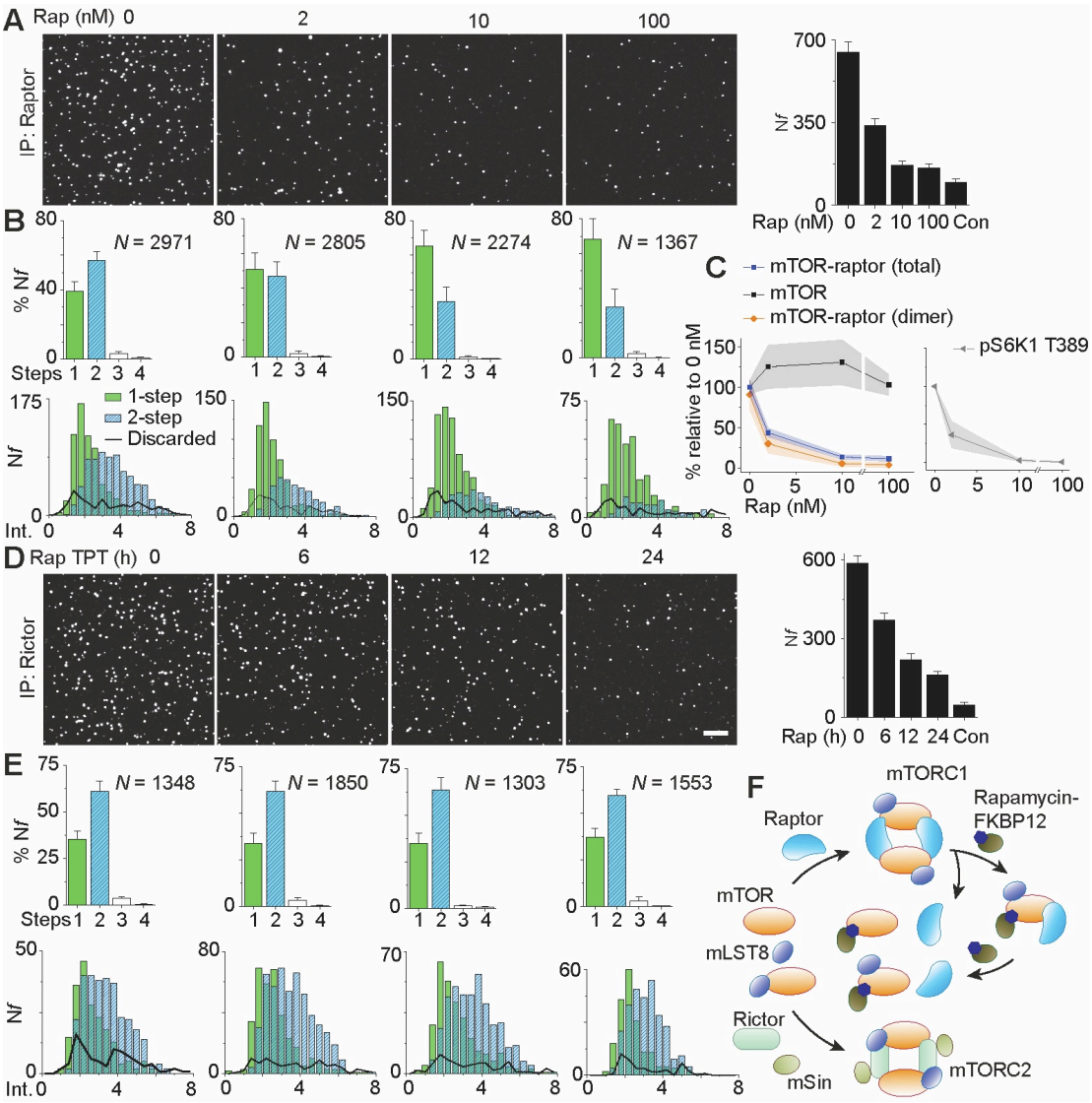

Figure III. 15. Effect of rapamycin on mTORCs. YFP-mTOR stable cells were treated with (A-C) increasing doses of rapamycin (Rap) for 30 min or (D-E) 100 nM rapamycin over the indicated time course. mTORC1 (A, B) and mTORC2 (D, E) were captured via endogenous raptor and rictor, respectively. Representative SiMPull images and number of molecules observed per imaging area are shown in (A, D). Scale bar: 5 μm. Distributions of fluorescence photobleaching steps are shown in (B, E). *N*, total number of molecules analyzed. (C) Left: relative levels of mTOR, mTOR-raptor (total), and mTOR-raptor (dimer) were obtained from SiMPull. Right: phosphorylation of S6K1 (pT389) was measured by Western blotting under similar conditions, and quantified by densitometry. TPT: time post treatment. (F) A model for the assembly of mTOR complexes. Individual mTORC components are monomeric and assemble into homo-dimeric holocomplexes, mTORC1 or mTORC2. Rapamycin directly disrupts the mTOR-raptor interaction leading to monomeric mTORC1 and single proteins. Rapamycin-FKBP12-associated mTOR cannot be incorporated into mTORC1 or mTORC2, resulting in indirect depletion of mTORC2 over time.

III. 6. References

Bakkenist, C. J. and M. B. Kastan (2003). "DNA damage activates ATM through intermolecular autophosphorylation and dimer dissociation." Nature 421(6922): 499-506.

Ball, H. L. and D. Cortez (2005). "ATRIP oligomerization is required for ATR-dependent checkpoint signaling." J Biol Chem 280(36): 31390-31396.

Dibble, C. C., J. M. Asara, et al. (2009). "Characterization of Rictor phosphorylation sites reveals direct regulation of mTOR complex 2 by S6K1." Mol Cell Biol 29(21): 5657-5670.

Dunne, P. D., R. A. Fernandes, et al. (2009). "DySCo: quantitating associations of membrane proteins using two-color single-molecule tracking." Biophys J 97(4): L5-7.

Fang, Y., M. Vilella-Bach, et al. (2001). "Phosphatidic acid-mediated mitogenic activation of mTOR signaling." Science 294(5548): 1942-1945.

Frias, M. A., C. C. Thoreen, et al. (2006). "mSin1 is necessary for Akt/PKB phosphorylation, and its isoforms define three distinct mTORC2s." Curr Biol 16(18): 1865-1870.

Goodsell, D. S. and A. J. Olson (2000). "Structural symmetry and protein function." Annu Rev Biophys Biomol Struct 29: 105-153.

Guertin, D. A., D. M. Stevens, et al. (2006). "Ablation in mice of the mTORC components raptor, rictor, or mLST8 reveals that mTORC2 is required for signaling to Akt-FOXO and PKCalpha, but not S6K1." Dev Cell 11(6): 859-871.

Huang, J. and B. D. Manning (2009). "A complex interplay between Akt, TSC2 and the two mTOR complexes." Biochem Soc Trans 37(Pt 1): 217-222.

Jain, A., R. Liu, et al. (2011). "Probing cellular protein complexes using single-molecule pull-down." Nature 473(7348): 484-488.

Jain, A., R. Liu, et al. (2012). "Single-molecule pull-down for studying protein interactions." Nat Protoc 7(3): 445-452.

Julien, L. A., A. Carriere, et al. (2010). "mTORC1-activated S6K1 phosphorylates Rictor on threonine 1135 and regulates mTORC2 signaling." Mol Cell Biol 30(4): 908-921.

Kim, D. H., D. D. Sarbassov, et al. (2002). "mTOR interacts with raptor to form a nutrient-sensitive complex that signals to the cell growth machinery." Cell 110(2): 163-175.

Kim, S. G., G. R. Hoffman, et al. (2013). "Metabolic stress controls mTORC1 lysosomal localization and dimerization by regulating the TTT-RUVBL1/2 complex." Mol Cell 49(1): 172-185.

Laplante, M. and D. M. Sabatini (2009). "mTOR signaling at a glance." J Cell Sci 122(Pt 20): 3589-3594.

Laplante, M. and D. M. Sabatini (2012). "mTOR signaling in growth control and disease." Cell 149(2): 274-293.

McMahon, L. P., K. M. Choi, et al. (2002). "The rapamycin-binding domain governs substrate selectivity by the mammalian target of rapamycin." Mol Cell Biol 22(21): 7428-7438.

Oshiro, N., K. Yoshino, et al. (2004). "Dissociation of raptor from mTOR is a mechanism of rapamycin-induced inhibition of mTOR function." Genes Cells 9(4): 359-366.

Peterson, T. R., M. Laplante, et al. (2009). "DEPTOR is an mTOR inhibitor frequently overexpressed in multiple myeloma cells and required for their survival." Cell 137(5): 873-886.

Riley, K. J., T. A. Yario, et al. (2012). "Association of Argonaute proteins and microRNAs can occur after cell lysis." RNA 18(9): 1581-1585.

Sarbassov, D. D., S. M. Ali, et al. (2004). "Rictor, a novel binding partner of mTOR, defines a rapamycin-insensitive and raptor-independent pathway that regulates the cytoskeleton." Curr Biol 14(14): 1296-1302.

Sarbassov, D. D., S. M. Ali, et al. (2006). "Prolonged rapamycin treatment inhibits mTORC2 assembly and Akt/PKB." Mol Cell 22(2): 159-168.

Sarbassov, D. D., D. A. Guertin, et al. (2005). "Phosphorylation and regulation of Akt/PKB by the rictor-mTOR complex." Science 307(5712): 1098-1101.

Spagnolo, L., A. Rivera-Calzada, et al. (2006). "Three-dimensional structure of the human DNA-PKcs/Ku70/Ku80 complex assembled on DNA and its implications for DNA DSB repair." Mol Cell 22(4): 511-519.

Takahara, T., K. Hara, et al. (2006). "Nutrient-dependent multimerization of the mammalian target of rapamycin through the N-terminal HEAT repeat region." J Biol Chem 281(39): 28605-28614.

Tao, Z., J. Barker, et al. (2010). "Steady-state kinetic and inhibition studies of the mammalian target of rapamycin (mTOR) kinase domain and mTOR complexes." Biochemistry 49(39): 8488-8498.

Ulbrich, M. H. and E. Y. Isacoff (2007). "Subunit counting in membrane-bound proteins." Nat Methods 4(4): 319-321.

Ulbrich, M. H. and E. Y. Isacoff (2008). "Rules of engagement for NMDA receptor subunits." Proc Natl Acad Sci U S A 105(37): 14163-14168.

Vander Haar, E., S. I. Lee, et al. (2007). "Insulin signalling to mTOR mediated by the Akt/PKB substrate PRAS40." Nat Cell Biol 9(3): 316-323.

Vilella-Bach, M., P. Nuzzi, et al. (1999). "The FKBP12-rapamycin-binding domain is required for FKBP12-rapamycin-associated protein kinase activity and G1 progression." J Biol Chem 274(7): 4266-4272.

Wang, L., C. J. Rhodes, et al. (2006). "Activation of mammalian target of rapamycin (mTOR) by insulin is associated with stimulation of 4EBP1 binding to dimeric mTOR complex 1." J Biol Chem 281(34): 24293-24303.

Wullschleger, S., R. Loewith, et al. (2005). "Molecular organization of target of rapamycin complex 2." J Biol Chem 280(35): 30697-30704.

Yang, H., D. G. Rudge, et al. (2013). "mTOR kinase structure, mechanism and regulation." Nature 497(7448): 217-223.

Yip, C. K., K. Murata, et al. (2010). "Structure of the human mTOR complex I and its implications for rapamycin inhibition." Mol Cell 38(5): 768-774.

Yoon, M. S., G. Du, et al. (2011). "Class III PI-3-kinase activates phospholipase D in an amino acid-sensing mTORC1 pathway." J Cell Biol 195(3): 435-447.

Zhang, Y., C. J. Billington, Jr., et al. (2006). "Drosophila target of rapamycin kinase functions as a multimer." Genetics 172(1): 355-362.

CHAPTER IV

Single-molecule analysis of lipid-protein interactions in crude cell lysates

IV. 1. Introduction

Lipid second messengers represent a small fraction of the cell membrane and organelles, and their levels are precisely controlled. They play essential signaling roles in diverse cellular processes such as cell growth, proliferation, metabolism, and differentiation (Wymann and Schneiter 2008). Phosphoinositides constitute a well-known group of signaling lipids, which play fundamental roles in cells. Phosphatidylinositol 3-phosphate (PI(3)P) is a well-studied phosphoinositide that is involved in endocytic and phagocytic trafficking, autophagy, and growth factor signaling (Gillooly, Morrow et al. 2000; Burman and Ktistakis 2010; Yoon, Du et al. 2011). Phosphatidylinositol 4,5-bisphosphate (PIP_2) is involved in the regulation of cell shape, migration, cytokinesis, and membrane trafficking events (Di Paolo and De Camilli 2006). Phosphatidylinositol 3,4,5-triphosphate (PIP_3) is found at low levels at the plasma membrane but is dramatically increased by growth factor stimulation (Hawkins, Jackson et al. 1992). PIP_3 is involved in cell proliferation, survival, metabolism, and it is implicated in diseases such as diabetes and cancer (Cantley 2002). Another important signaling lipid is phosphatidic acid (PA), which is involved cytoskeletal rearrangement, cellular trafficking for secretion and endocytosis, and growth factor signaling (Jenkins and Frohman 2005).

These signaling lipids are recognized by conserved lipid-binding domains (LBDs) that are widely present in proteins (DiNitto, Cronin et al. 2003). For example, FYVE domain has a conserved basic amino acid motif (RR/KHHCR) that contributes to a shallow, positively charged binding pocket for PI(3)P. PH domains exhibit a range of lipid selectivity depending on the amino acid residues present and on the cellular context. The PH domain of PLCδ is a specific effector for PIP_2 (Lemmon, Ferguson et al. 1995) while the PH domain of Akt binds preferentially to PIP_3, with an affinity in the nanomolar range (James, Downes et al. 1996; Frech, Andjelkovic et al. 1997; Rowland, Gong et al. 2012). In some instances, the LBD is not a well conserved module, as in the case of PA binding proteins, where the region involved in binding varies in sequence and structure from protein to protein, although a common feature is the presence of positively

charged amino acids that form electrostatic interactions with the head group of PA (Stace and Ktistakis 2006).

Several in-vitro ensemble assays such as surface plasmon resonance, isothermal titration calorimetry, size-exclusion chromatography, and centrifugation-based methods have traditionally been employed to investigate lipid-protein interactions to determine binding affinities of LBDs, and a handful of studies have probed these interactions with single-molecule resolution (Scott, Musselman et al. 2012). A major limitation of these studies lies in using purified recombinant proteins, which does not recapitulate the intracellular environment of a cell. Additionally, these assays typically require the separation of the unbound protein or lipid from the lipid-protein complex and therefore are not performed under equilibrium conditions. We previously reported the development of a single-molecule pulldown assay (SiMPull) to study protein complexes directly captured from cell lysates (Jain, Liu et al. 2011). In SiMPull, protein complexes are pulled down from freshly prepared cell lysates for single-molecule total internal reflection fluorescence microscopy. When proteins are stoichiometrically labeled, for example using fluorescent protein tags, SiMPull can reveal the stoichiometry of the protein complexes via single-molecule fluorescence photobleaching step analysis (Jain, Liu et al. 2011).

Here we present a novel approach based on the principle of SiMPull to interrogate lipid-protein interactions in crude cell lysates. We provide evidence of high sensitivity and specificity of our assay for a variety of LBDs and the full-length protein Akt. We also uncover new insights into the assembly of the LBDs and Akt on lipid vesicles.

IV. 2. Materials and methods

IV. 2. 1. Antibodies and reagents

All antibodies used were obtained from commercial sources as follows: mouse anti-GFP from Roche and Rockland Immunochemicals; biotinylated mouse anti-GFP from Jackson ImunoResearch Labs. 1-palmitoyl-2-oleoyl-sn-glycero-3-phosphocholine (POPC), 1-palmitoyl-2-oleoyl-sn-glycero-3-phosphate (POPA), 1-palmitoyl-2-oleoyl-sn-glycero-3-phospho-L-serine (POPS), 1,2-dioleoyl-sn-clycero-3-phopho-(1′-myo-inositol-4′,5′-bisphosphate) (PIP_2), 1,2-dioleoyl-sn-clycero-3-phopho-(1′-myo-inositol-3′,4′,5′-

trisphosphate) (PIP_3), and 1,2-dipalmitoyl-sn-glycero-3-phosphoethanolamine-N-(Cap Biotinyl) (biotinPE) were from Avanti Lipids Inc. Phosphatidylinositol-3-phosphate (PI(3)P) was from Echelon Biosciences Inc. 1,1′-dioctadecyl-3,3,3′,3′-tetramethylindodicarbocyanine perchlorate (DiD) was from Invitrogen. Purified GFP protein was from Abcam (ab84191).

IV. 2. 2. Plasmids

The GFP-2xHrs-FYVE construct was previously reported by the Stenmark laboratory (Gillooly, Morrow et al. 2000). GFP-2xSpo20-PABD was from the Du laboratory at The University of Texas Health Science Center at Houston (Zeniou-Meyer, Zabari et al. 2007) The following plasmids were obtained from Addgene: GFP-PLC-PH (#21179) (Botelho, Teruel et al. 2000), 2xPH-PLC-GFP (#35142) (Bohdanowicz, Cosio et al. 2010), GFP-Akt (#39531), and GFP-Akt-PH (#39533) (Watton and Downward 1999). GFP-Akt mutants (T308D/S473D; T308A/S473A; T308A/S473D; T308D/S473A) were created using QuickChange II mutagenesis kit (Stratagene). GFP-1xSpo20-PABD and GFP-1xHrs-FYVE were created by inserting a single copy of Spo20-PABD and Hrs-FYVE, respectively, into a gateway destination plasmid pCDNA5 with AttR1/R2 recombination sites and GFP fused at the N-terminus.

IV. 2. 3. Cell culture, transfection, and cell lysis

HEK293 cells were cultured in DMEM containing 10%(vol/vol) FBS at 37 °C with 5% (vol/vol) CO_2. Cells seeded in 6-well plates were transfected at 70-80% confluency with various plasmids (3 μg each well) using PolyFect following the manufacturer's recommendation (Qiagen). After 24 hr, cells were wash twice in ice-cold PBS and re-suspended in 150 μL per well of detergent-free buffer (40mM Hepes, pH 8, 150mM NaCl, 10mM ß-glycerophosphate, 10mM sodioum pyrophostate, 2mM EDTA, 1x Sigma protease inhibitor cocktail). Cells were lysed by passing 11 times through a 25G1 needle (BD PrecisionGlide), followed by centrifugation for 20 min at 14,000 xg to remove cell debris. The concentrations of GFP-fused LBDs in cell lysates were determined by western blotting followed by quantification of x-ray band intensities using the ImageJ software, with purified recombinant as GFP reference. All GFP-LBDs were

present at 2-3 μM in cell lysates in our study. Lysates were then diluted 10 to 100-fold with dilution buffer (20mM Tris·HCl , pH 8, 150mM NaCl) before loading into the imaging chamber.

IV. 2. 4. Vesicle preparation

Lipids in chloroform (0.5 μmol total) were dried under nitrogen gas, and resuspended in 300 μL vesicle buffer (10mM Tris·HCl, pH 8, 150mM NaCl) to a final concentration of 1.66 mM. Vesicles were formed by water bath sonication followed by probe sonication. Unilamellar vesicles were collected as the supernatant after ultracentrifugation at 194,398xg in a TLA100.3 rotor for 2hr at 25°C. Lipid compositions for the phosphoinositide vesicles were 5% PI(3)P, PIP_2, or PIP_3, 95% phosphatidylcholine (PC) as a carrier, 0.05% biotin-phosphatidylethanolamine (biotin-PE) for immobilization of the vesicles on imaging surface, and 0.1% C-18 DiD for fluorescence imaging of the vesicles. The composition of PA vesicles was similar as above except with 20% PA and 80% PC. Vesicles were diluted 500-fold to yield ~700 vesicles per 2,500 μm^2, loaded into imaging chamber, and incubated for 20 min before loading of cell lysates.

IV. 2. 5. Single-molecule imaging and quantification

A prism-type total internal reflection fluorescence microscope was used to acquire single-molecule data. Quartz slides were passivated with methoxy polyethylene glycol (PEG). The surfaces were doped with 2-5% biotinylated PEG. Immobilized DiD-labeled vesicles were excited at 647 nm and GFP-tagged LBDs were excited at 488 nm. Band pass filters (red dichroic 635 plus a 665 long pass from Semrock for DiD, and HQ 535/30 from Chroma Technology for GFP) were used to detect emission signal. All experiments were performed at room temperature (22–25°C).

Number of molecules, *S*, were determined by quantifying the number of GFP and DiD spots per imaging area (2,500 μm^2). The emission signal from each spot was recorded for 16 frames (100 ms each) and an intensity average calculated. Standard deviation was calculated from data collected from 10 or more different imaging areas. Cell lysate was present in the flow chamber during data acquisition.

IV. 2. 6. Single molecule co-localization

The percentage of colocalization between vesicles and proteins was quantified by determining the number of molecules, S, and position of each DiD and GFP spot present in the same imaging region. Positions of DiD and GFP spots were determined to 2-pixel accuracy by fitting a Gaussian point spread function. Spots lying within 2-pixel distance (pixel size, 150 nm) were considered to be co-localized. The percentage of GFP-positive spots that overlapped with DiD spots was calculated. To determine false co-localization by chance, two different regions were imaged for DiD and GFP, and similar analysis was performed. Co-localization by chance was observed to be ~6%.

IV. 2. 7. Single-molecule analysis for assembly plots

After addition of cell lysates into imaging chambers, several movies of 200-500 frames were recorded at different incubation times. The first 50 frames were taken with 647-laser excitation to localize DiD-labeled vesicles, followed by additional frames taken with 488-laser excitation to detect GFP molecules. Single-molecule fluorescent traces obtained from the movies were divided in three different categories: empty vesicles (only DiD signal), bound vesicles (DiD and GFP signals), and non-specifically bound GFP (only GFP signal). Single-molecule fluorescence traces showing DiD and GFP signal (bound vesicles) were further analyzed by Chung-Kennedy filtration algorithm to remove noise from raw GFP intensity profiles. Filtrated traces were manually scored for the number of bleaching steps to determine the number of GFP molecules per vesicle, N_{GFP}. The fluorescence traces were classified as having 1–10 bleaching steps. The fraction of vesicles bound (F_v) was calculated from the number of empty vesicles and bound vesicles. N_{GFP} per vesicle at different incubation times were used to build the assembly plots.

To determine the stoichiometry of vesicle-free proteins, GFP-LBDs in cell lysates were captured using biotinylated GFP antibodies immobilized to the surface via biotin-NeutrAvidin interaction. Copy number of GFP was determined by photobleaching step analysis as described above. To avoid false colocalization, samples were immobilized at a surface density of (~400 molecules per 2,500 μm^2 imaging area) by adjusting the dilution factor for diluting each lysate (1000 to -5000- fold). The fluorescence trace of each

molecule was classified as having one to four bleaching steps or was discarded if no clean bleaching steps could be identified. At least 300 molecules were evaluated for each experiment; the total number of molecules successfully scored as bleaching in one to four steps is depicted in the figures.

IV. 3. Results

IV. 3. 1. Detection of lipid-protein interaction in crude mammalian cell lysates

To establish a single-molecule assay for lipid-protein interactions in crude cell lysates, we chose three signaling lipid and LBD pairs that have been reported to display specific interactions: PI(3)P and Hrs-FYVE domain (Gillooly, Morrow et al. 2000); PIP_2 and PLCδ-PH domain (Lemmon, Ferguson et al. 1995); PA and Spo20-PABD domain (Nakanishi, de los Santos et al. 2004). Small unilamellar vesicles were prepared containing each of these signaling lipids and PC as a carrier, biotinylated phosphatidylethanolamine (biotin-PE) for immobilizing the vesicles on imaging surfaces, and C18-DiD to label the vesicles fluorescently. The vesicles were immobilized on biotin-polyethylene glycol (biotin-PEG)-passivated microscopic slides aided by NeutrAvidin at a density that allowed single-vesicle resolution. The LBDs were expressed in HEK293 cells as GFP-fusions of tandem repeats (i.e., 2xFYVE, 2xPH, and 2xPABD), which have been commonly used as specific lipid sensors (Balla and Varnai 2002). Detergent-free cell lysates expressing the LBDs were added to chambers of slides coated with the vesicles, and TIRF microscopy was performed to visualize vesicles via DiD and bound proteins via GFP. A schematic of the method is depicted in Figure IV.1A. The number of DiDs incorporated into each vesicle was determined by single-step photobleaching analysis, with most vesicles containing 6-8 dyes (Fig. IV.2), which is in agreement with the concentration of DiD used and the expected size of vesicles.

As shown in Figure IV.1B, when lysates expressing the 2xFYVE sensor were added to various vesicles, we observed single-vesicle GFP fluorescent spots specifically in the PI(3)P-containing vesicles; all other vesicles displayed only background levels of GFP signals coming from surface impurities or nonspecific binding to the surface. Quantification of the GFP and DiD fluorescent spots are shown in Figure IV.1C.

Similarly, specific binding was observed from lysates expressing 2xPABD and 2xPH to PA and PIP_2 vesicles, respectively (Fig. IV. 1D-G).

To confirm that LBDs were indeed captured by vesicles and not interacting non-specifically with the surface, we super-imposed the DiD images of vesicles with the corresponding GFP images of the LBDs, and found ~50-60% of GFP molecules colocalized to vesicles (Fig. IV. 3A-D). The colocalization did not reach 100% most likely because of unlabeled vesicles, inactive chromophores and surface impurities. Colocalization occurring due to chance was determined by overlapping DiD and GFP images from two different regions and was found to be approximately 6%. In summary, our assays detected lipid-protein interactions from whole cell lysates with high specificity.

IV. 3. 2. Acquisition of assembly properties for LBDs

Next, we sought to determine the binding dynamics of each LBD to its target phospholipid vesicles. Using single-molecule TIRF microscopy we monitored binding-dissociation events of the GFP-LBDs with the immobilized vesicles. We obtained two-minute duration movies, where DiD was first briefly excited followed by longer GFP excitation (Fig. IV.4A). This strategy allowed us to eliminate GFP spots derived from surface impurities and LBDs bound to unlabeled vesicles. Therefore, we could monitor in real-time only LBDs that were bound to labeled vesicles. The movies were acquired after incubating LBD-expressing lysates with vesicles for different times ranging from 0 to 30 minutes. Cell lysates were present in the flow chamber during movie acquisition to ensure that any transient binding events were also captured.

For all the single-molecule analyses we obtained two parameters: the fraction of LBD-bound vesicles (F_v), and the number of LBDs per vesicle (N_{GFP}) derived from the number of photobleaching steps of GFP. The percentage of vesicles with a particular number of LBD-bound molecules was then calculated. Because the noise in single-molecule traces of GFP made it difficult to clearly distinguish real photobleaching steps from inherent noise in GFP fluorescence (Dickson, Cubitt et al. 1997), we used Chung-Kennedy filtration algorithm to average out noise from the raw GFP intensity profiles

(Chung and Kennedy 1991) (Fig. IV. 4B,C). This enabled us to count clearly the number of photobleaching steps when more than 4 molecules were bound (Fig. IV.4D).

Applying this analysis scheme, we observed over an incubation time course increased binding of 2xFYVE to PI(3)P vesicles (Fig. IV. 5A), as well as N_{GFP}, reflected by an increase in brightness of GFP spots (Fig. IV. 5B, left panels). Single-vesicle fluorescent traces of 2xFYVE revealed two distinct binding behaviors: transient binding of one 2xFYVE per vesicle and stable binding of multiple 2xFYVE per vesicle (Fig. IV. 5B, right panels). The increase in N_{GFP} over time is more clearly depicted in Figure IV. 5C. Immediately after the loading of lysates, most vesicles (~80%) were unbound and a few (~10%) had one or two proteins per vesicle. After 30 minutes of incubation, more than half of the vesicles were occupied by two to 5 proteins.

We next analyzed 2xPABD binding to PA vesicles. The fraction of bound vesicles, F_v, increased with the incubation time, although at a different rate from 2xFYVE (Fig. IV. 5A). At the same time, N_{GFP} also increased, as reflected by an increase in brightness of GFP spots (Fig. IV. 5D, left panels). Single-vesicle fluorescent traces at three different incubation times revealed that 2xPABD assembled stably onto PA vesicles, without transient binding events as observed for 2xFYVE (Fig. IV. 5D, right panels). The percentage of vesicles with various N_{GFP} was plotted over incubation time as shown in Figure IV. 5E. Immediately after the addition of 2xPABD lysate, we observed unbound vesicles (40%) and vesicles with one copy of the protein (37%) . Over time, more vesicles became populated with multiple copies of 2xPABD, such that by 30 minutes almost 90% of the vesicles had two or more copies of the protein.

Analysis of 2xPH interaction with PIP_2 vesicles revealed two distinct populations of vesicles that displayed stable and transient binding, respectively (Fig. IV. 5F). Interestingly, although the fraction of bound vesicles, F_v, increased over incubation time (Fig. IV. 5A), the number of proteins per vesicle, N_{GFP}, did not change markedly (Fig. IV. 5G). Most vesicles had one (50%) and two copies (25%) of 2xPH bound, and only 16% vesicles had three copies by 30 minutes. To rule out the possibility that the GFP-tagged fusion proteins might oligomerize independent of vesicle binding, we analyzed the stoichiometry of tandem LBDs pulled down by an anti-GFP antibody under the same

conditions as above. As shown in Figure IV. 6A-C, all these fusion proteins were monomeric in the absence of vesicles.

IV. 3. 3. Assembly of lipid binding domains in a monomer configuration

Having established our assay to study lipid-protein interactions using tandem lipid-domains that are commonly used as biosensors, we decided to investigate the binding of single-copy LBDs, which is the most common configuration present in cellular proteins. Cell lysates expressing 1xPABD or 1xPH were prepared and subjected to analyses as described above. Specific pulldown of each LBD by its expected target lipid was observed (Fig. IV. 7A-D). These LBDs showed a colocalization of 55-60% with their respective vesicles (Fig. IV.7E-G, confirming specific lipid-protein interaction.

We also tested 1xFYVE but could not detect any interaction with PI(3)P. This consistent with the previously reported lack of monomeric Hrs-FYVE binding to PI(3)P in live cell imaging experiments (Gillooly, Morrow et al. 2000), and the requirement of Hrs-FYVE dimerization for PI(3)P recognition (Gillooly, Morrow et al. 2000; Hayakawa, Hayes et al. 2004).

Next we examined the assembly behavior of monomeric LBDs, in order to compare them to their tandem dimeric counterparts. Most of the vesicles ($F_v \approx 0.9$) were occupied by 1xPABD within 2 min of cell lysate loading (Fig. IV. 8A) indicating a fast binding rate. Single-vesicle fluorescent traces revealed transient binding of 1xPABD, as seen by many short-lived binding-dissociation events in a single movie (Fig. IV. 8B). Photobleaching step analysis indicated that the distribution of N_{GFP} for 1xPABD was up to five copies per vesicle and did not change markedly over incubation time (Fig. IV. 8C). These results are in contrast to those for 2xPABD, which displayed only stable binding events (Fig. IV. 5D,E), higher N_{GFP} over time, and slower rate of vesicle occupancy. The dimeric and monomeric PABD were present at a similar level in cell lysates, as determined by western blotting (data not shown).

The monomeric PH sensor also had a faster rate of vesicle occupancy (Fig. IV. 8A) compared to 2xPH (Fig. IV. 5A). Again, expression levels of the monomeric and dimeric PH were comparable. Additionally, only transient binding events were observed for 1xPH (Fig. IV. 8D), with a dissociation rate of 2.33 ± 0.3 sec^{-1} (Fig. IV. 8E).

Consistent with these short-lived binding events, 1xPH was found to bind PIP_2 only at 1 copy per vesicle. We measured transient binding at two different laser intensities and obtained the same results, confirming that the lifetime and photoblinking of GFP emission did not contribute to k_{off} determination (Fig. IV. 8D,E). These monomeric LBDs did not oligomerize by themselves, as shown by anti-GFP pull-down followed by photobleaching analysis (Fig. IV. 8F,G).

Overall, our results suggest that tandem LBDs bind lipid vesicles at a slower rate but more stably and at higher copy numbers than their monomeric counterparts.

IV. 3. 4. Assay applicability to protein kinase Akt

After validating the versatility and specificity of our assay using LBDs, we deemed it necessary to explore the applicability of the assay to intact proteins. To that end, we decided to pursue Akt, a protein kinase of vast biological significance. Akt contain a PH domain that binds to PIP_3 with nanomolar affinity (James, Downes et al. 1996; Frech, Andjelkovic et al. 1997; Rowland, Gong et al. 2012). We expressed GFP-tagged full-length Akt in HEK293 cells and observed its specific pulldown by immobilized PIP_3 vesicles (Fig. IV. 9A,B), with ~ 47% of Akt colocalizing with the vesicles (Fig. IV. 9E,G). We further investigated the PH domain of Akt, in order to make comparisons with full-length Akt. Specific pull-down of Akt-PH by PIP_3 vesicles was observed (Fig. IV. 9C,D), with 53% of GFP signals colocalizing with the vesicles (Fig. IV. 9F,G).

Next, we determined the assembly properties of Akt and Akt-PH on PIP_3 vesicles. Akt-PH association with vesicles occurred very rapidly, and within 2 min of lysate loading 90% of the vesicles were bound (Fig. IV. 10A black line). In contrast, only ~40% of vesicles were occupied by full-length Akt even after 30 min incubation (Fig. IV. 10A gray line). Interestingly, Akt binding seemed highly stable as revealed by the single-vesicle traces (Fig. IV. 10B). Additionally, we found that most bound vesicles had one or two copies of Akt irrespective of the lysate incubation time (Fig. IV. 10C). In contrast, single-vesicle fluorescent traces of Akt-PH revealed both stable and transient interactions between the domain and the lipid (Fig. IV. 10D), and the number of molecules per vesicle, $N_{GFP,}$ increased with the incubation time (Fig. IV. 10E). Akt and Akt-PH were

present at similar levels in the cell lysates as confirmed by Western blotting (data not shown). GFP-Akt by itself was monomeric, as shown by photobleaching analysis following anti-GFP pull-down (Fig. IV. 10F).

We wondered if the difference in binding behavior between Akt and its PH domain could be due to intra-molecular interactions within Akt. Indeed, it has long been speculated that activation of Akt, primarily through membrane recruitment (via PIP_3) and phosphorylation on T308 and S473, involves conformational change of the protein. An extension of that speculation is that Akt membrane association is influenced by its phosphorylation or activation state. We compared serum-starved and serum-stimulated cells for the analysis of Akt-PIP_3 interaction, but did not observe any difference (data not shown). However, it was possible that only a small fraction of Akt was activated in cells upon serum stimulation. To unequivocally examine a possible role of phosphorylation (and thus activation) of Akt on its lipid binding properties, we created the following nonphosphorylatable and phosphomimetic mutants of Akt and analyzed their binding to PIP_3 vesicles: T308A/S473A, T308D/S473D, T308A/S473D, and T308D/S473A. As shown in Figure IV. 11A,B, all the mutants bound and colocalized with PIP_3 to a similar extent. These results suggest that phosphorylation of T308 and S473 does not impact Akt binding to PIP_3. This conclusion is surprising and important, as it disproves a long-held model of Akt activation.

IV. 4. Discussion

We have developed a new approach to study lipid-protein interactions that allow acquisition of kinetic parameters and detection of distinctive assembly properties in crude cell extracts. We first demonstrated the versatility of our assay to detect specific binding of several LBDs to their lipid target, followed by the application to a full-length protein binding to its lipid target. A distinctive advantage of our approach is that it addresses proteins expressed in human cell lines and the assay is conducted in a more physiological context where unknown components are present in the cell extract.

The single-molecule fluorescence and CK filtration allowed comprehensive understanding of assembly mechanisms of the lipid-binding domains and protein. We were able to monitor each binding and unbinding event of LBDs to single immobilized

vesicles and discovered novel and distinct assembly properties of the three common domains present in lipid binding proteins: PH, FYVE and PABD in their monomeric and dimeric form, binding to PIP_2, PI(3)P and PA respectively. The monomers for all LBDs displayed transient binding occurring at different dissociation rates. The difference between the monomers could result from the chemical and structural properties of lipid-protein interaction or could occur as an effect of other proteins present in the cell extract competing for the phospholipid binding. At this point, we cannot distinguish between the two. A striking result was that tandem LBDs displayed higher stability in terms of their residence time on the lipid vesicles likely due to two lipid-binding pockets. 2xPABD shows only stable interaction and could assemble up to nine copies per vesicle. Interestingly, 2xPH shows stable and transient interactions, but the distribution of copies per vesicle did not change over time. This may be explained by faster dissociations events maintaining this distribution, as evidenced by binding-unbinding events observed in the single-molecule fluorescence traces. Similar to 2xPH , tandem FYVE showed transient and stable binding characteristics. We propose that 2xFYVE sensor by itself shows transient interaction with PI(3)P, and its binding becomes stable when it encounters more copies of itself during the lysate incubation period. Additionally, this suggests a spatial rearrangement of the bound proteins and lipids on the vesicle resulting in formation of membrane nanodomains. These nanodomains could be small clusters of many 2xFYVE and PI(3)P lipids. This hypothesis is also supported by the inability of monomer FYVE to show PI(3)P binding in our assay, most likely due to very short-lived and unstable interactions beyond the scope of our measurement.

We observed differences in binding behavior between two different PH domains: the PH domain of PLCδ and of Akt. PLCδ-PH shows only transient interactions with a dissociation rate of 2.33 ± 0.3 sec^{-1}. This rate is consistent with its biological function of detecting the lipid PIP_2 but rapidly dissociate to allow subsequent cleavage by the catalytic domain of PLCδ to produce inositol 1,4,5-trisphosphate and diacylglycerol. On the other hand, the PH domain of Akt bound both transiently and stably to its target lipid PIP_3. In this case, it may be beneficial for Akt to have a longer residence time on the membrane to allow the protein kinases, such as PDK1 and mTORC2, to bind and phosphorylate Akt on the membrane before it is dissociates.

We used Akt as model system, validating that our assay can be used with full-length proteins expressed in cell lysates. We were also able to compare the binding properties of full-length Akt and its isolated PH domain. Our results indicate a striking difference in binding kinetic and binding dynamic between full-length Akt and its isolated PH domain. To our knowledge, such a difference in the assembly properties and binding between Akt and its isolated PH domain has not been reported before (Frech, Andjelkovic et al. 1997), and could be possible because of the single-molecule resolution in our lipid-binding assay.

It has been proposed that inactive Akt is in a conformation where the PH domain is protected from binding to the lipid (Calleja, Alcor et al. 2007), and this configuration may change due to regulatory proteins or post-translational modification. Our data indicates that phosphorylation at T308 and S473 sites do not affect Akt binding to PIP_3. These results challenge the model where phosphorylation plays a key role in regulating membrane recruitment of Akt, and indicates that other regulatory proteins or different posttranslational modifications are playing a key role in this process.

Further development of this assay, such as an extension to large macromolecular complexes interacting with signaling lipids, and coupling with microfluidic devices, high-throughput technologies, and single cell sensitivity, will allow the investigation of lipid-protein interactions at a new scale.

IV. 5. Figures

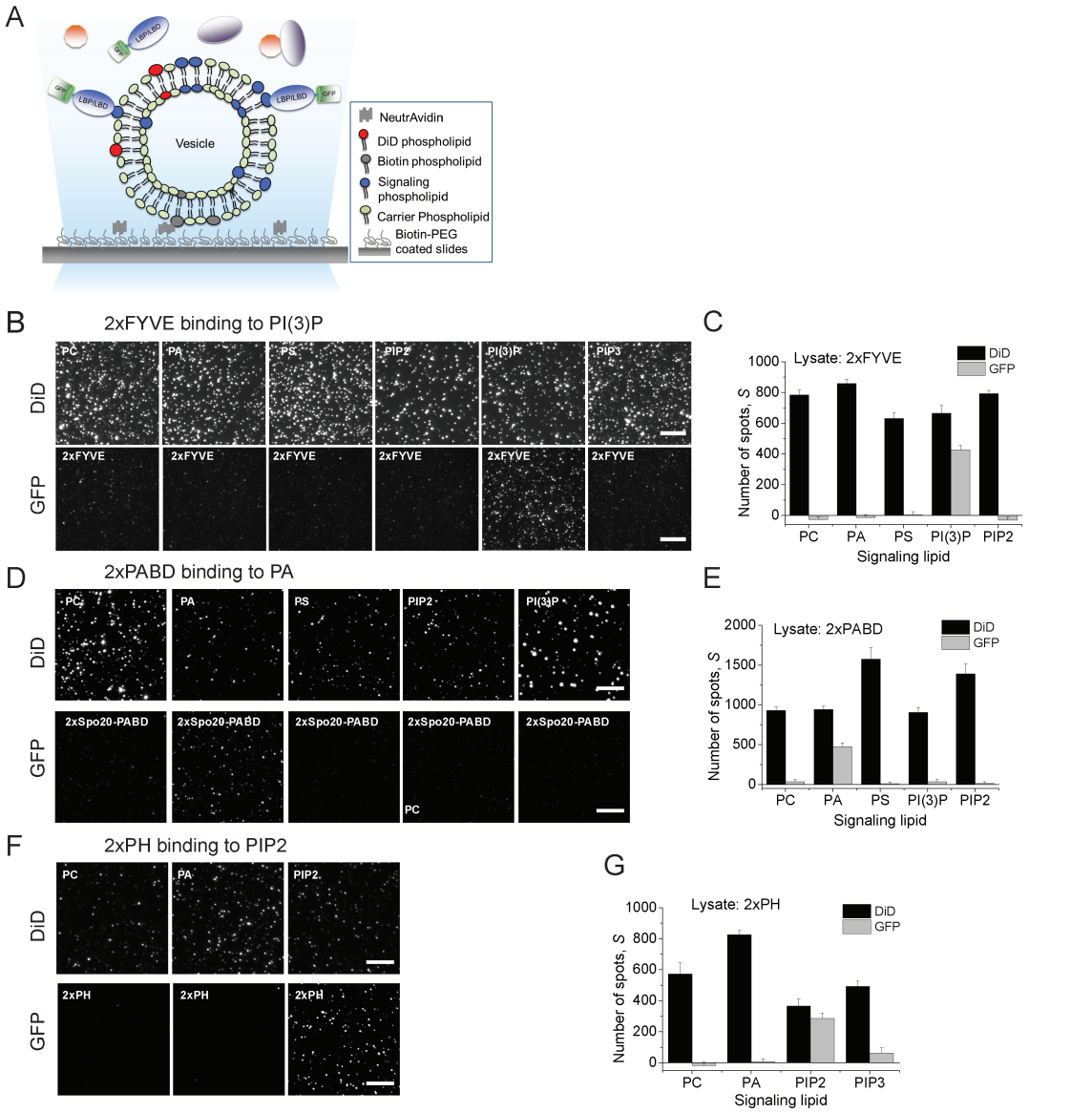

Figure. IV. 1. Detection of lipid-protein interactions in crude cell lysates.
(A) Schematic of the single-molecule lipid-protein interaction assay. (B) Single-molecule TIRF images of different vesicles (DiD, shown in top row) and the corresponding 2xFYVE (GFP, shown in bottom row). (C) Quantification of 2xFYVE pull-down by different lipid vesicles (D) Single-molecule TIRF images of different vesicles (DiD, shown in top row) and the corresponding 2xPABD (GFP, shown in bottom row). (E). Quantification of 2xPABD pull-down by different lipid vesicles. (F) Single-molecule TIRF images of different vesicles (DiD, shown in top row) and the corresponding 2xPH (GFP, shown in bottom row) (G) Quantification of 2xPH pull-down by different lipid vesicles. Error bars depict standard deviation of the mean across 10 or more imaging areas. Scale bar is 10μm.

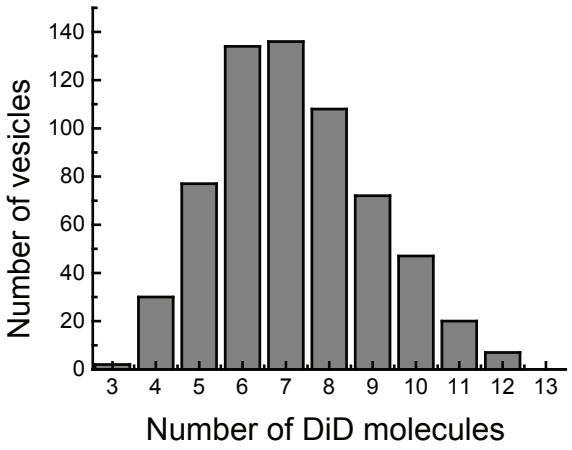

Figure. IV. 2. Number of DiD molecules per vesicle. Vesicles (containing Biotin-PE) where captured on the surface via biotin-NeutrAvidin interaction. Number of DiD molecules was determined by fluorescent photobleaching analysis after laser excitation at 647 nm. Most vesicles have 6-8 DiD molecules per vesicle.

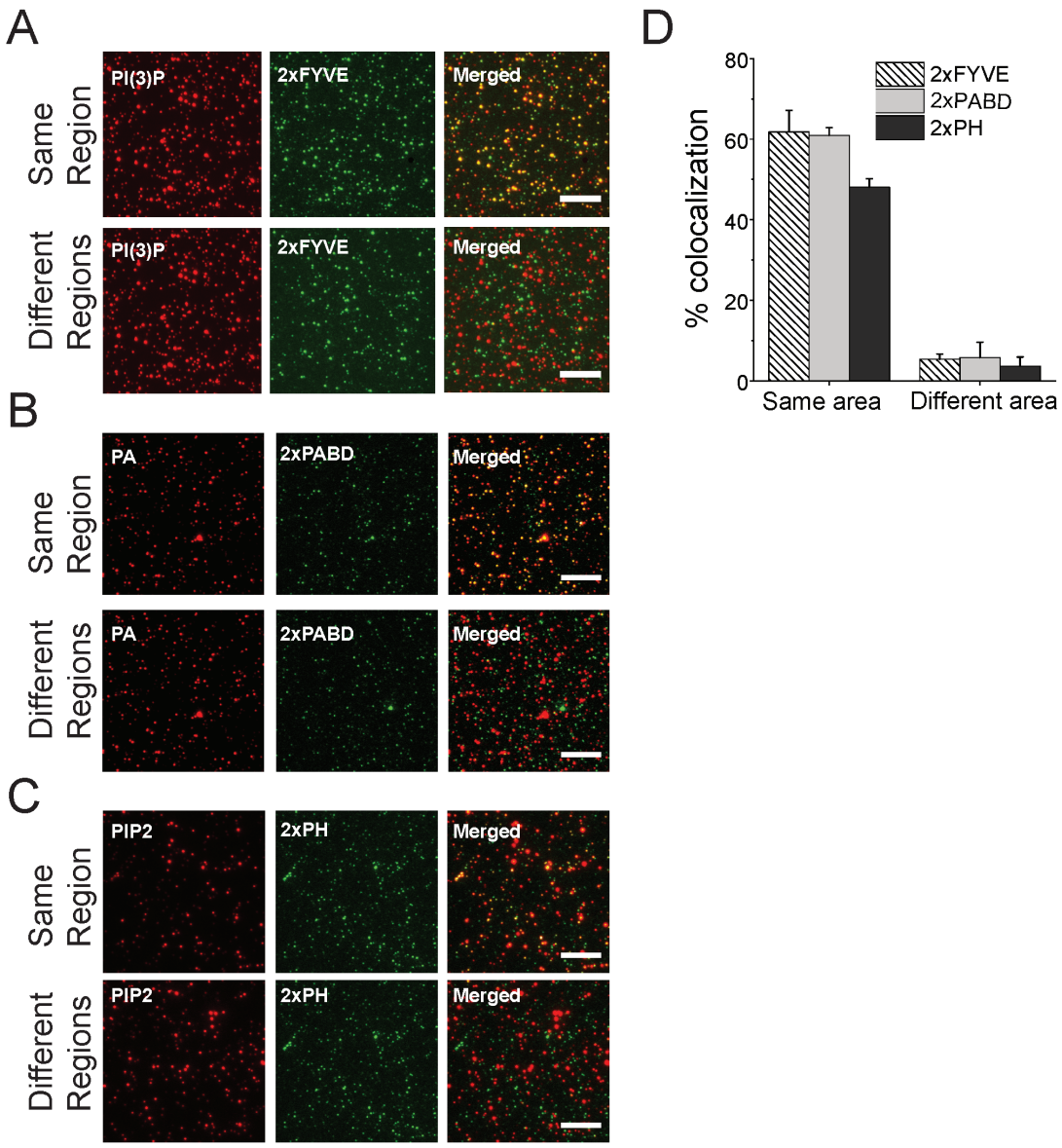

Figure. IV. 3. Colocalization of tandem LBDs with lipid vesicles. (A-C) TIRF images show the overlay of 2xFYVE, 2xPABD, and 2xPH with PI(3)P, PA, and PIP_2 vesicles, respectively. Overlay from the same region is shown in top rows and from different regions is shown in bottom rows. (D) Percentage colocalization of 2FYVE, 2xPABD, and 2xPH to PI(3)P, PA, and PIP_2 vesicles, respectively, from same and different regions. Error bars depict standard deviation of the mean across 10 or more imaging areas. Scale bar is 10μm.

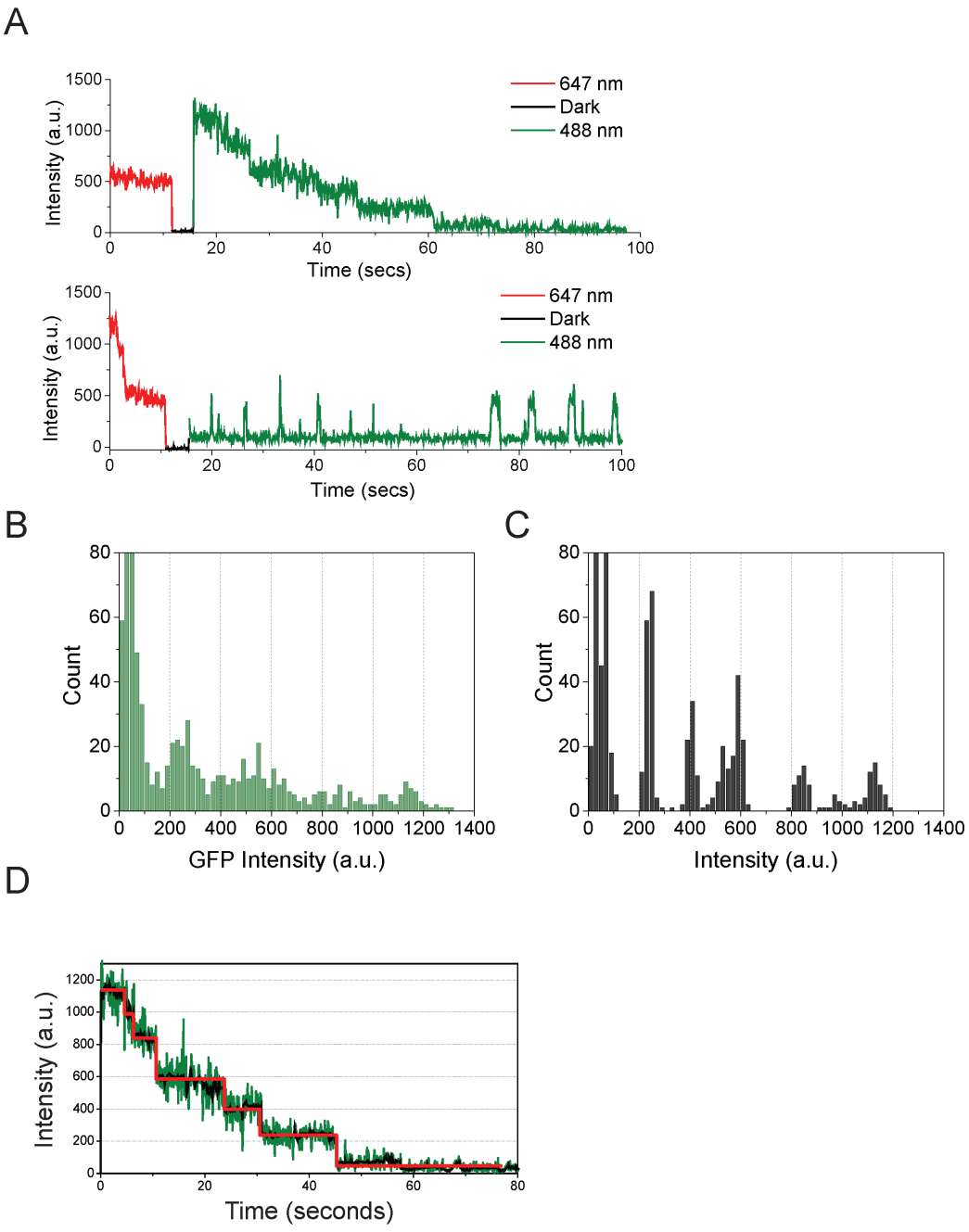

Figure. IV. 4. Framework for data acquisition and analysis. (A) Single molecule fluorescent traces depicting DiD labeled vesicle (red line, 647 nm excitation) and GFP signal (green line, 488 nm excitation). (B-C) Chung-Kennedy filtration algorithm: Intensity histogram of GFP fluorescence before (B) and after CK filtration (C), for calculating number of photobleaching steps. (D) Visualization of 6 photobleaching steps (red line) after CK filtration. Raw single-molecule trace (green) over-imposed with trace generated by CK filtration (red line).

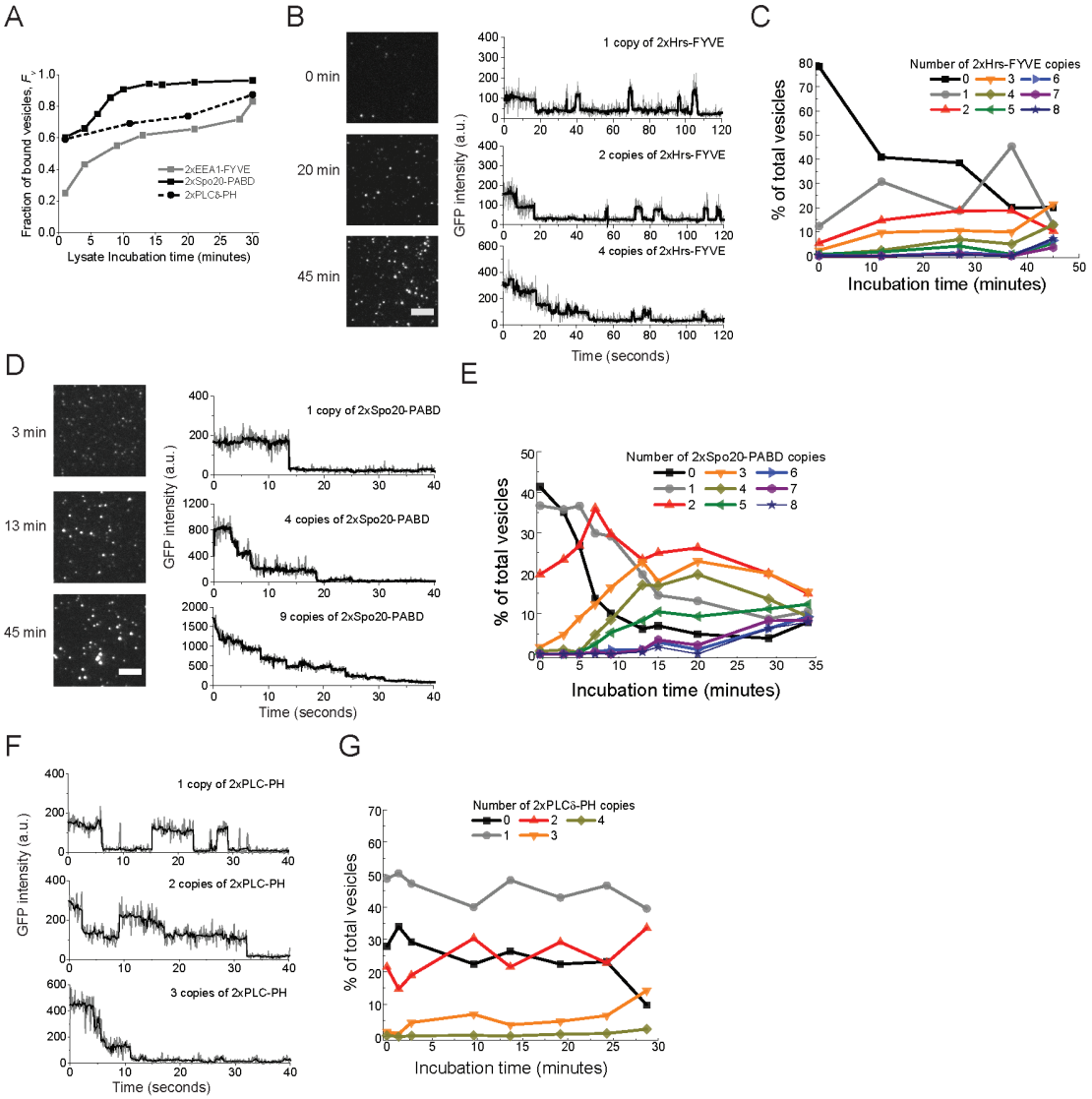

Figure. IV. 5. Assembly properties of tandem LBDs on lipid vesicles. (A) Time course of 2xFYVE, 2xPABD, and 2xPH binding to lipid vesicles. (B) Single-molecule TIRF images of 2xFYVE bound to PI(3)P vesicles from three different incubation times to show increasing intensity and number of GFP spots. Single-molecule fluorescence traces show the increase in total intensity along with stable and transient binding properties seen for 2xFYVE. (C) Assembly plot depicts an increase in number of 2xFYVE copies with longer incubation time. Example of 1, 2 and 4 copies are shown in (B). (D) Single-molecule TIRF images of 2xPABD bound to PA vesicles obtained from three different incubation times to show increasing intensity of each GFP spot. This can also be seen in the single-molecule fluorescent traces with higher total intensity. (E) Assembly plot depicts an increase in number of 2xPABD copies with longer incubation time. Example of 1, 4, and 9 copies are shown in (D). (F) Single-molecule fluorescent traces show examples of 1, 2, and 3 copies, taken at three different incubation times. (G) Assembly plot shows that the number of 2xPH copies do not change over the incubation time. Scale bar is 5μm.

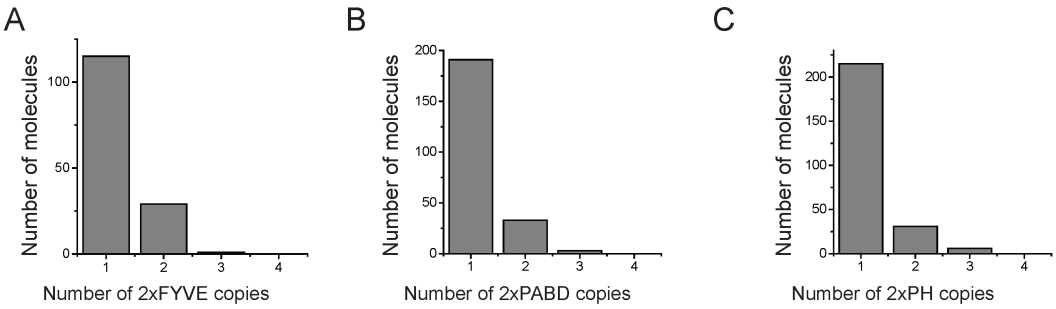

Figure. IV. 6. Stoichiometry of tandem LBDs. (A-C) Distribution of fluorescent photobleaching steps for 2xFYVE, 2xPABD, and 2xPH, respectively. Tandem LBDs were captured from cell lysate using biotinylated antiGFP antibody.

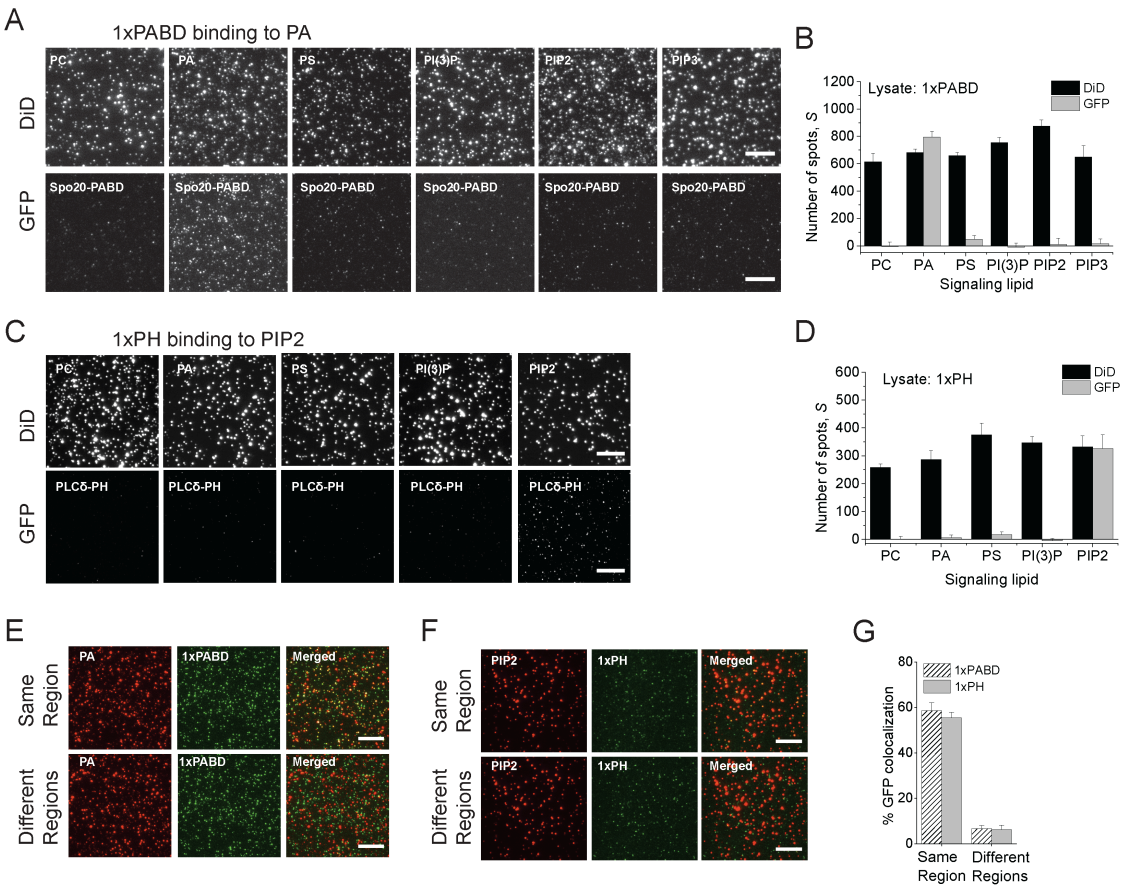

Figure. IV. 7. Specific binding and colocalization of single-copy LBDs. (A) Single-molecule TIRF images of different lipid vesicles (DiD, shown in top row) and the corresponding 1xPABD (GFP, shown in bottom row). (B) Quantification of 1xPABD pull-down by different lipid vesicles. (C) Single-molecule TIRF images of different lipid vesicles (DiD, shown in top row) and the corresponding 1xPH (GFP, shown in bottom row). (D) Quantification of 1xPH pull-down by different lipid vesicles. (E-F) TIRF images show the overlay of 1xPABD with PA vesicles and of 1xPH with PIP_2 vesicles, respectively. Overlay from the same region is shown in top rows and overlay from different regions is shown in bottom rows. (G) Percentage colocalization of 1xPABD and 1xPH to PA and PIP_2 vesicles, respectively, from same and different and regions. Error bars depict standard deviation of the mean across 10 or more imaging areas. Scale bar is 10μm.

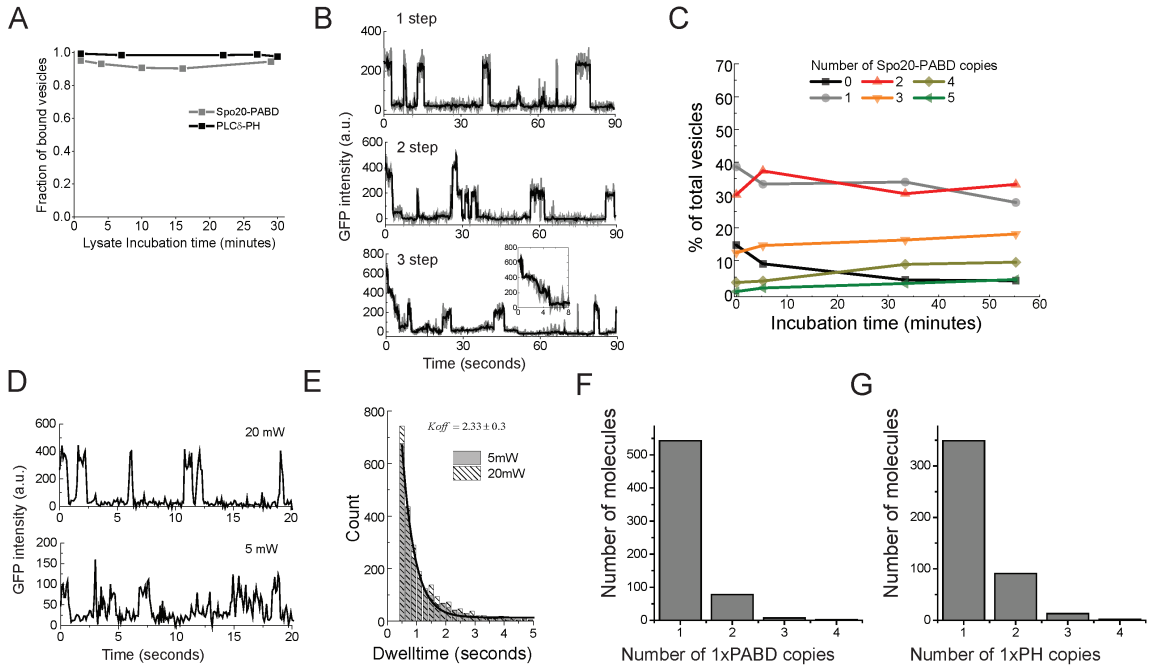

Figure. IV. 8. Assembly properties of single-copy LBDs on lipid vesicles. (A) Time course of 1xPABD and 1xPH binding to lipid vesicles. (B) Single-molecule fluorescent traces of 1xPABD bound to PA vesicles to show examples of 1, 2, and 3 copies per vesicle. (C) Assembly plot shows that the number 1xPABD copies per vesicle do not change with longer incubation time. (D) Single-molecule fluorescent traces of 1xPH bound to PIP_2 to show transient binding events. The two traces correspond to two different laser intensities (20 mW and 5 mW). (E) Dwelltime histogram of 1xPH molecules fitted to exponential decay to give off-rate of 2.33 ± 0.3 sec^{-1}.
(F-G) Distribution of fluorescent photobleaching steps for 1xPABD and 1xPH, respectively. GFP-LBDs were captured from cell lysate using biotinylated antiGFP antibody.

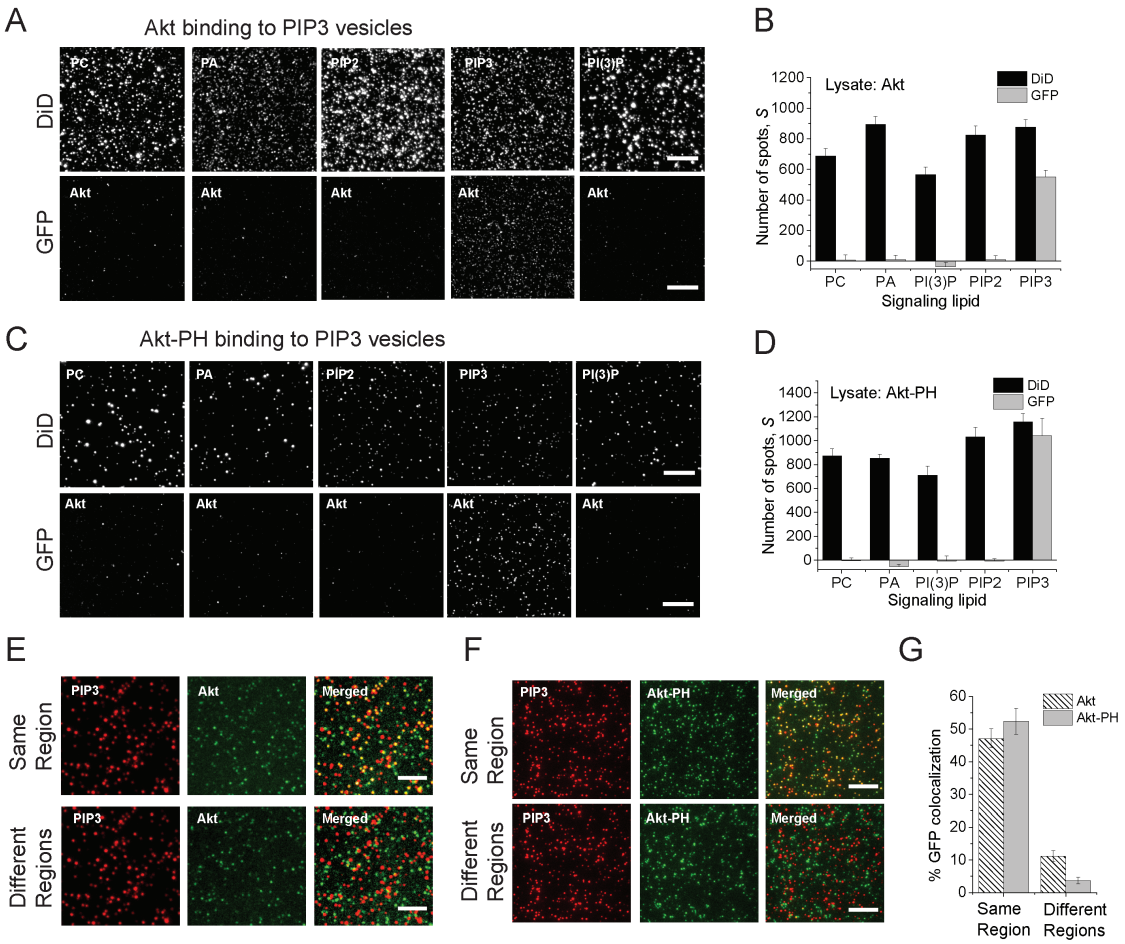

Figure. IV. 9. Assay applicability to protein kinase Akt. (A) Single-molecule TIRF images of several vesicles (GFP, shown in top rows) and the corresponding Akt (GFP, shown in bottom row). (B) Quantification of Akt pull-down by different lipid vesicles. (C) Single-molecule TIRF images of several vesicles (DiD, shown in top rows) and the corresponding Akt-PH (GFP, shown in bottom row). (D) Quantification of Akt-PH pull-down by different lipid vesicles. (E-F) TIRF images show the overlay of Akt (E) and Akt-PH (F) with DiD-labeled PIP_3 vesicles. Overlay from the same region is shown in top rows and overlay from different regions is shown in bottom rows. (G) Percentage colocalization of Akt and Akt-PH to PIP_3 vesicles, from same and different regions. Error bars depict standard deviation of the mean across 10 or more imaging areas. Scale bar is 10μm.

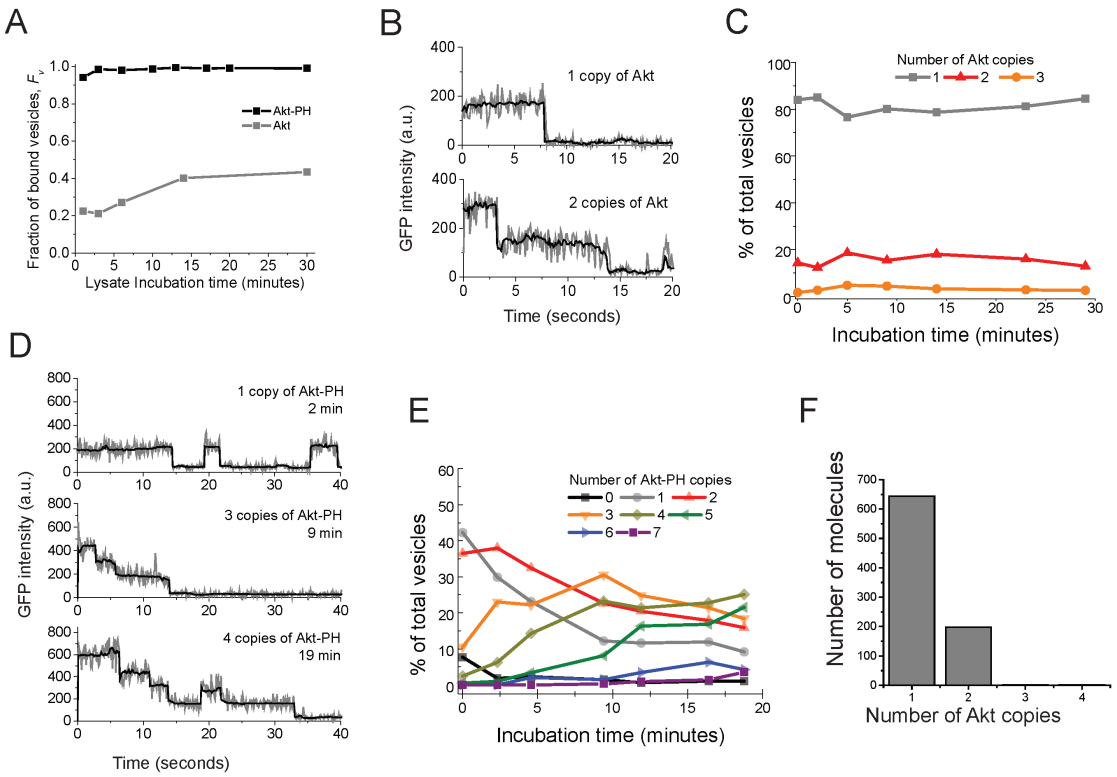

Figure. IV. 10. Assembly properties of Akt and Akt-PH. (A) Time course of Akt and Akt-PH binding to PIP_3 vesicles. (B) Representative single-molecule fluorescence traces of Akt bound to PIP_3, showing 1 and 2 copies per vesicle. (C) Assembly plot shows that the number of Akt copies per vesicle do not change with incubation time. (D) Single-molecule fluorescent traces for Akt-PH show an increase in total intensity along with stable and transient binding events. (E) The assembly plot depicts an increase in number of Akt-PH copies with increasing lysate incubation time. Example of 1, 3, and 4 copies per vesicle are shown in (D). (F) Distribution of fluorescent photobleaching steps for Akt. Akt was directly captured from cell lysates using a biotinylated anti-GFP antibody.

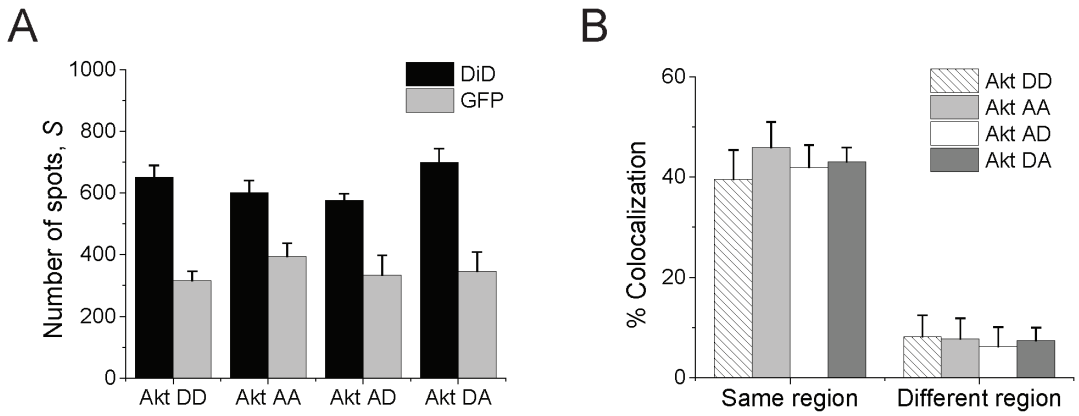

Figure IV. 11. T308 and S473 phosphorylation sites do not regulate Akt binding to PIP_3. (A) Comparision of Akt double mutants on T308 and S473 (DD, AA, AD, and DA respectively) binding to PIP_3 vesicles (B) Percentage colocalization of GFP-Akt double mutants to PI(3)P vesicles from same and different regions. Error bars depict standard deviation of the mean across 10 or more imaging areas.

IV. 6. References

Balla, T. and P. Varnai (2002). "Visualizing cellular phosphoinositide pools with GFP-fused protein-modules." Sci STKE 2002(125): pl3.

Bohdanowicz, M., G. Cosio, et al. (2010). "Class I and class III phosphoinositide 3-kinases are required for actin polymerization that propels phagosomes." J Cell Biol 191(5): 999-1012.

Botelho, R. J., M. Teruel, et al. (2000). "Localized biphasic changes in phosphatidylinositol-4,5-bisphosphate at sites of phagocytosis." J Cell Biol 151(7): 1353-1368.

Burman, C. and N. T. Ktistakis (2010). "Regulation of autophagy by phosphatidylinositol 3-phosphate." FEBS Lett 584(7): 1302-1312.

Calleja, V., D. Alcor, et al. (2007). "Intramolecular and intermolecular interactions of protein kinase B define its activation in vivo." PLoS Biol 5(4): e95.

Cantley, L. C. (2002). "The phosphoinositide 3-kinase pathway." Science 296(5573): 1655-1657.

Chung, S. H. and R. A. Kennedy (1991). "Forward-backward non-linear filtering technique for extracting small biological signals from noise." J Neurosci Methods 40(1): 71-86.

Di Paolo, G. and P. De Camilli (2006). "Phosphoinositides in cell regulation and membrane dynamics." Nature 443(7112): 651-657.

Dickson, R. M., A. B. Cubitt, et al. (1997). "On/off blinking and switching behaviour of single molecules of green fluorescent protein." Nature 388(6640): 355-358.

DiNitto, J. P., T. C. Cronin, et al. (2003). "Membrane recognition and targeting by lipid-binding domains." Sci STKE 2003(213): re16.

Frech, M., M. Andjelkovic, et al. (1997). "High affinity binding of inositol phosphates and phosphoinositides to the pleckstrin homology domain of RAC/protein kinase B and their influence on kinase activity." J Biol Chem 272(13): 8474-8481.

Gillooly, D. J., I. C. Morrow, et al. (2000). "Localization of phosphatidylinositol 3-phosphate in yeast and mammalian cells." EMBO J 19(17): 4577-4588.

Hawkins, P. T., T. R. Jackson, et al. (1992). "Platelet-derived growth factor stimulates synthesis of PtdIns(3,4,5)P3 by activating a PtdIns(4,5)P2 3-OH kinase." Nature 358(6382): 157-159.

Hayakawa, A., S. J. Hayes, et al. (2004). "Structural basis for endosomal targeting by FYVE domains." J Biol Chem 279(7): 5958-5966.

Jain, A., R. Liu, et al. (2011). "Probing cellular protein complexes using single-molecule pull-down." Nature 473(7348): 484-488.

James, S. R., C. P. Downes, et al. (1996). "Specific binding of the Akt-1 protein kinase to phosphatidylinositol 3,4,5-trisphosphate without subsequent activation." Biochem J 315 (Pt 3): 709-713.

Jenkins, G. M. and M. A. Frohman (2005). "Phospholipase D: a lipid centric review." Cell Mol Life Sci 62(19-20): 2305-2316.

Lemmon, M. A., K. M. Ferguson, et al. (1995). "Specific and high-affinity binding of inositol phosphates to an isolated pleckstrin homology domain." Proc Natl Acad Sci U S A 92(23): 10472-10476.

Nakanishi, H., P. de los Santos, et al. (2004). "Positive and negative regulation of a SNARE protein by control of intracellular localization." Mol Biol Cell 15(4): 1802-1815.

Rowland, M. M., D. Gong, et al. (2012). "Microarray analysis of Akt PH domain binding employing synthetic biotinylated analogs of all seven phosphoinositide headgroup isomers." Chem Phys Lipids 165(2): 207-215.

Scott, J. L., C. A. Musselman, et al. (2012). "Emerging methodologies to investigate lipid-protein interactions." Integr Biol (Camb) 4(3): 247-258.

Stace, C. L. and N. T. Ktistakis (2006). "Phosphatidic acid- and phosphatidylserine-binding proteins." Biochim Biophys Acta 1761(8): 913-926.

Watton, S. J. and J. Downward (1999). "Akt/PKB localisation and 3' phosphoinositide generation at sites of epithelial cell-matrix and cell-cell interaction." Curr Biol 9(8): 433-436.

Wymann, M. P. and R. Schneiter (2008). "Lipid signalling in disease." Nat Rev Mol Cell Biol 9(2): 162-176.

Yoon, M. S., G. Du, et al. (2011). "Class III PI-3-kinase activates phospholipase D in an amino acid-sensing mTORC1 pathway." J Cell Biol 195(3): 435-447.

Zeniou-Meyer, M., N. Zabari, et al. (2007). "Phospholipase D1 production of phosphatidic acid at the plasma membrane promotes exocytosis of large dense-core granules at a late stage." J Biol Chem 282(30): 21746-21757.